NAVAL POSTGRADUATE SCHOOL
Monterey, California

THESIS

AN INVARIANT DISPLAY STRATEGY FOR HYPERSPECTRAL IMAGERY

by

David Ivan Diersen

December 2000

Thesis Advisor:	Scott Tyo
Second Reader:	Roberto Cristi

20010402 111

REPORT DOCUMENTATION PAGE		*Form Approved* *OMB No. 0704-0188*

Public reporting burden for this collection of information is estimated to average 1 hour per response, including the time for reviewing instruction, searching existing data sources, gathering and maintaining the data needed, and completing and reviewing the collection of information. Send comments regarding this burden estimate or any other aspect of this collection of information, including suggestions for reducing this burden, to Washington headquarters Services, Directorate for Information Operations and Reports, 1215 Jefferson Davis Highway, Suite 1204, Arlington, VA 22202-4302, and to the Office of Management and Budget, Paperwork Reduction Project (0704-0188) Washington DC 20503.

1. AGENCY USE ONLY *(Leave blank)*	2. REPORT DATE December 2000	3. REPORT TYPE AND DATES COVERED Master's Thesis	
. TITLE AND SUBTITLE: Title (Mix case letters) AN INVARIANT DISPLAY STRATEGY FOR HYPERSPECTRAL IMAGERY		**5. FUNDING NUMBERS**	
6. AUTHOR(S) David Ivan Diersen			
7. PERFORMING ORGANIZATION NAME(S) AND ADDRESS(ES) Naval Postgraduate School Monterey, CA 93943-5000		**. PERFORMING ORGANIZATION EPORT NUMBER**	
9. SPONSORING / MONITORING AGENCY NAME(S) AND ADDRESS(ES) N/A		**10. SPONSORING / MONITORING AGENCY REPORT NUMBER**	

11. SUPPLEMENTARY NOTES The views expressed in this thesis are those of the author and do not reflect the official policy or position of the Department of Defense or the U.S. Government.

12a. DISTRIBUTION / AVAILABILITY STATEMENT Approved for public distribution; distribution unlimited	12b. DISTRIBUTION CODE

13. ABSTRACT *(maximum 200 words)*

Remotely sensed data produced by hyperspectral imagers contains hundreds of contiguous narrow spectral bands at each spatial pixel. The substantial dimensionality and unique character of hyperspectral imagery requires display techniques that differ from traditional image analysis tools.

This study investigated the appropriate methodologies for displaying hyperspectral images based on the physical principles of human color vision and a generalized set of linear transformations. Principal components (PC) analysis is a powerful tool for reducing the dimensionality of a data set, and PC-based strategies were explored in creating a broadly applicable image display strategy. It is shown that the invariant display strategy and generalized eigenvectors developed within this study offer a first look capability for a wide variety of spectral scenes. PC transformations utilizing this generalized set of eigenvectors allow for 'real time' initial classification. Detailed investigation of the relationship between the PC eigenvectors and dissimilar image content shows that this strategy is robust enough to provide an accurate initial scene classification.

14. SUBJECT TERMS			15. NUMBER OF PAGES 104
			16. PRICE CODE
17. SECURITY CLASSIFICATION OF REPORT Unclassified	18. SECURITY CLASSIFICATION OF THIS PAGE Unclassified	19. SECURITY CLASSIFICATION OF ABSTRACT Unclassified	20. LIMITATION OF ABSTRACT UL

THIS PAGE INTENTIONALLY LEFT BLANK

AN INVARIANT DISPLAY STRATEGY FOR HYPERSPECTRAL IMAGERY

David I. Diersen
Captain, United States Marine Corps
B.S.E.E., University of Minnesota, 1993

Submitted in partial fulfillment of the
requirements for the degree of
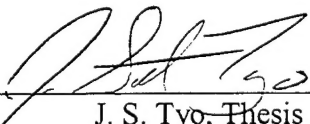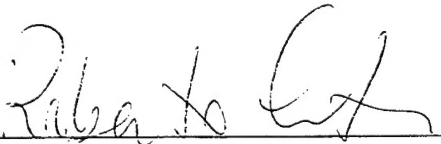
MASTER OF SCIENCE IN ELECTRICAL ENGINEERING

from the

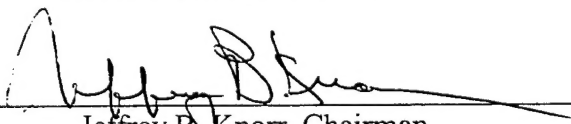## NAVAL POSTGRADUATE SCHOOL
December 2000

Author: _____

David I. Diersen

Approved by: _____

J. S. Tyo, Thesis Advisor

_____

Roberto Cristi, Second Reader

_____

Jeffrey B. Knorr, Chairman
Department of Electrical and Computer Engineering

iii

THIS PAGE INTENTIONALLY LEFT BLANK

ABSTRACT

Remotely sensed data produced by hyperspectral imagers contains hundreds of contiguous narrow spectral bands at each spatial pixel. The substantial dimensionality and unique character of hyperspectral imagery requires display techniques that differ from traditional image analysis tools.

This study investigated the appropriate methodologies for displaying hyperspectral images based on the physical principles of human color vision and a generalized set of linear transformations. Principal components (PC) analysis is a powerful tool for reducing the dimensionality of a data set, and PC-based strategies were explored in creating a broadly applicable image display strategy. It is shown that the invariant display strategy and generalized eigenvectors developed within this study offer a first look capability for a wide variety of spectral scenes. PC transformations utilizing this generalized set of eigenvectors allow for 'real time' initial classification. Detailed investigation of the relationship between the PC eigenvectors and dissimilar image content shows that this strategy is robust enough to provide an accurate initial scene classification.

THIS PAGE INTENTIONALLY LEFT BLANK

TABLE OF CONTENTS

THIS PAGE INTENTIONALLY LEFT BLANK

LIST OF FIGURES

THIS PAGE INTENTIONALLY LEFT BLANK

LIST OF TABLES

THIS PAGE INTENTIONALLY LEFT BLANK

EXECUTIVE SUMMARY

An invariant methodology has been developed in response to the need for coherent and consistent display of the hundreds of contiguous narrow spectral bands present within hyperspectral imagery. The methodology builds upon traditional hyperspectral imagery processing techniques and provides a more robust first look capability for unsupervised classification.

This study investigated the appropriate techniques for displaying hyperspectral images based on the physical principles of human color vision and a generalized set of linear transformations. Principal components (PC) analysis reduced the dimensionality of a data sets, and PC-based strategies were explored in creating a broadly applicable image display strategy. Analysis of hyperspectral images and display strategies were accomplished utilizing MATLAB and ENVI software.

From analysis and comparison of imagery data from Davis-Monthan Air Force Base to image data obtained from similar and dissimilar scenes, it is clear to see that for comprehensive analysis, it would be appropriate to maintain scenes such as Davis-Monthan (which consists of desert background) within one group and scenes such as Jasper Ridge (forest) and Lake Tahoe (forest/water) within another group. But, for first order unsupervised classification, the first few eigenvalues and associated eigenvectors which contain the largest amount of scene variance can appropriately represent a scene. Extending this concept further, it is clear that a generalized set of eigenvectors can depict any scene content. The average eigenvectors investigated in this study provides such a

basis and can be further improved upon with an increase in the number of data sets utilized.

A principal component-based mapping strategy provides an easy way to perform first order unsupervised display. The inclusion and utilization of generalized eigenvectors decreases the overhead required to perform first order display and will allow for 'real time' classification of hyperspectral imagery. By visually inspecting the resultant image, an analyst can then direct attention to appropriate areas of the scene for further processing without the time consuming requirement of calculating the scene specific statistics. The generalized PC and RGB transformation eigenvectors utilized in this study can be applied to a broad range of spectral imagery classes. These eigenvectors can become even more robust as the number of 'averaged' scenes is increased.

The 1st PC will always be related to the mean solar radiance, but the 2nd, 3rd and subsequent PCs depend on the specific contents of the image. However, it is also shown that only the first three PCs are required for a color mapping corresponding to human color vision. It remains to be investigated whether or not the RGB transformation of the HSV image presented here can be arranged so that materials are presented in a straightforward manner, i.e. water always mapped to blue, vegetation to green, etc, vice having the dominant scene constituent set the base hue of the image.

The presentation strategy discussed here is best suited to broadscale geographical classification, not for identifying small, isolated targets. However, objects and variances within the scene which occur only at a few pixels in an image and thus have little effect on the overall covariance matrix and do not contribute significantly to the 2nd and 3rd PCs,

do appear to be discernable in this mapping strategy. For this reason, this aspect of the mapping strategy merits further investigation.

The invariant display strategy and generalized eigenvectors presented here is offered as a way to have a first look at a wide variety of spectral scenes. By performing a PC transformation with these eigenvectors and analyzing the three most significant PCs, an initial classification decision can be made 'real time'.

THIS PAGE INTENTIONALLY LEFT BLANK

ACKNOWLEDGMENTS

THIS PAGE INTENTIONALLY LEFT BLANK

I. INTRODUCTION

The introduction of imaging spectroscopy with the Airborne Imaging Spectrometer in 1982 established a powerful new tool for the earth sciences, but also created a fundamentally new class of data requiring new approaches to information extraction and display methodologies (Vane and Goetz, 1988, p.1). This new class of data provides a representation of the spectral character of materials on the ground and will be referred to as spectral imagery throughout the study. Hyperspectral data, a particular type of spectral imagery, is produced when solar electromagnetic energy reflected form the earth's surface is dispersed into many contiguous narrow spectral bands by an airborne spectrometer (Vane and Goetz, 1988, p. 3). Each picture element (pixel) of a hyperspectral image can be thought of as a high resolution trace of radiation versus wavelength, or a spectrum (Rinker, 1990, p. 6). The characteristic wavelength dependent changes in the emissivity and reflectivity of a given material can be related to the chemical composition and types of atomic and molecular bonds present in that material (Gorman, et. al., 1995, p. 2805). The chemical composition of different materials is thus manifested in the spectral properties of these materials, and can serve as a means of differentiating materials observed in a hyperspectral image with great detail.

Analysis and display of hyperspectral imagery is complicated by several factors. The first is the volume of data inherent in a hyperspectral image. A typical 224-band Airborne Visible/Infrared Imaging Spectrometer (AVIRIS) image contains approximately 134 Mbytes of data (Roger and Cavenor 1996). Algorithms for processing data sets of this magnitude must be computationally efficient to be of any service and if possible, must seek to eliminate redundant data prior to processing. The second factor is that the

1

radiances recorded at the spectrometer output are subjected to noise, additive and possibly multiplicative (Tyo, et. al., 2000), from the atmosphere, sensor instrumentation, data quantization procedure, and transmission back to earth. The cumulative effect of these noise terms is a spectrum that has been corrupted by noise which impacts meaningful image representation and target detection becomes even more complicated. It is here where a signal processing point of view is helpful, as the problem has now become the classical signal in noise problem. The third factor is that because of the finite spatial resolution of the imaging spectrometer and the actual ground scene, the observed spectrum for a pixel may not be that of a single material, but could be a mixture of several different materials which exist within the spatial dimensions of the sensor's ground instantaneous field of view (GIFOV). Although the third factor is primarily concerned with target detection and classification, it will impact the overall display representation. The sea level GIFOV of the AVIRIS sensor at sea level is nominally 20m x 20m (Farrand and Harsanyi, 1995, p. 1566) and the implication is that several materials could contribute to the observed spectrum for that pixel depending on the complexity of the ground scene. A fourth factor that complicates analysis efforts is that spectra of the same type of material may appear very different. This variability within the spectra of a species or target class dictates a statistical approach vice a deterministic one. (Tyo, et. al. 2000, Kerekes, et. al., 2000)

There are many types of data processing techniques which address the unique issues raised by hyperspectral imagery. Many grew out of earlier techniques which had been successfully applied to multispectral imagery, the precursor of hyperspectral imagery. Others have a foundation in the discipline of pattern recognition. Another

approach, which is naturally suited to the task of detecting signals in the presence of noise and multiple interfering signals, is based on signal processing. The signal processing approach efficiently handles the data by viewing it from the vantage of vectors and matrices, performs processing by various linear transformations and will be the methodology utilized in this study.

The major goal of this study is to expand the knowledge and methodology of hyperspectral image display strategies and a secondary goal is to provide a mapping strategy that can be used on a wide variety of hyperspectral images. This study is organized in a manner that will facilitate the goal of an orderly approach to invariant display strategies for hyperspectral images. Chapter II presents an overview of hyperspectral imagery and introduces the statistical signal processing approach to data analysis. Chapter III describes human vision and relates it to a statistical signal processing approach. This chapter also details why human visual perception must be accounted for in any display methodology. Chapter IV details the methods utilized in this study for the processing of hyperspectral image files and identifies specific types of data that it is applied to. Chapter IV also contains an analysis of the various display strategies found to be most effective for a variety of hyperspectral image types. Chapter V concludes the study and seeks to solidify the connections between specific hyperspectral data sets and the most appropriate display strategies.

THIS PAGE INTENTIONALLY LEFT BLANK

II. BACKGROUND

A.   PROBLEM STATEMENT

Within the past several decades, many strategies for target identification, material classification, terrain mapping, etc., have been developed to exploit the information in the hundreds of spectral samples taken at each pixel in a scene. Once a classification algorithm or image processing tool has been applied to a spectral image, the resulting processed data is invariably mapped into a pseudocolor image. While many display methodologies are quite powerful, there is no standard tool used to render spectral imagery in false-color images for presentation.

Currently, the use of false color displays is generally reserved as a tool for presenting data after processing. Once a scene has been classified by a particular algorithm, a specifically tailored colormap is created to emphasize the performance of the classification system. Commonly, in an attempt to distinguish scene elements, one displays the data as an initial processing step, but rarely is visualization in and of itself used as a tool that allows the spectral analyst to perform identification before cueing more powerful processing strategies. Most colormaps in use today have been developed based on the mathematics of spectral images without considering the workings of the human vision system. It has been demonstrated that failure to consider how the observer processes data visually can make information difficult to find in an image, even when the data are clearly available. (Tyo, et. al. 1998)

B. HYPERSPECTRAL IMAGERY OVERVIEW

In order to fully understand the need of an invariant false-color mapping strategy, a review of the historical perspective and paradigms in the analysis of hyperspectral images is necessary. Figure 2.1 illustrates the major image analysis paradigms over the past seventy years. This is not an all inclusive history, but a quick synopsis of the major ideas behind hyperspectral imagery analysis. Note that there is no visual representation strategy within any of the paradigms.

Photointerpretation (1930s)
: 2-D Images
: good qualitative analysis (human)
: poor quantitative analysis

Digital Imagery (1960s)
: 2-D Images
: Pattern Recognition, Computer Vision
: Emphasis on Classification Techniques

Multispectral Imagery (1970s)
: 3-D Images
: Principal Components Analysis
: Land Usage Classification

Hyperspectral imagery (1980s)
: 3-D
: Need to reduce data dimensionality
: Software Packages with Spectral Libraries
: Need efficient processing techniques

Figure 2.1: Major Imagery Analysis Paradigms.

The analysis of imagery began in the early part of this century with photointerpretation. The analysis of aerial photographs to extract information of interest was a strictly human operation. The strength of the human element in interpretation was

6

the ability to recognize large scale patterns (Richards, 1986, p. 75) and make inferences based on these patterns. However, the weakness of human image interpretation is the inability to accurately quantify the results in a consistent manner.

The computing power that began to become available in the 1960's and the ability to represent data in a digital fashion provided the impetus for automation of the photointerpretation task into digital imagery analysis. Here, the computer was programmed to work within narrow parameters, such as counting the number of occurrences of certain brightness values, a job that it performed more quickly and accurately than any human analyst. The fields of pattern recognition and computer vision became important, and a statistical description of the data was needed to form the basis of classification schemes which could accurately determine the number of pixels in the scene belonging to a certain class. Linear prediction and spatial principal components analysis (PCA) were tools that assisted in the automated detection of a target in the two-dimensional digital images.

The advent of multispectral imagery with Landsat data in the 1970's added the spectral dimension to the problem of imagery analysis. (i.e. If the number of spectral samples at each pixel is N, there is now N times the amount of data for analysis.) PCA played a significant role in reducing the dimensionality of the data (decrease from N number of samples to M<N linear combinations) by exploiting redundancy within the data and assisted in the classification of large land areas. The relationship between PCA techniques and classification techniques was a sequential operation in that PCA was first applied to an image to remove the redundant information or create a better class separation before application of a classifier. This preprocessing application of PCA still

7

continues today. It is important to note also that PCA in MSI and HSI is performed in the spectral dimension while in pattern recognition and photography, it is performed spatially.

The 1980's and hyperspectral imagery ushered in a new challenge to the existing methods of analyzing data. Hyperspectral imagery increased the number of spectral bands from less than 10 to more than 200, increasing the volume of data by a factor of 20-50. Thus, data compression became an important concern. The search for new techniques to deal with the large amount of information and commensurate amount of redundancy prompted new views of the analysis paradigm. Ideas from the signal processing community provided a means of handling the large amount of data and confronting the mixed pixel problem. Software packages dedicated to the analysis of hyperspectral imagery, such as ENVI, incorporated spectral libraries and found particular interest in the geological remote sensing community.

C.   DEFINITIONS

An understanding of the fundamental ideas behind the various spectral imagery analysis techniques is important because it forms the basis for all imagery analysis and image display methodologies. The fundamental ideas involve concepts from statistics, linear algebra, and signal processing theory. Discussion of these ideas in the context of spectral imagery sets the stage for the detailed discussion of display strategies that follow.

This section presents multispectral and hyperspectral images as a means of further highlighting certain properties of the spectral concept. The images are also

characterized from a statistics view which assists in better understanding the image content and the statistical principles used in spectral imagery analysis. Some concepts from linear algebra and signal processing are defined to provide a framework through which certain spectral imagery analysis techniques and display methodologies are understood. These perspectives offer a means of defining key concepts that appear throughout this study. An effort has been made to make these definitions simple yet comprehensive through the use of illustrative examples.

1. Spectral Imagery

Spectral imagery is the acquisition of images at multiple wavelengths by spectrometers onboard aircraft or spacecraft. Two primary classes of such measurements are the traditional multispectral images, as with those produced by the Thematic Mapper (TM) radiometer on the Landsat satellites, and hyperspectral imagery, produced by imaging spectrometers such as in the Airborne Visible/Infrared Imaging Spectrometer (AVIRIS) and Hyperspectral Digital Imaging Collection Experiment (HYDICE) systems. Typical Landsat TM and AVIRIS images will be used here to introduce many of the concepts needed for this study. These data sets will also be used to illustrate display strategies in future sections. The Landsat TM scene in Figure 2.2 is a six-band, 640-pixel x 400-pixel image of Canon City, Colorado which is provided with ENVI software on the ENVI-DATA CD-ROM. The scene is an image of a city surrounded by mountains. The six distinct image planes present in Figure 2.2 represent the various wavelength ranges sensed by Landsat TM. Notice how objects which appear bright in one band may appear dark in another band. The mountain ridgeline, found on the left side of the image,

illustrates this effect. Through this sort of contrasting, Landsat imagery offers a very basic means of discerning the spectral character of a particular class of material.

A representative AVIRIS scene of Jasper Ridge, which is also provided on the ENVIDATA CD-ROM, was chosen for comparison. The scene shows a biological preserve surrounded by a small city. Data sets of this area are typically utilized for vegetation analysis.

$\lambda=0.485um$ $\lambda=0.560um$ $\lambda=0.660um$ $\lambda=0.830um$ $\lambda=1.650um$ $\lambda=2.215um$
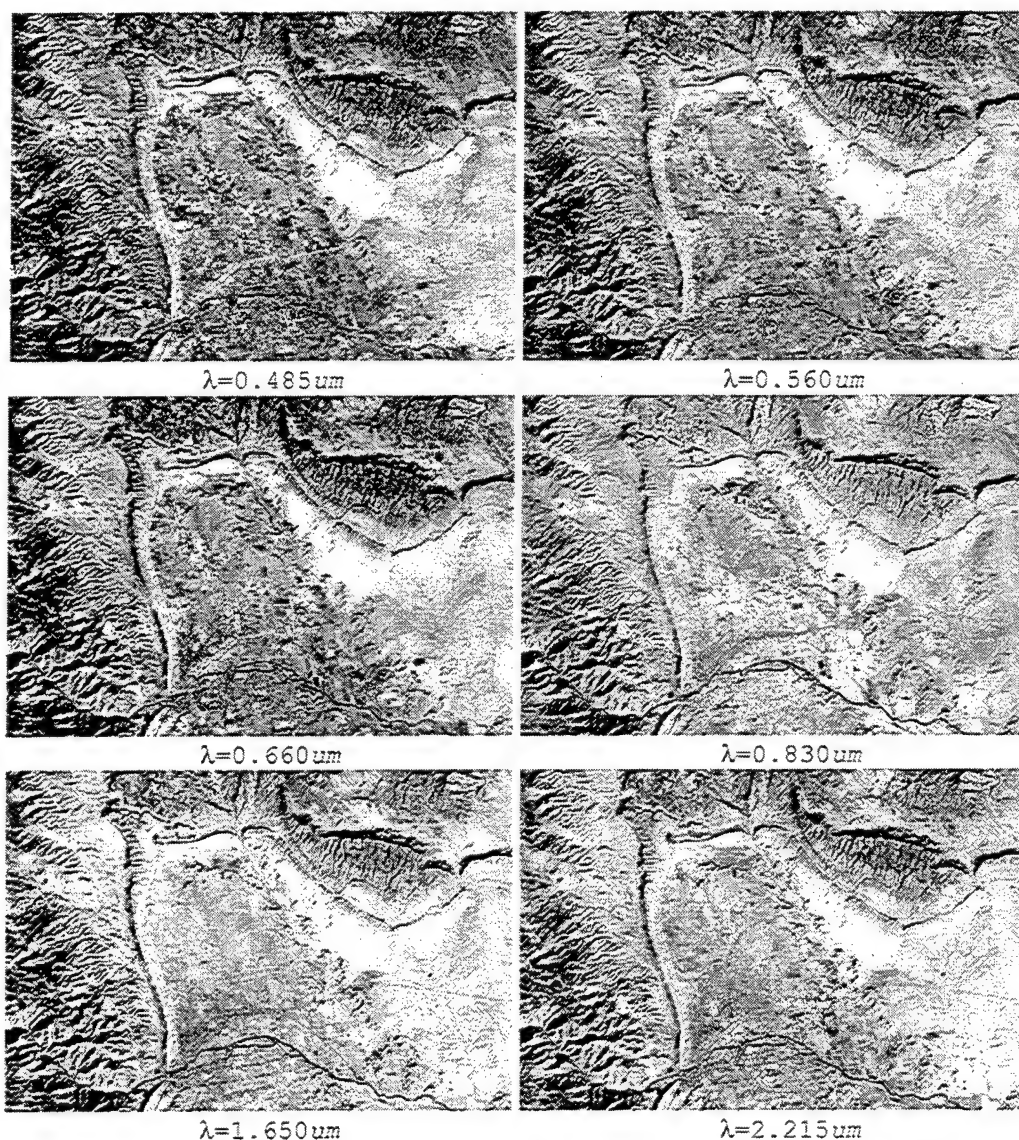
Figure 2.2: A Typical 6-Band Multispectral Image Produced by Landsat TM. (Note different shadings between bands.)

Figure 2.3 shows three representations of the hyperspectral image consisting of 300 samples, 250 lines, and 224 bands. This first image is a grayscale representation of band 37, the second image is a red, green, blue composite formed using bands 176, 91, and 31, and the third image is a red, green, blue composite formed using bands 25, 120, and 200. The Jasper Ridge representation in Figure 2.3 shows only a small subset of the wide range of color mappings available to an analyst.

Figure 2.3: Jasper Ridge Color Representation. Panel a is an achromatic representation of Band 37 (702.5nm). Panel b is a R-G-B representation with Red 2208.7nm, Green 1221.0nm and Blue 665.7nm. Panel c is a R-G-B representation with Red 606.4nm, Green 1483.4nm and Blue 2268.4nm.

One way of visualizing data that has two spatial and one spectral dimension is as a cube. Due to 'finer' resolution of spectral frequencies, the ability to identify materials based on spectral detail is more effective with hyperspectral imagery as opposed to multispectral imagery (Goetz,1995). Figure 2.4 emphasizes the high spectral resolution of hyperspectral data by extracting information in the spectral dimension, or downward in the axes of the cube. It shows the construction of an observed spectrum associated with a particular spatial location, called a pixel vector.

EACH PIXEL HAS
AN ASSOCIATED,
CONTINUOUS SPECTRUM
THAT CAN BE USED TO
IDENTIFY THE SURFACE
MATERIALS

IMAGES TAKEN
SIMULTANEOUSLY
IN 100-200 SPECTRAL BANDS,
INHERENTLY REGISTERED

R

0.4   2.5

WAVELENGTH, μm
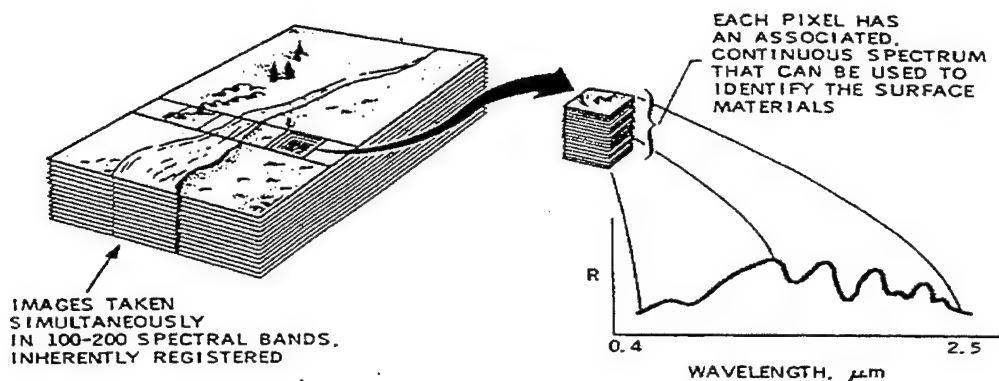
Figure 2.4: The Concept of a Pixel Vector. From Vane and Goetz, 1988, P.2.

The pixel vector is central to the discussion which follows, since the pixel vector may be viewed as a unique signal associated with a material of interest. Figure 2.5 further illustrates the pixel vector concept using randomly chosen observed spectra from the Landsat and AVIRIS images. The fine spectral detail that can be discerned in the hyperspectral image spectrum is a stark contrast to the coarse detail that comes from six data points, as in the Landsat observed spectrum. The implication is that the characteristic shape of the pixel vectors obtained using hyperspectral imagery allows a more definitive identification of material based on unique spectral characteristics.

The hyperspectral sensors AVIRIS and HYDICE have spectral bands that are configured to cover a range of 400 to 2500nm. The observations of the reflected energy at the sensor are measured in terms of radiance, which has units of watts per square meter per steradian, ($Wm^{-2}sr^{-1}$). The spectral irradiance is how much power density is available incrementally across the wavelength range and is measured in ($Wm^{-2}um^{-1}$). (Richards, 1986)

12
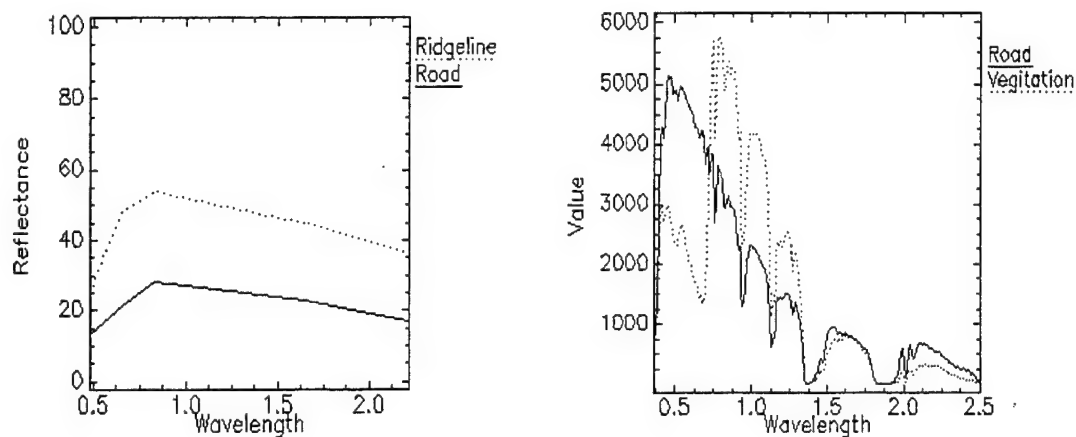
Figure 2.5: Typical Pixel Vectors From Multispectral and Hyperspectral Images.

A significant portion of the spectrum imaged in the AVIRIS system is dominated by solar energy reflected from the earth's surface. This solar energy accounts for the characteristic "hump" in roughly the 15th to the 37th bands (500nm-700nm). At times, it is desirable to mitigate the effect of the dominant solar curve so that other spectral details may be discerned. One means of doing so entails converting radiance measurements to reflectance measurements by dividing the radiance observations by the scene average spectrum. Other methods include the use of calibration panels, flat field calibration, and numerical techniques (ATREM, etc.) The net effect is to normalize the radiance measurements in such a manner that the solar bias is removed and the resulting reflectance spectrum appears flatter. For the purposes of this study, raw radiance data will primarily be utilized because analysis of this data will limit the amount of preprocessing required and allow for a better understanding of overall scene characteristics.

13

2. Statistical Interpretation

In order to assist in the quantitative discussion of characterizing the data statistically, we need to formally define the concept of the observed pixel vector. Assume that the observed pixel vector x is a real valued random vector

$$\mathbf{x} = \begin{bmatrix} x_1 \\ \vdots \\ \vdots \\ x_L \end{bmatrix} \tag{2.1}$$

where the components $\{x_i,...,x_L\}$ correspond to measured brightness values in each of L spectral bands. Since a stochastic view of the data assumes that these vectors are random entities, one means of characterizing them is to describe their behavior using statistical concepts. Exact statistical descriptions of their behavior are unavailable in real applications, so we must rely on methods that estimate the statistics of the observed random vectors.

There are three major statistical definitions of interest in this respect. The first is the concept of expectation. The expectation of a random vector is called the mean or the average value that the random vector assumes and is denoted as $E\{\mathbf{x}\}$. The mean is also called the first moment since it involves only the random vector itself and not products of the components of the vector $\mathbf{x}$ (Therrien, 1992, p. 33). In using the observed data, it is often desirable that the statistical expectation of the estimated mean equal the actual mean. This is called an unbiased estimate of the mean. The framework for this estimation is to view the spectral image or scene as a collection of N random pixel vectors. This implies that the scene is comprised of N pixel vectors, each consisting of an L-band spectrum. The unbiased estimate of the mean spectrum for the scene is given by:

14

$$\mathbf{m} = \frac{1}{N} \sum_{j=1}^{N} \mathbf{x}_j = \begin{bmatrix} m_1 \\ \vdots \\ \vdots \\ m_L \end{bmatrix} \tag{2.2}$$

where $\mathbf{x}_j$ represents the spectrum of the jth pixel of the scene. The mean spectrum vector, $\mathbf{m}$, of Equation 2.2 can also be interpreted as a L-dimensional vector with each component representing the average brightness value over the entire image for one particular band.

The second definition of importance in characterizing random vectors is that of the covariance matrix. The covariance matrix is defined in vector and expanded component form as:

$$\sum_{x} = E\{(\mathbf{x}\text{-}\mathbf{m})(\mathbf{x}\text{-}\mathbf{m})^T\} =$$

$$\begin{bmatrix} E\{(x_1-m_1)^2\} & E\{(x_1-m_1)(x_2-m_2)\} & \cdots & E\{(x_1-m_1)(x_L-m_L)\} \\ E\{(x_2-m_2)(x_1-m_1)\} & E\{(x_2-m_2)^2\} & \cdots & E\{(x_2-m_2)(x_L-m_L)\} \\ \vdots & \vdots & \ddots & \vdots \\ E\{(x_L-m_L)(x_1-m_1)\} & E\{(x_L-m_L)(x_2-m_2)\} & \cdots & E\{(x_L-m_L)^2\} \end{bmatrix} \tag{2.3}$$

where $\mathbf{m}$ is the mean vector of the entire image defined in Equation 2.2. The covariance matrix is symmetric, and the elements of the main diagonal represent the variances associated with each of the component variables of the random vector $\mathbf{x}$. In the case of spectral imagery, the variance is a measure of how the brightness value of a particular band varies over all spatial image pixels and the covariance describes the scatter of pixel points in the principal components vector space.

The covariance matrix is the set of second central moments of the distribution, which are also referred to as moments about the mean since the mean component is

15

subtracted from each random variable. The unbiased estimate of the covariance matrix is generated by:

$$\sum_x = \frac{1}{N-1} \sum_{j=1}^{N} (\mathbf{xj}\text{-}\mathbf{m})(\mathbf{xj}\text{-}\mathbf{m})^T \tag{2.4}$$

where $\mathbf{x}_j$ is again the pixel vector associated with the jth spatial location (Richards, 1993, p. 134). When the covariance of two random variables is zero, then the random variables are said to be uncorrelated, which implies that those random variables were generated by separate random processes (Leon-Garcia, 1994, p. 337). In the calculation of the unbiased estimates of statistical quantities, the computational expense of the covariance matrix for a large number of samples, N, must be balanced with the desired degree of accuracy for the estimate. More samples imply better estimates, and in order to ensure sufficient accuracy, the number of samples must be sufficiently large (Fukunaga, 1971, p.242).

The third statistical definition involves an issue that requires clarification regarding the term "correlation" matrix. In signal processing terminology, the correlation matrix stated as $E\{\mathbf{xx}^T\}$ is formed exactly as the covariance matrix, except that the mean vector is not subtracted from the random vector $\mathbf{x}$ (Therrien, 1992, p. 33). Figure 2.6 demonstrates the concept of mean removal using the scatter plots of two bands of Landsat data. The scatter plots are a representation of many two-dimensional random vectors which have a two-dimensional mean vector. The subtraction of this mean vector from every random vector results in a centering of the data about the origin. This introduces negative numbers into the previously positive data values.

16
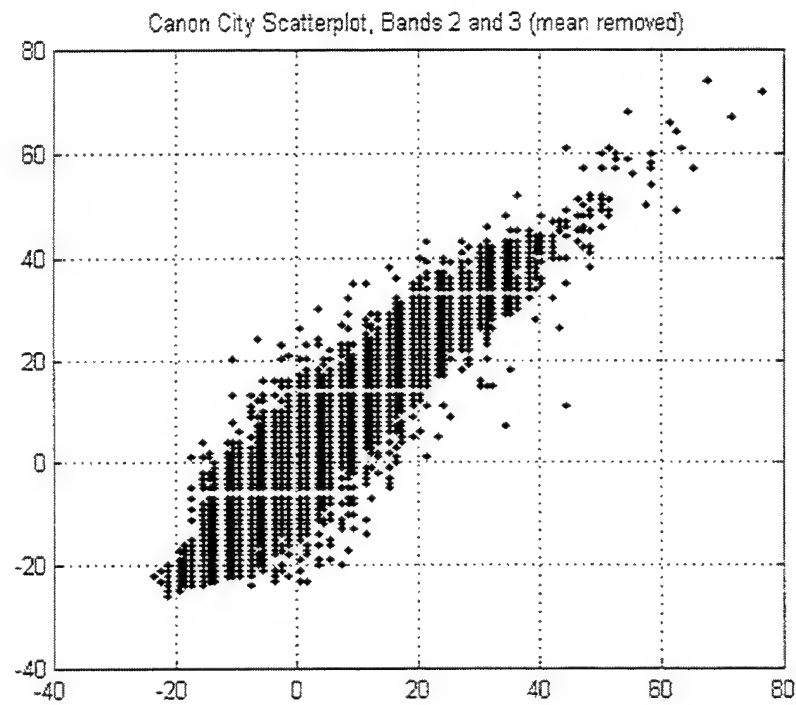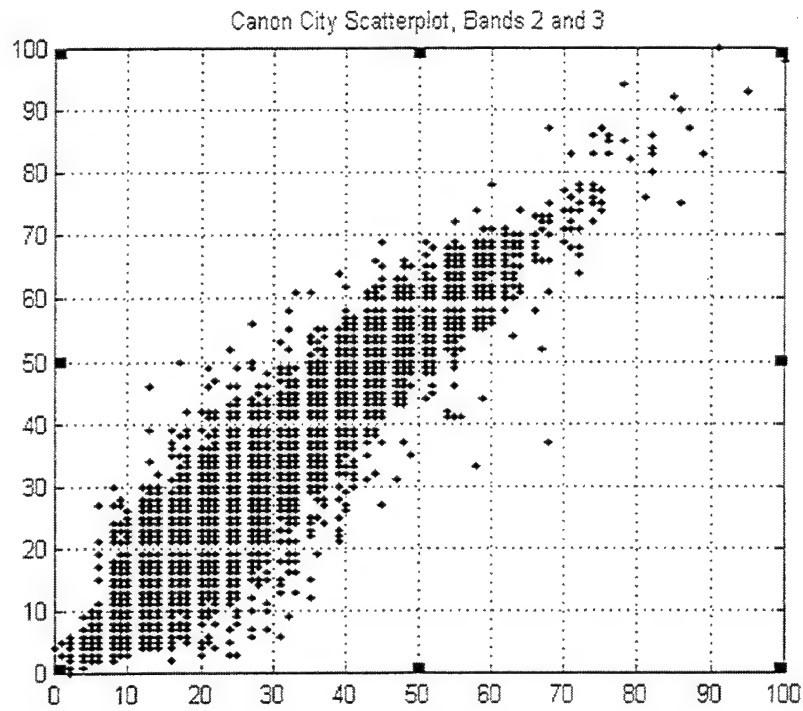
Figure 2.6: Mean Removal Illustration With Scatter Plots.

While the correlation matrix is more frequently used in signal processing where zero mean signals are the norm, remote sensing uses the covariance matrix since negative radiance values do not have a clear physical significance.

In statistical and remote sensing applications, the correlation matrix is usually defined in terms of the covariance matrix. The ij^{th} element of the statistical version of the correlation matrix is:

$$\rho_{ij} = \frac{\sigma_{ij}}{\sqrt{\sigma_{ii}\sigma_{jj}}} \qquad (2.5)$$

where σ_{ij} is an element of the covariance matrix and is the covariance between bands i and j in Σ_x, σ_{ii} represents the variance of the ith band of data, and the square root of variance is defined as the standard deviation (Richards, 1993, p. 135).

The statistical and signal processing versions of correlation do not produce the same matrix. The statistical definition produces a matrix which has a unit main diagonal and can be represented as:

$$\mathbf{R}_x = \begin{bmatrix} 1 & \rho_{12} & \dots & \rho_{1N} \\ \rho_{21} & 1 & \dots & \rho_{2N} \\ \vdots & \vdots & \ddots & \vdots \\ \rho_{N1} & \rho_{N2} & \dots & 1 \end{bmatrix} \qquad (2.6)$$

(Searle, 1982, P. 348). It is apparent that dividing the covariance matrix elements by their standard deviations has the effect of reducing all the variables to an equal importance since all have unit variance. The signal processing definition does not produce a unit diagonal matrix, though it is symmetric. The off diagonal elements of $\mathbf{R}_x$, represented by ρ_{ij} are called correlation coefficients. They range between -1 and +1 in value, and provide a measure of how well two random variables vary jointly by

18

quantifying the degree of fit to a linear model (Research Systems, Inc., 1995, p. 20-6). A value near +1 or -1 represents a high degree of fit between the random variables to a positive or negative linear model, whereas a values near zero implies that the random variables exhibit a poor fit to the linear model. The conclusion that may be drawn is that a high degree of fit implies well-correlated random variables, whereas a correlation coefficient of zero is indicative of statistically orthogonal random variables. We will assume that we are dealing with the statistical definition of the correlation matrix, though a more descriptive term for the "correlation" matrix might be the "normalized" or "standardized" covariance matrix.

The definitions of statistical properties become clearer when they are linked to a physically observable phenomenon. The next few illustrations attempt to show the large amount of information revealed by the statistics of the data. Table 2.1 shows the covariance and correlation matrices for the Landsat data of Canon City.

Covariance Matrix for Canon City TM Data

Band	Band 1	Band 2	Band 3	Band 4	Band 5	Band 6
1	45.391430	54.157121	62.472157	48.824654	48.318837	43.826169
2	54.157121	69.760492	79.432844	64.610172	64.421129	57.616349
3	62.472157	79.432844	96.376932	77.863810	79.247686	70.393457
4	48.824654	64.610172	77.863810	100.500970	74.711596	57.981971
5	48.318837	64.421129	79.247686	74.711596	87.056432	70.991722
6	43.826169	57.616349	70.393457	57.981971	70.991722	63.739045

Correlation Matrix for Canon City TM Data

Band	Band 1	Band 2	Band 3	Band 4	Band 5	Band 6
1	1.000000	0.962418	0.944524	0.722881	0.768651	0.814786
2	0.962418	1.000000	0.968744	0.771633	0.826653	0.864049
3	0.944524	0.968744	1.000000	0.791159	0.865166	0.898138
4	0.722881	0.771633	0.791159	1.000000	0.798735	0.724444
5	0.768651	0.826653	0.865166	0.798735	1.000000	0.953025
6	0.814786	0.864049	0.898138	0.724444	0.953025	1.000000

Table 2.1: Covariance and Correlation Matrices of Landsat TM Data.

In examining the Landsat covariance matrix, we see that the highest variance results from band four, the lowest covariance is between bands one and six, and the highest covariance is between bands two and three. The correlation coefficient is highest between bands two and three and is lowest between bands one and four. We can draw some conclusions from these statistics. First, band four has more variance, or contrast over the scene, than any other band. Before we assume that this means that band four can detect some sort of unique information better than other bands, we must ask if this variance was caused by signal coming from the ground or if it was noise introduced by our sensor or the atmosphere in that particular band. If we know the signal-to-noise ratio of our sensor in band four then we can answer the question. Signal-to-noise ratio (SNR) is the ratio of signal power to noise power, and can be obtained using the variances as the power. Second, band one exhibits the lowest correlation coefficient when compared to all other bands. Again, before we assume that band one detects unique information, we must ask about the signal-to-noise characteristics of band one. For example, if band one were purely noise, then it would exhibit an even lower correlation with other bands, perhaps even zero. This is because it is independent of the other bands, not because it carries any information.

The scatter plot is another means of characterizing the statistics of the data by visually presenting the two-dimensional distribution of pixels using two selected bands. Two band combinations are shown in Figure 2.7. The scatter plot is a representation of all of the two-dimensional random pixel vectors formed by the two bands of interest. By plotting the data of one band against that of another, information regarding the statistical similarity of bands may be inferred. The scatter plots for the Landsat image show a

20

definite linear feature when a high correlation coefficient exists, as between bands two and three. Thus, bands two and three are statistically similar, to the extent that there appears to be a near linear relationship between their random variables. The correlation coefficient of 0.9687 substantiates this observation. This is in contrast to the more distributed shape for the scatter plot of band one data versus band four where the correlation coefficient is .7229.
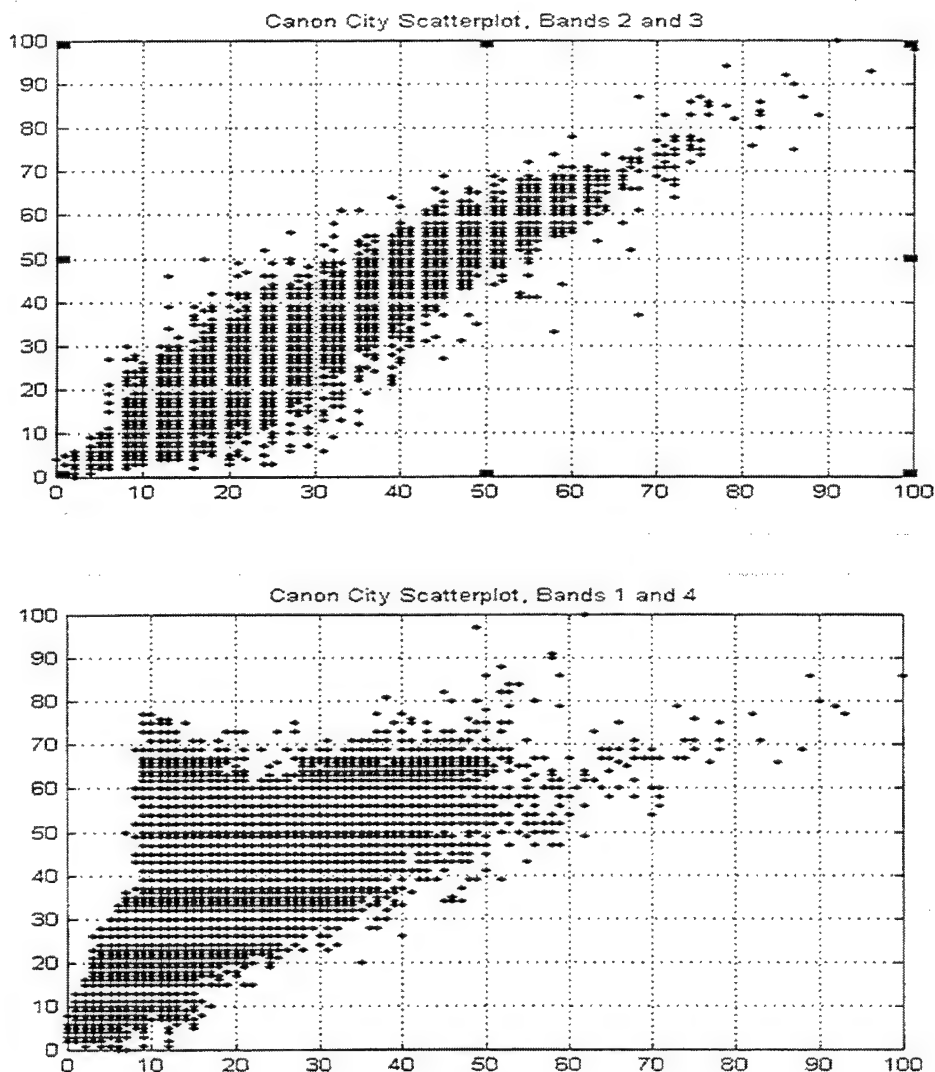
Figure 2.7: Scatter Plots of Canon City Landsat TM Data Showing Highly Correlated (2nd & 3rd) and Less Correlated (1st & 4th) Band Combinations.

This graphically depicts the more independent and less correlated nature of the data in band four, as evidenced by the lower correlation coefficient of 0.7229. The scatter plot also clearly shows groupings of pixels that have the most variance and will form the basis for the studies false-color mapping strategy.

In order to show the second order statistics of a hyperspectral image, another visualization technique is introduced. With 224 bands, manually examining the covariance matrix would be tedious, and comparing two bands at a time with scatter plots would be similarly ineffective and time consuming. For hyperspectral data statistics, the elements in the covariance matrices are assigned color values corresponding to their value. The result is a color matrix which helps in explaining trends. Figure 2.8 illustrates the covariance and correlation matrices for the radiance data in the AVIRIS Jasper Ridge scene.
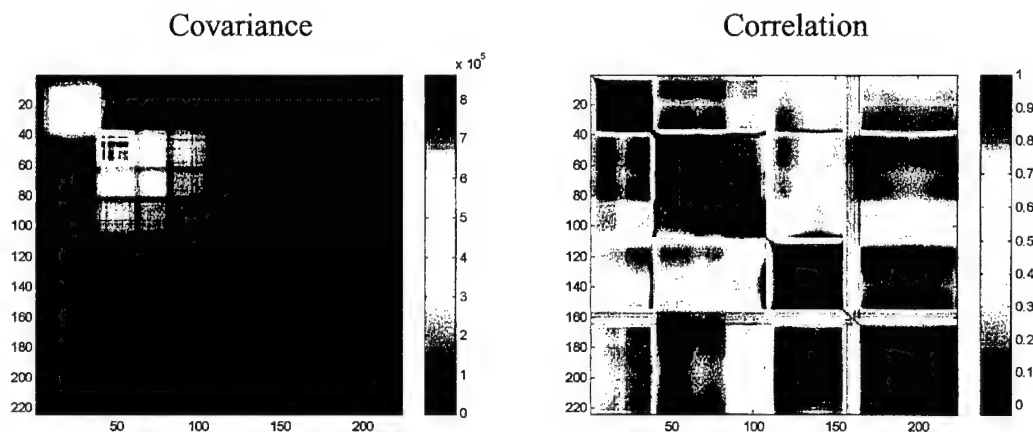
Figure 2.8: Second Order Statistics of the AVIRIS Jasper Ridge Scene.

There are several notable features in the two matrices. In the radiance covariance matrix, we see the effect of the sun on bands 50 to 70 manifested in the higher variance and covariance values. This is because the covariance matrix is constructed in a manner

22

that uses the absolute radiance values, which are very large in these bands for radiance data. The correlation matrix of the radiance does not show this uneven weighting of variances. Instead, the correlation coefficients closest to the main diagonal exhibit a fairly similar value over all image bands, indicating that the correlation matrix has normalized the variances and covariances with respect to their standard deviations. The high values in the vicinity of the main diagonal are indicative of an important characteristic of hyperspectral imagery, namely the high correlation between adjacent bands. Both of the matrices show the effects of the absorption bands as areas of very low covariances and correlation coefficients. This is intuitively pleasing, since the absorption bands should be very uncorrelated with all other bands. These dark vertical and horizontal features on the matrices represent the presence of atmospheric absorption features and are a good illustration of the effect of additive noise. The bands corresponding to these absorption features have had the "signal" drowned out by "noise" introduced by the atmosphere. This is multiplicative in nature, the additive noise is introduced at the sensor. Note also that the main diagonal trace is specifically $\Sigma \sigma^2_{ii}$ and represents the variance associated with each band.

The blocky, segmented nature of the second order statistics matrices reveals important details about the scene. The low covariances in the absorption bands are easily explained because the brightness values in those bands are so statistically different than all other bands. More subtly, these matrices show the degree of difference or similarity between the brightness values in other parts of the observed spectra.

In order to illustrate this concept, a Davis-Monthan Air Force Base HYDICE radiance data set is introduced. Figure 2.9 shows the covariance and correlation

23

matrices for this data set. The scene is a good contrast to the Jasper Ridge image because the predominant background material is sand instead of vegetation.
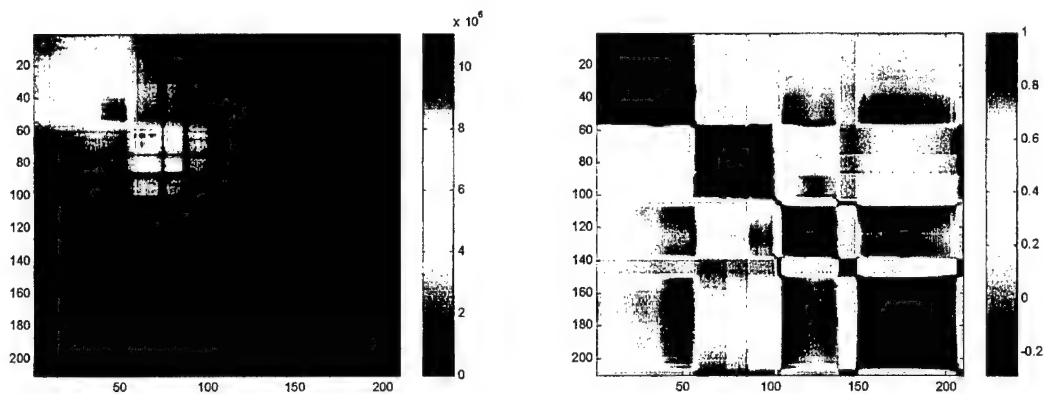
Figure 2.9: Second Order Statistics of a HYDICE Davis Monthan Scene.

Recalling the plots of various pixel vectors seen in Figure 2.5, note how the spectrum of the vegetation sharply spiked up at wavelength 700nm whereas the spectrum of the road remains relatively unchanged. This corresponds to the chlorophyll absorption band edge that occurs at a wavelength of about 700nm. In Figure 2.8 note how a "block" of high covariances rapidly transitions to a "block" of low covariances at band 55. This feature is an indicator of the fact that there are significant differences in the spectral shapes of the observed pixel vectors which start at this wavelength. This can be interpreted to mean that the scene consists of both vegetation and non-vegetation pixel vectors. If the pixel vectors did not posses significantly different shapes, then this feature would not have manifested itself. The Davis Monthan scene is comprised predominantly of a sandy background, and as a result, the area between bands one and 100 appears to have high covariances and correlation coefficients without the sharp

transition at band 55. The blocky appearance in the first 100 bands, evident when vegetation was present, is now not present.

While these observations are cursory, they demonstrate how the statistics of the scene reveal a great deal of useful information. A more refined study of scene statistics, such as that pursued by Brower, et. al., (1996), finds that the scene statistics can be used to differentiate urban and rural areas. This idea can be carried further to the problem of differentiating small man-made objects in a natural background but is beyond the scope of this study. Considered independently, the scene statistics are interesting in that they provide further perspective and understanding into the nature of the scene. More importantly, they bring us closer to the invariant display problem by setting the stage for an understanding of the techniques which use statistics to describe the background.

3.   Related Signal Processing and Linear Algebra Concepts

a.   *Linear Transformations of Random Variables*

The fundamental basis of the hyperspectral image analysis technique utilized by this study is that of linear transformations. Our statistical definitions of the data using the covariance matrix and its standardized form, the correlation matrix, are central to an invariant display strategy. Understanding the effect of a linear transformation on these matrices is also important and will be addressed.

A linear transformation of a vector $\mathbf{x}$ into a vector $\mathbf{y}$ is accomplished by the matrix $\mathbf{A}$ in the relation $\mathbf{y} = \mathbf{Ax}$. Figure 2.10 illustrates this concept using two-dimensional vectors.

25
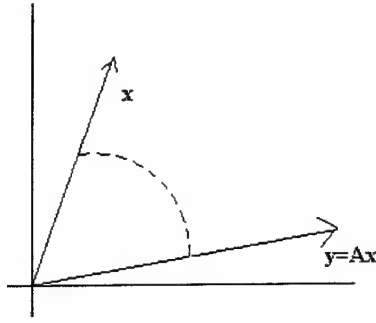
Figure 2.10: Linear Transformation of a Two-dimensional Vector.

The transformation matrix $\mathbf{A}$ rotates and scales the vector $\mathbf{x}$ into the new vector $\mathbf{y}$. Since second order moment matrices of random vectors are symmetric, we may assume that $\mathbf{A}$ is symmetric. The expectation operator is linear, which implies that the mean of the random vector x is transformed as:

$$E\{\mathbf{y}\} = E\{\mathbf{Ax}\} = \mathbf{A}E\{\mathbf{x}\} \tag{2.7}$$

which can be restated as $\mathbf{m_y} = \mathbf{Am_x}$, where the subscript on the mean vector denotes which random vector the mean vector represents. Similarly, using the definition of the second order moment, the covariance matrix is transformed by the matrix $\mathbf{A}$ so that (Therrien, 1992, p. 45)

$$\Sigma_y = \mathbf{A}\Sigma_x\mathbf{A}^T \tag{2.8}$$

A particularly useful transformation is one which transforms a random vector $\mathbf{x}$ into another random vector $\mathbf{y}$ whose k^{th} and l^{th} components have the property of statistical orthogonality such that (Therrien, 1992, p. 50):

$$E\{y_k y_l\} = 0 \quad k \neq l. \tag{2.9}$$

The statistically orthogonal or uncorrelated random variables which result from such a transformation cause the transformed data covariance matrix to be diagonal. The means

26

of achieving such a transformation that diagonalizes the covariance matrix is provided by the concept of eigenvectors and eigenvalues.

b. *Eigenvectors and Eigenvalues*

The eigenvalues of a L x L matrix $\mathbf{A}$ are the scalar roots of its characteristic equation, and are denoted as $\{\lambda_1,\dots \lambda_L\}$. The nonzero vectors, $\{\mathbf{e}_1,\dots,\mathbf{e}_L\}$ which satisfy the equation

$$\mathbf{A}\mathbf{e}_k = \lambda_k\,\mathbf{e}_k \tag{2.10}$$

are called the eigenvectors of $\mathbf{A}$. An eigenvector defines a one-dimensional subspace that is invariant with respect to premultiplication by $\mathbf{A}$ (Golub and Van Loan, 1983, P. 190). In applying the above definitions of the eigenvalue and eigenvector to the L x L covariance matrix, we obtain

$$\Sigma_x\mathbf{e}_k = \lambda_k\,\mathbf{e}_k. \tag{2.11}$$

The covariance matrix in this relation may be viewed as a linear transformation which maps the eigenvector $\mathbf{e}_k$ into a scaled version of itself (Therrien, 1992, p. 50). Because of the symmetry of the real covariance matrix, the L eigenvalues are guaranteed to be non-negative and real (Searle, 1982). It is also possible to find L orthonormal eigenvectors $\{\mathbf{e}_1,\dots,\mathbf{e}_L\}$, that correspond to the L eigenvalues (Therrien, 1992, p. 50) that satisfy

$$\mathbf{e}_i^T\mathbf{e}_j = \delta_{ij}. \tag{2.12}$$

27

c.   *Unitary Transformations*

Suppose that the eigenvectors of the L x L covariance matrix Σ_x are packed into a matrix $\mathbf{E}$ as column vectors. Then, because of the orthonormality of the eigenvectors, the matrix $\mathbf{E}$ transforms the covariance matrix in the following manner:

$$\mathbf{E}^T\Sigma_x\mathbf{E} = \begin{bmatrix} \leftarrow & e_1^T & \rightarrow \\ & \vdots & \\ \leftarrow & e_l^T & \rightarrow \end{bmatrix} \Sigma_x \begin{bmatrix} \uparrow & & \uparrow \\ e_1 & \cdots & e_1 \\ \downarrow & & \downarrow \end{bmatrix} = \begin{bmatrix} \lambda_1 & & 0 \\ & \ddots & \\ 0 & & \lambda_l \end{bmatrix} = \Lambda, \tag{2.13}$$

following the rules of linear transformations (Therrien, 1992, p. 45). The transformation matrix $\mathbf{E}^T$ defines a linear transformation of a random vector $\mathbf{x}$ into a random vector $\mathbf{y}$, by the relation

$$\mathbf{y} = \mathbf{E}^T\mathbf{x} \tag{2.14}$$

in which the covariance matrix of $\mathbf{y}$ is a diagonal matrix represented by Λ. This diagonalization of the covariance matrix Σ_x is another manner of stating that the components of random vector $\mathbf{y}$ are now uncorrelated since all off-diagonal elements of Λ are zero. The orthonormal columns of $\mathbf{E}$ imply that the transformation matrix $\mathbf{E}^T$ represents a unitary transformation defined by (Therrien, 1992, p. 51)

$$\mathbf{E}^T\mathbf{E}=\mathbf{E}\mathbf{E}^T=\mathbf{I}. \tag{2.15}$$

d.   *A Geometric Interpretation of the Unitary Transform*

If we assume that our data has a Gaussian distribution, then we can describe its probability density function (pdf) with a family of ellipsoids as:

$$(\mathbf{x}-\mathbf{m}_x)^T \Sigma_x^{-1}(\mathbf{x}-\mathbf{m}_x) = \text{constant} \tag{2.16}$$

28

Because the matrix **E** is orthonormal, the implication is that the eigenvectors of Σ_x are the same as those of its inverse, and the eigenvalues of Σ_x^{-1} are simply the reciprocals of those of Σ_x (Jolliffe, 1986, p. 14). Thus, the inverse transformation may be written as

$$\mathbf{x} = \mathbf{E}^T\mathbf{y} \qquad (2.17)$$

and the equation defining the contours of constant density may be rewritten as:

$$(\mathbf{x}\text{-}\mathbf{m_x})^T \mathbf{E}\, \Lambda^{-1}\mathbf{E}^T\, (\mathbf{x}\text{-}\mathbf{m_x}) = (\mathbf{y}\text{-}\mathbf{m_y})^T \Lambda^{-1}(\mathbf{y}\text{-}\mathbf{m_y}) = \sum_{k=1}^{l}\frac{|\, y_k - m_k\, \|\, y_k - m_k\, |}{\lambda_k} = \text{constant} = C \quad (2.18)$$

which is the equation for an ellipse with the principal axes of the ellipse being aligned with the eigenvectors and the magnitudes proportional to $\lambda_k^{1/2}$ (Jolliffe, 1986, P. 19). This geometrically illustrates the role that eigenvalues and eigenvectors play in the unitary transform. Figure 2.11 shows that the unitary transformation is equivalent to a rotation of the coordinate axes. The tilt of the ellipse with respect to the original coordinate system is indicative of the fact that correlation exists between the original vector components (Therrien, 1992, p. 59). In the new coordinate system defined by the unitary transformation, the axes of the ellipse are parallel to the new axes, showing that the vector components are indeed uncorrelated in this coordinate system. Although the assumption was made that the data was Gaussian, this concept of two-dimensional ellipsoids is a useful one in understanding the workings of the transformation even for non-Gaussian data. In this context, the scatter plots of the Landsat data are useful in portraying a rough idea of the distribution of the probability density function of the random vectors.
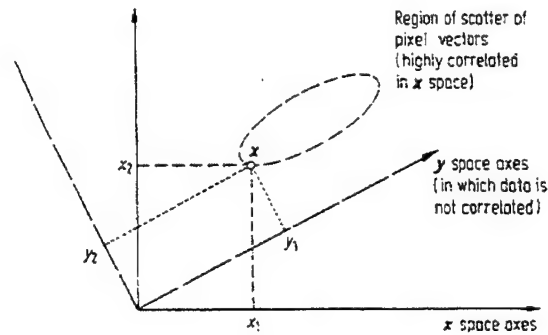
Figure 2.11: The Unitary Transformation as a Rotation of Axes. From Richards, 1993.

4. Principal Component Analysis

a. Description

Principal components analysis (PCA) as applied in multispectral and hyperspectral remote sensing is an analytical technique based on the linear transformation of the observed spectral axes to a new coordinate system in which spectral variability is maximized. The impetus for such a transformation is the high correlation that exists between adjacent bands in spectral imagery. The spectral overlap of the sensors and the wide frequency range of the energy reflected from the ground account for this high correlation (Rao and Bhargava, 1996, p. 385). This implies that a great deal of spectral redundancy exists in the data. The principal components transformation decorrelates the information in the original bands and allows the significant information content of the scene to be represented by a smaller number of linear combinations of the original bands called principal components. The transformation effected by the PCA is a unitary transformation and is graphically depicted in Figure 2.12 as operating on observed pixel vectors to produce new pixel vectors with uncorrelated components.

30

The immediate applications of the principal components transformation for this study are data compression and information extraction. In the problem of target detection and development of an invariant display strategy, the latter is of considerable interest. PCA techniques are based exclusively on the statistics of the observed variables, requiring no *a priori* deterministic information about the variables in the image. This will allow for a methodology whereby no preprocessing need be performed prior to displaying the data utilizing "global" *a priori* knowledge.
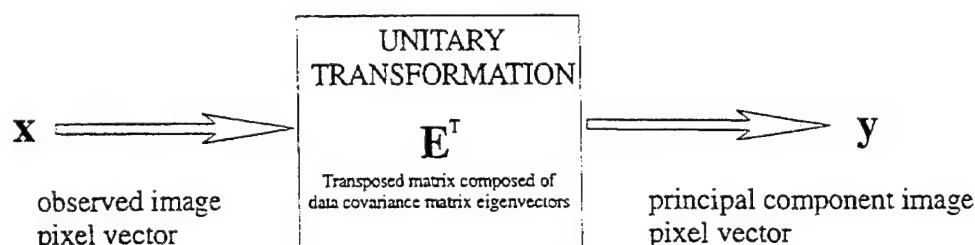
Figure 2.12: PC Transformation Depicted as a Linear Transformation.

b.   *Background*

Principal components analysis is an extremely versatile tool in the analysis of multidimensional data. In tracing the historical roots of this technique, it is clear that it is based upon ideas drawn from the fields of statistics and linear algebra. The mathematical underpinnings of PCA deal with the diagonalization of the covariance matrix via eigendecomposition of the data by unitary transform and serves as a bridge between matrix algebra and stochastic processes (Haykin, 1996). The wide applicability of PCA is due to the fact that it assumes a stochastic outlook of the data, which is fundamental to the analysis of data in many scientific disciplines. We will investigate the

31

views of two disciplines which employ PCA to better understand some of the mechanics of this seemingly simple transformation. The two views are those of multivariate data analysis and signal processing. A thorough understanding of the ideas that motivate the PCA will assist in understanding why it is such a commonly used technique in remotely sensed imagery analysis, and why this strategy is most appropriately applied to an invariant display strategy.

(1)   Multivariate Data Analysis View. PCA was described by Pearson in 1901 and introduced as the Hotelling transform in 1933 by Hotelling for application in educational psychology (Singh and Harrison, 1985, p. 884). Hotelling's goal was to find a fundamental set of independent variables of smaller dimensionality than the observations that could be used to determine the underlying nature of the observed variables (Hotelling, 1933, P. 417). In many scientific experiments, the large number of variables makes the problem of determining the relative importance of specific variables intractable. Hotelling's method makes the problem manageable by discarding the linear combinations of variables with small variances, and studying only those linear combinations with large variances. Since the important information in the data is usually contained in the deviation of the variables from a mean value, it is logical to seek a transform which provides a convenient means of identifying the combinations of variables most responsible for the variances (Anderson, 1984, p. 451). The linear combination of the original variables which behave sufficiently similarly are combined into new variables called principal components. In this context, principal components analysis studies the covariance relationships within a data set by investigating the number of independent variables, and identifies the natural associations of the variables.

32

Mathematically represented, each principal component is a scalar formed by a linear combination of the elements of the observed random vector **x**, where each vector component corresponds to a random variable. The principal components are constructed in such a manner as to be uncorrelated with all other principal components and ordered so that variance is maximized (Jolliffe, 1986, p. 2). The kth principal component is obtained by multiplying the transposed k^{th} eigenvector of Σ_x by the data vector **x**, as depicted in the equation

$$y_k = e_k^T x. \tag{2.19}$$

The kth principal component is also called a score, and the components of the eigenvector are called loadings because they determine the contribution of each original variable to the principal component. Generalizing the scalar result of Equation 2.18 to a vector result:

$$\mathbf{y} = \mathbf{E^T x} \tag{2.20}$$

we obtain a vector of L principal components when we take the product of all of the transposed eigenvectors of Σ_x and the data vector, **x**.

While the property of the unitary transform to produce new uncorrelated variables has been previously discussed, the property of the unitary transform to maximize the variance, which is central to the PCA, will be discussed further. The best illustration of this property is the algebraic derivation of the PCA. The goal is to maximize the variance of the first principal component, denoted as $VAR[y_1]$ or $VAR[e_1^T x]$. By the definition of variance as a second order moment, this is equivalent to maximizing $e_1^T \Sigma_x e_1$, where the eigenvectors are orthonormal, so that $e_1^T e_1 = 1$. The

33

method of LaGrange multipliers is employed so that the expression to be maximized is differentiated with respect to the eigenvector and set equal to zero as

$$\frac{\partial}{\partial e_1} [e_1^T \Sigma_x e_1 - \lambda(e_1^T e_1 - 1)] = 0 \Rightarrow (\Sigma_x - \lambda I) e_1 = 0. \qquad (2.21)$$

In Equation 2.21, λ is a Langrangian multiplier in the left hand expression and corresponds to the largest eigenvalue of Σ_x in the right hand expression, and e_1 is the eigenvector corresponding to the largest eigenvalue (Jolliffe, 1986, p. 4). Thus, the eigenvalues of Σ_x represent the variances of the principal components, and are ordered from largest to smallest magnitude. If the original variables have significant linear intercorrelations, as spectral imagery does, then the first few principal components account for a large part of the total variance. (Singh and Harrison, 1985, p. 883). Figure 2.13 depicts the eigenvalues and associated variance percentage for a typical Davis-Monthan scene.
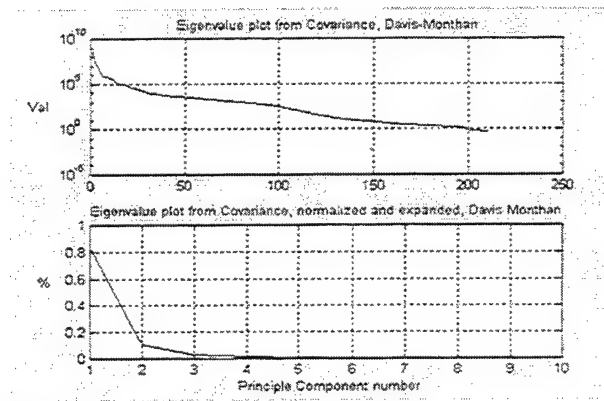
Figure 2.13: Eigenvalue Plot of Davis-Monthan. Note the large fraction of the overall variance within first few PCs.

(2) Signal Processing View. In the analysis of random signals, the key is to have a set of basis functions that make the components of the signal

34

statistically orthogonal or uncorrelated (Therrien, 1992, p. 173). The Karhunen-Loeve Transform (KLT) was introduced in 1947 for the analysis of continuous random processes, and is developed here in its discrete form, the DKLT. It is the same unitary transform previously presented, but is posed to solve the problem from a different perspective. The motivation for the DKLT is actually an expansion, best seen by Figure 2.14, which shows a discrete observed signal as a weighted sum of basis functions, which are in fact the eigenvectors of the covariance matrix. The observed pixel vector spectrum may be thought of as a discrete signal, indicated by the square brackets in the notation of Figure 2.14. Whereas in the PCA approach the original variables are weighted by eigenvector components to form principal components, in the DKLT the eigenvector basis functions, $\{e_1,...,e_N\}$, are weighted by the principal component scores, $\{y_1,...,y_N\}$, to form a representation of the observation. The DKLT has an optimal representation property in that it is the most efficient representation of the observed random process if the expansion is truncated to use fewer than N orthonormal basis functions. This makes it very attractive from a compression perspective, and explains the popularity of DKLT as a compression scheme.

Another important property associated with the DKLT is the equivalence between the total variance in the vector x and the sum of the associated eigenvalues. This property is mathematically stated by the equation

$$\sum_{i=1}^{L} \sigma^2_i = \sum_{i=1}^{L} \lambda_i \tag{2.22}$$

35
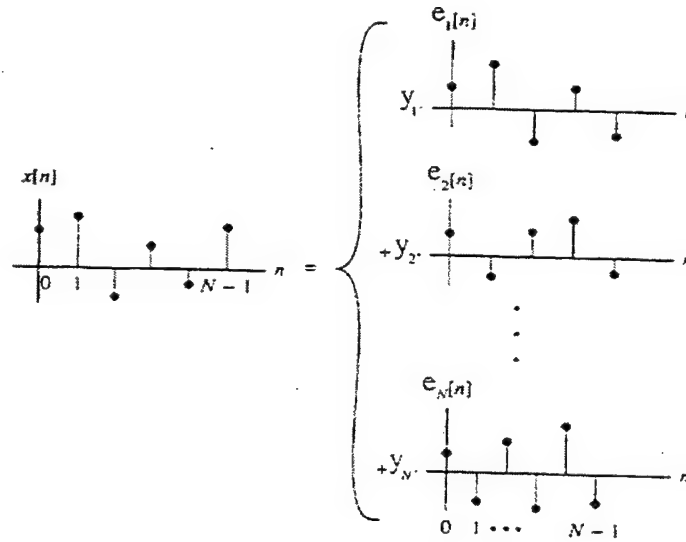
Figure 2.14: The Karhunen- Loeve Expansion in Terms of Discrete Signals. After Therrien, 1992, p. 175.

In Equation 2.22, σ^2_i is the variance of the original variables and λ_i is the eigenvalue representing the variances of the transformed variables and the index i ranges over all L bands. This property only holds for the orthonormal vectors which are eigenvectors of Σ_x and not for other orthonormal basis sets of vectors (Kapur, 1989, p. 501).

When a representation of a signal is formed by using fewer than L basis functions, the mean square error (MSE) is a means of quantifying how well the representation corresponds to the original signal by measuring the power of the difference between the representation and original signals. The MSE incurred by truncating the representation is equal to the sum of the eigenvalues of the covariance matrix that were left out of the representation. (Therrien, 1992, p. 179) Conversely, the largest eigenvalues and their corresponding eigenvectors can be used to represent the intrinsic dimensionality of the signal. This corresponds to the number of dimensions that would be needed to represent the signal to some predetermined MSE.

36

In signal processing applications, the DKLT is a means of compressing data by representing it with a truncated number of eigenvectors. It is also an optimum way of detecting a signal in noise and works particularly well for the detection of narrowband signals. Since a significant portion of the signal energy lies in the direction of the first few eigenvectors, those eigenvectors can be said to define a subspace for the signal and all other eigenvectors define the subspace for the noise. This simple example is the basis for several high resolution methods of spectral estimation used to detect sinusoids in noise (Scharf, 1991, p. 483).

c.   *Operation*

PCA uses the eigenvectors of Σ_x to assemble a unitary transformation matrix which, when applied to each pixel vector, transforms the original pixel vector into a new vector with uncorrelated components ordered by variance. The eigenvector components act as weights in the linear combination of the original band brightness values that form the principal components (Richards, 1993). The new image associated with each eigenvector is referred to as the principal component image. The principal component images are ordered from largest to smallest in terms of variance, and are revealing in their composition. As Singh and Harrison (1985) point out, it must be kept in mind that the PCA is an exploratory technique that constructs new variables called the principal components (PCs). These new variables are artificial and do not necessarily have a physical meaning, as they represent linear combinations of the observed variables and cannot themselves be observed directly, but they should be related because the first

37

eigenvector in spectral imaging is a representation of the mean solar energy of the scene and the next few eigenvectors deviate as the variance changes.

In traditional application of PCA, the hope is that the transformation will enhance the contrast of the image by grouping like areas together to such an extent that objects or areas of interest can be more readily discriminated in the principal component images. Jenson and Waltz (1979) give an analogy which clearly explains the role of PCA in the traditional application. They imagine a tube filled with ping pong balls. Looking at the tube directly from an end, only one ball is apparent, the same way that the original spectral image is. Turning the tube sideways, all of the balls become visible (Jenson and Waltz, 1979, p. 341). PCA has the effect of decorrelating the data so that independent sources of spectral features can be discerned.

Though PCA assumes no *a priori* knowledge of the scene, PCA as described here depends intrinsically on the scene because scene-specific features will dictate the shape of the eigenvalues. Nevertheless, certain general observations can be made regarding the PCA and an associated physical meaning without any knowledge of the scene. The following two figures highlight these observations. Figure 2.15 shows the first 20 PC images of the Jasper Ridge AVIRIS scene. For a non-negative symmetric matrix, the first eigenvector is all positive. A weighted sum loosely corresponds to the average spectral radiance. All other eigenvectors must have at least one sign change to be orthogonal to the first eigenvector. This is due to the fact that in forming the first principal component image, the first eigenvector has heavily weighted the original bands possessing the most variance. Thus, the first principal component image will have a variance that is larger than that of any single original band image.

38

1   $\lambda/\Sigma\lambda = .616$ 2 $\lambda/\Sigma\lambda = .348$ 3 $\lambda/\Sigma\lambda = .027$ 4 $\lambda/\Sigma\lambda = .003$

5   $\lambda/\Sigma\lambda = .002$ 6 $\lambda/\Sigma\lambda = .002$ 7 $\lambda/\Sigma\lambda = .001$ 8 $\lambda/\Sigma\lambda = 3\times10^{-4}$

9   $\lambda/\Sigma\lambda = 2\times10^{-4}$ 10 $\lambda/\Sigma\lambda = 1.5\times10^{-4}$ 11 $\lambda/\Sigma\lambda = 1\times10^{-4}$ 12 $\lambda/\Sigma\lambda = 1\times10^{-4}$

13 $\lambda/\Sigma\lambda = 8.8\times10^{-5}$ 14 $\lambda/\Sigma\lambda = 6.5\times10^{-5}$ 15 $\lambda/\Sigma\lambda = 5.3\times10^{-5}$ 16 $\lambda/\Sigma\lambda = 5.2\times10^{-5}$

17 $\lambda/\Sigma\lambda = 4.7\times10^{-5}$ 18 $\lambda/\Sigma\lambda = 4.4\times10^{-5}$ 19 $\lambda/\Sigma\lambda = 3\times10^{-5}$ 20 $\lambda/\Sigma\lambda = 2.6\times10^{-5}$
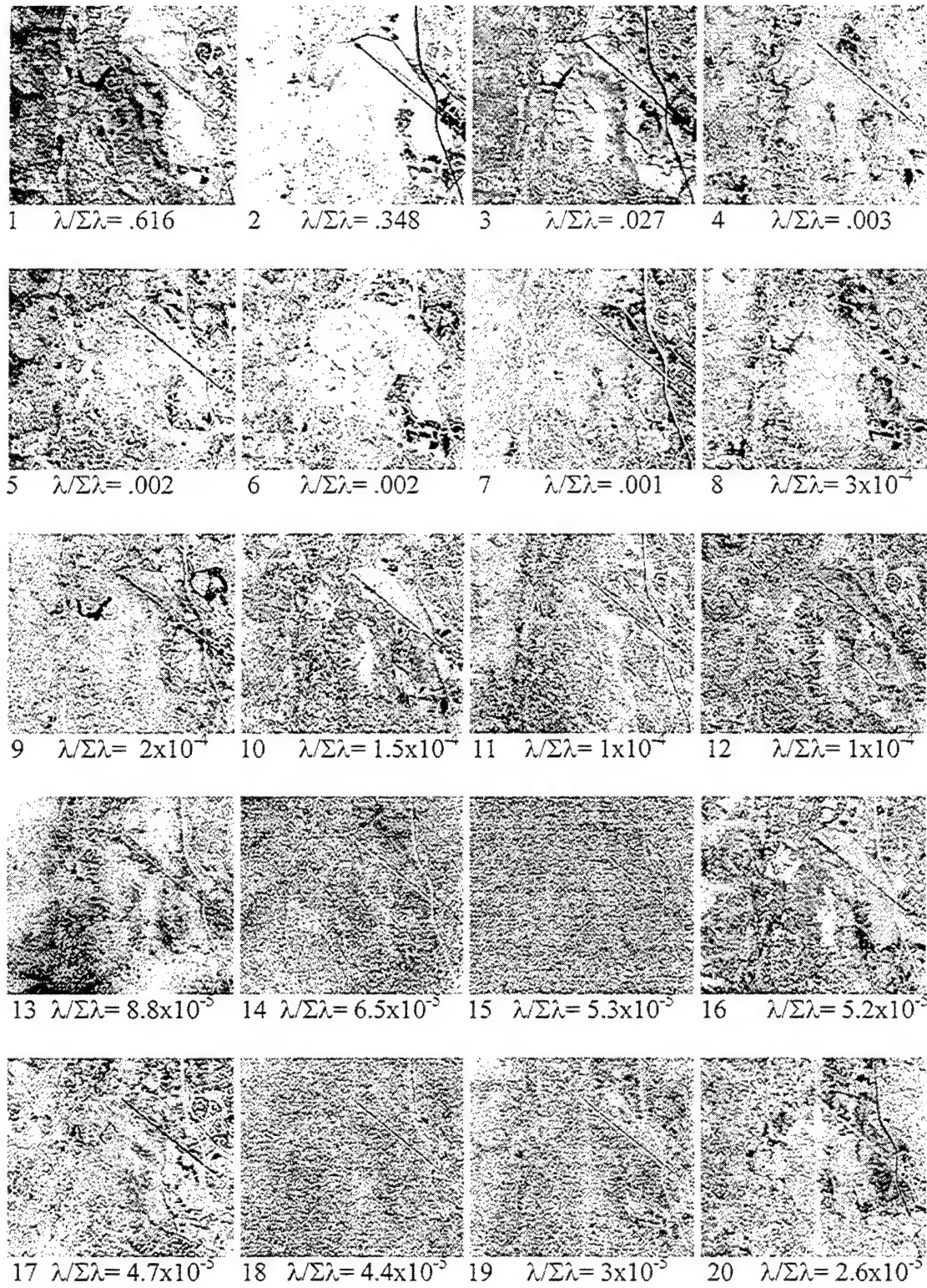
Figure 2.15: First 20 PC Images of Jasper Ridge Scene

It is the weighted sum of the overall response level in all original band images. The second principal component image is the difference between certain original band images. As the principal component image number increases, the PC image holds less of the data variance. This effect manifests itself as a rough decrease in image quality with increasing PC image number. In Figure 2.15, the fact that the first twelve PC images contain relatively clear details of the scene indicates that these PC images together account for the majority of the overall spectral variance in the scene. It is interesting to note that when using PCA, the higher numbered PC images sometimes contain a large amount of local detail. Though it is tempting to dismiss the higher numbered PC images as not containing any useful information because they have low variance, one must keep in mind that the covariance matrix on which PCA is based is a global measure of the variability of the original image (Richards, 1986, p. 138). This implies that small areas of local detail will not appear until higher PC images since they do not make a statistically significant impact on the covariance matrix. Another point that is noteworthy is the issue of SNR. PCA orders PC images based on total variability. It does not differentiate between the variability representing desirable information and the variability representing undesirable noise (Jenson and Waltz, 1979, p. 338). Ready and Wintz (1973) argue that PCA improves the SNR of the spectral image. Their definition of noise is additive white Gaussian noise with a variance of σ_n^2. The SNR of the original image is

$$(SNR)_x = \frac{\sigma_{x\,max}^2}{\sigma_n^2} \tag{2.23}$$

which is the maximum original band variance over the noise variance. The SNR of the PC images is

$$(SNR)_y = \frac{\lambda_1}{\sigma_n^2} \qquad (2.24)$$

which is the largest eigenvalue (or new variance) over the noise variance. Since the first

eigenvalue always has a greater variance than any of the original bands, the improvement

in SNR is

$$\Delta SNR = \frac{(SNR)_y}{(SNR)_x} = \frac{\lambda_1}{\sigma_{x\,max}^2} \qquad (2.25)$$

and will be greater than one. The SNR improvement applies as long as the variance of

the eigenvalue exceeds that of the original bands. The diminishing SNR manifests itself

in Figure 2.15 as an increased fuzziness of the image that begins to appear around the

ninth PC image. Figure 2.16 further accentuates the above observations using the Cuprite

radiance and reflectance images. The first ten PC images are shown for each data set.

The same general trends noted for Figure 2.15 appear. The first few PC images offer the

greatest amount of contrast. The effects of noise become apparent sooner in decreased

image quality with the reflectance data than the radiance data.

A traditional means of presenting PCA images is to form a false color

composite image consisting of the first, second, and third PC images as the red, green

,and blue colors. Figure 2.17 presents such false color images for the Jasper Ridge and

Cuprite radiance PC images. This mode of presentation captures the major sources of

spectral variability in one image. The levels of detail and contrast apparent in the

composite image are interesting to compare with the original image shown in Figure 2.3.

41

RADIANCE REFLECTANCE
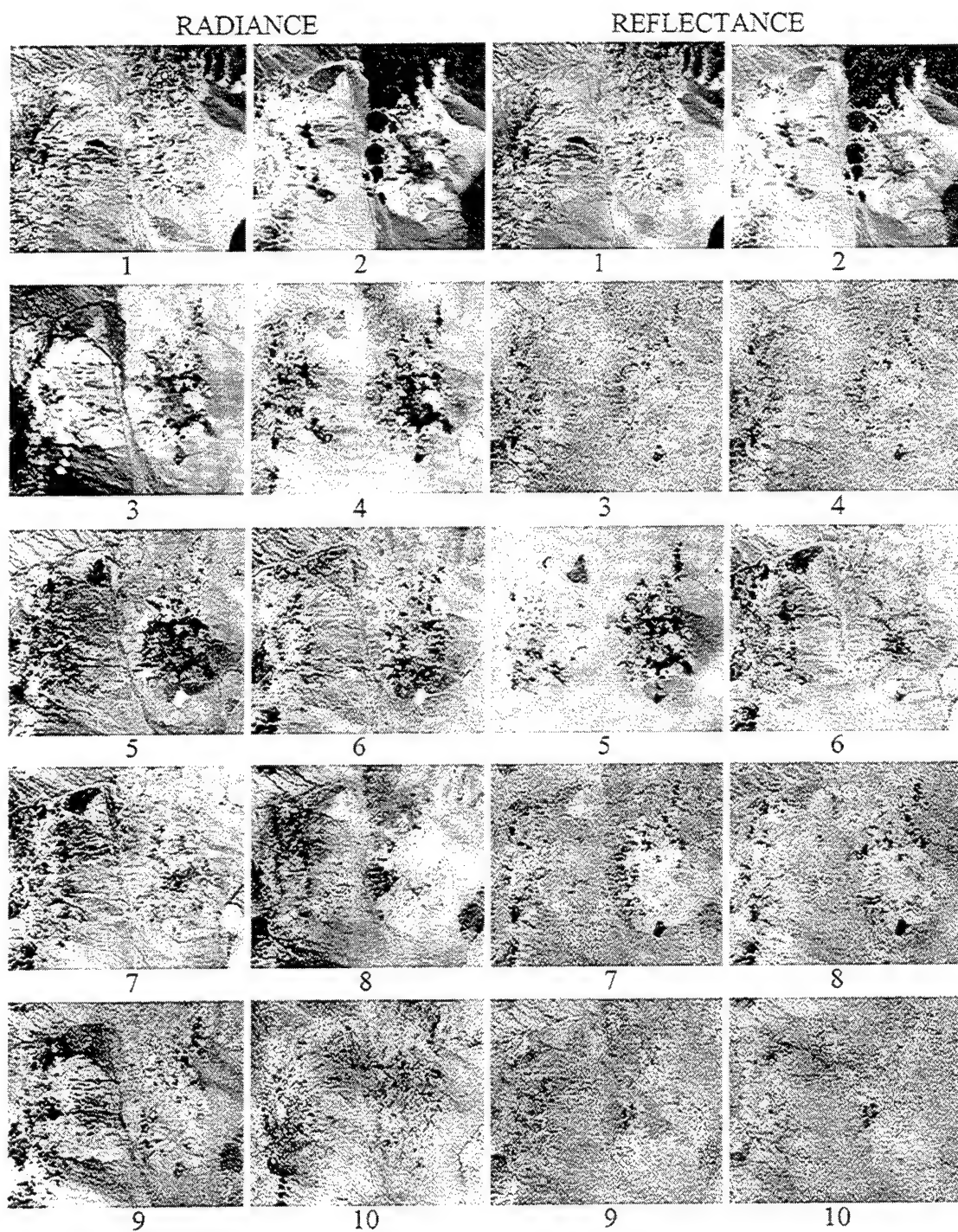
Figure 2.16: First 10 PC Images of Cuprite Radiance and Reflectance Scenes.

(Decreasing image quality as variance decreases for both radiance and reflectance. Noise effects more apparent earlier in reflectance.)

Jasper Ridge   Cuprite
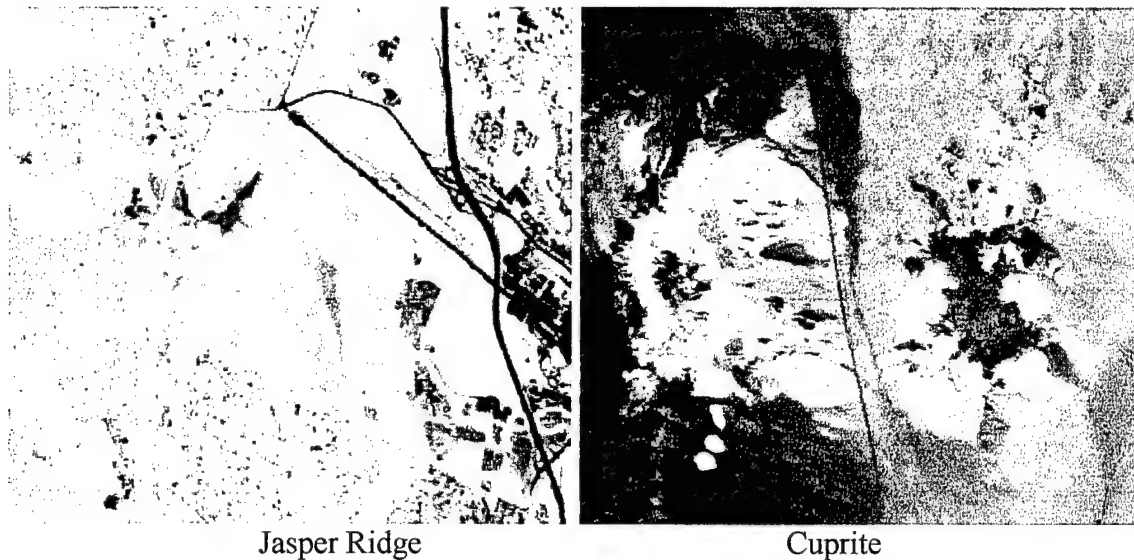
Figure 2.17: False Color Images of Jasper Ridge and Cuprite Radiance PC Scenes.

A facet of PCA rarely mentioned in the pertinent literature on PCA is the characterization of the original and PC images using the behavior of the eigenvalues and eigenvectors. The behavior of the eigenvalues and eigenvectors will be investigated more fully later in the study because these attributes form an important part of analyzing the scene information content. In spectral images, the typical trend in the eigenvalue magnitude is that a very small number of eigenvalues have a disproportionately large magnitude compared to the others. The obvious reason for this distinct grouping of eigenvalues is that the data in the original image exhibits a high degree of interband correlation and the magnitude of the eigenvalues reflects the degree of redundancy in the data. (Richards, 1986, p. 137). Phrased another way, the intrinsic dimensionality, which is represented by the number of large eigenvalues of the data, is much smaller than the original number of dimensions. This is good from a compression view, since the image variance will be accounted for by a very small number of principal components. From a

43

strict analysis viewpoint, it does not reveal as much information. If the problem were that of a narrowband signal embedded in noise, then the large eigenvalues would be associated with the signal. In the hyperspectral imagery analysis problem, the spectrum associated with a target is not narrowband, and hence is not clearly delineated from the eigenvalues of the background and other interfering signatures. The eigenvalues can be divided into a primary and a secondary set, where the secondary set roughly corresponds to the effects of instrumentation noise (Smith, Johnson, and Adams, 1985, p. C798). The primary set corresponds to the linear combinations of original bands that cause the most variance in the scene. Figure 2.18 illustrates the first ten eigenvalues of the Jasper Ridge and Cuprite radiance images together. The y-axis of this plot is normalized and represents the variance of each PC image. The Jasper Ridge PC images exhibit slightly higher variances (eigenvalues) than the Cuprite scene. The quality of the first eight PC images noted in Figure 2.15 corresponds to the steeper initial slope of the detailed eigenvalue plot.

Jasper Ridge and Cuprite PC Normalized Eigenvalues (Radiance)

	1	2	3	4	5	6	7	8	9	10
Cuprite	0.922	0.048	0.023	0.001	0.001	0.001	0.000	0.000	0.000	0.000
Jasper Ridge	0.615	0.348	0.027	0.003	0.002	0.002	0.001	0.000	0.000	0.000

PC Number
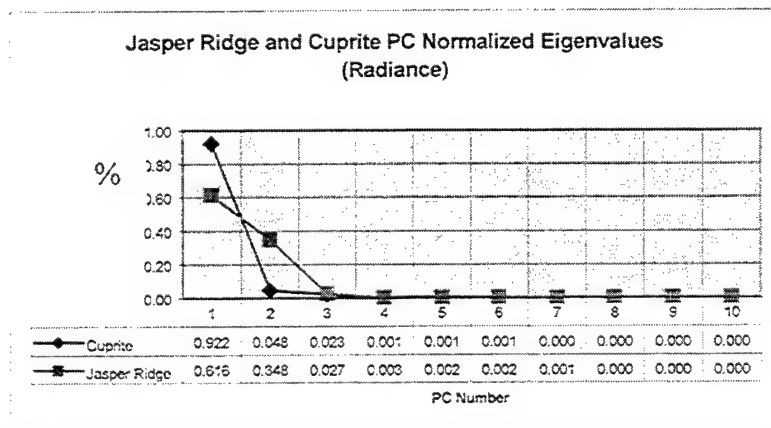
Figure 2.18: Eigenvalue Behavior of the Jasper Ridge and Cuprite Radiance Scene Covariance Matrices

Likewise, the first five images of the Cuprite radiance PC images in Figure 2.16 are reflected in the steeper slope of the first five eigenvalues of Figure 2.178.

Figure 2.19 shows the eigenvalues of the Cuprite reflectance image compared to the radiance. The sharp drop in the slope of the eigenvalues is paralleled by the drop in image quality noted in Figure 2.15 after the second PC image. In general, the AVIRIS reflectance eigenvalues are lower in magnitude than those of the radiance.

Cuprite Radiance and Reflectance PC Normalized Eigenvalues

	1	2	3	4	5	6	7	8	9	10
Radiance	0.922	0.048	0.023	0.001	0.001	0.001	0.000	0.000	0.000	0.000
Reflectance	0.901	0.063	0.022	0.005	0.002	0.001	0.001	0.001	0.001	0.000

PC Number
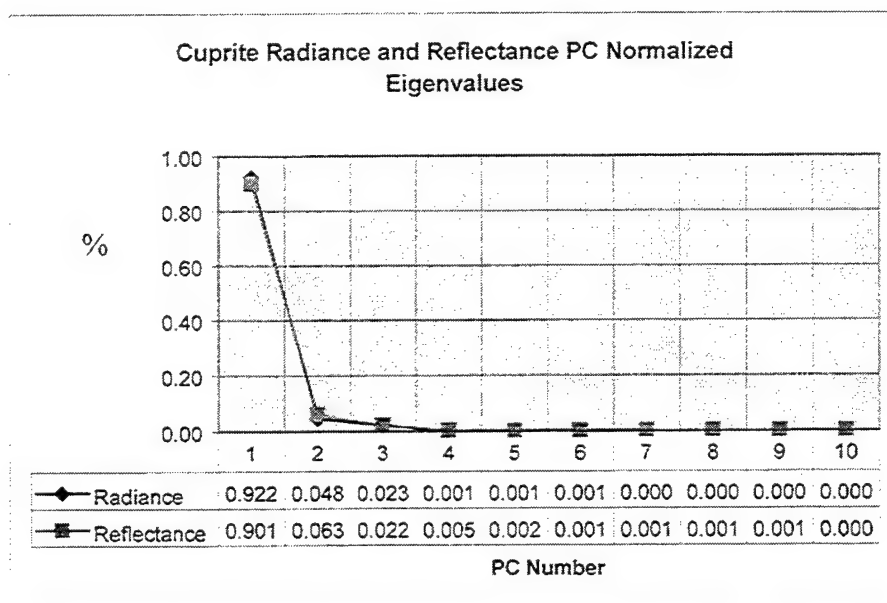
Figure 2.19: Eigenvalue Behavior of the Cuprite Radiance and Reflectance Scene Covariance Matrix.

The above results clearly indicate that the variance for the transformed data are concentrated in the first few PC bands, indicating that the dimensionality is on the order of 10 vice 200-225. It is important to note that the variance of the original data is equal to that of the transformed data. This property shows that the PC transformation merely redistributes the concentration of variance in the bands of a spectral image so that the higher variances occur in the first PC bands. (Stefanou, 1997)

The eigenvector behavior is less clear than that of the eigenvalues. The eigenvectors form the bases of the principal components subspaces. Physically, the eigenvectors correspond to the principal independent sources of spectral variation. As such, the wavelengths at which the maxima and minima of the eigenvectors occur account for the wavelengths that contribute the most to a particular independent axis of variation (Smith, Johnson, and Adams, 1985, p. C808). A signal processing interpretation of the eigenvectors is that the eigenvectors act as band pass filters that transform an input observed spectrum into a new spectrum that has fewer data points (Johnson, Smith, and Adams, 1985). This interpretation is analogous to the optimum representation property of the DKLT. It can be further shown that the eigenvectors of reflectance data will tend to have a more distributed appearance. The effect of the sun on the low numbered original bands can be mitigated in the conversion to reflectance, although this is not always desired, especially for real-time processing. Further examination of eigenvector behavior emphasizes the correlation between the eigenvectors and variance occurring in the original image bands and it can be shown that the eigenvectors of the PC transform tend to emphasize those original bands that contain the most variance with larger weights and inclusion in the low numbered eigenvectors. (Stefanou, 1997)

The PCA technique has been examined from the perspective of its results and the significance of its inner workings. Key points in PCA analysis are:

- In general, PCA provides an analysis of the data which guarantees an output set of images ordered by variance.

- Assuming white noise, it improves the SNR in the transformation from the original image cube to the PC images.

46

- The PC images accentuate spectral regions of high variance. However, an area of local detail may not be accentuated by a PC image due to its statistical insignificance.

- Because the variability of the covariance data is scale-dependent, PCA is sensitive to the scaling of the data to which it applied, and as a result, the PCA of radiance data will place more emphasis on the visible bands due to the sun than the PCA of reflectance data.

- PCA does not differentiate between noise and signal variances because it operates strictly on the variance of the observed data.

As a practical note in the implementation of PCA, the computation of the eigenvectors and eigenvalues of Σ_x is an expensive operation. Specific methods from computational linear algebra such as inverse iteration, QR factorization, and singular value decomposition (SVD) are all applicable in their calculation. (Watkins, 1991)

The previous discussion highlights three crucial issues in development of an invariant display strategy utilizing principal components. Issue number one is the fact that the first PC band is typically a representation of the scene average brightness and is generally dominated by solar radiance, but it can be affected by major scene constituents such as in Jasper Ridge. The second issue is that the PC transformation outputs a set of images ordered by variance with the 2nd, 3rd, ..N^{th} PCs dependant on the specific contents of the image and the third issue is that PCA is sensitive to scaling of the data to which it applied. Because of the scaling sensitivity, the PCA of radiance data will place more emphasis on the visible bands due to the sun than the PCA of reflectance data.

THIS PAGE INTENTIONALLY LEFT BLANK

III. PHYSICAL VISION

A. DESCRIPTION

The typical person can detect light with a wavelength in the range of about 400 nanometers (violet) to about 700 nanometers (red). Our visual system perceives this range of light wave frequencies as a smoothly varying rainbow of colors. This is called the visible spectrum. Figure 3.1 illustrates the visible spectrum approximately as a typical human eye experiences it.
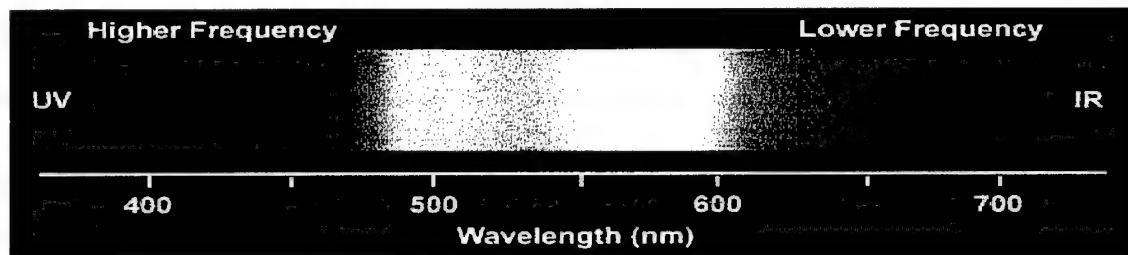
Figure 3.1: Human Visual Spectrum. (Scott, 1997)

The human eye has a lens and iris diaphragm which serve similar functions to the corresponding features of a camera. Other than this, the eye is quite different from a camera. Whereas a camera has a flat image plane where the resolution and spectral response is reasonable constant across the entire plane, the eye does not. The human eye also provides a motion sensor system with nearly 180 degrees horizontal coverage. The eye's peripheral vision system only supports low resolution imaging but offers an excellent ability to detect movement through a wide range of illumination levels. Peripheral vision also provides very little color information.

49

The retina is a thin layer of nerve cells which consists of light sensor cells called rods and cones. The majority of the eye's inside chamber has this retina layer, accounting for the very wide angle of our peripheral vision. Figure 3.2 is an illustration of the cross section of the human eye.
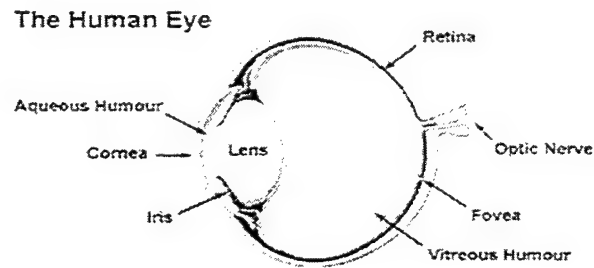
Figure 3.2: Cross Section of the Human Eye.

The rods in the retina are long and slender while the cones are generally shorter and thicker. Other than the physical differences, there is an important functional difference in that the rods are more sensitive to light than the cones. Figure 3.3 depicts the relative sensitivity of rods and cones as a function of illumination wavelength.
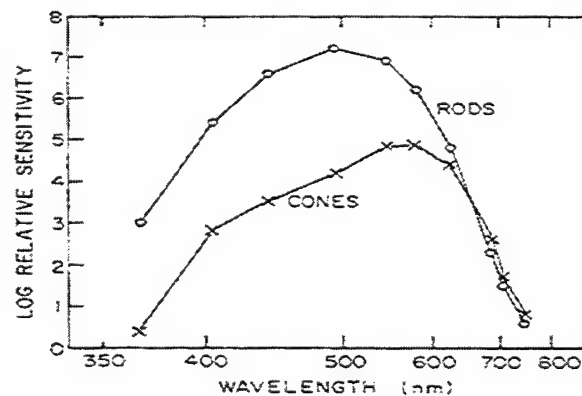
Figure 3.3: Sensitivity of Rods and Cones. (Pratt, 1991, p. 25)

50

It has been experimentally determined that there are three basic types of cones in the retina. (Wald, 1964) These cones have different absorption characteristics as a function of wavelength with peak absorptions in the red (580 nm), green (540 nm) and blue (450 nm) visible spectrum. Our perception of color is determined by the combination of cones are excited and by how much. Figure 3.4 illustrates the spectral sensitivity of the typical human visual system. The RGB sensors are denoted with the Greek letters Rho (red), Gamma (green) and Beta (blue). Human vision has a great deal of sensitivity to low ambient illumination situations. In low ambient illumination, the cones contribute little or no sensitivity and imaging is primarily accomplished by the rods.
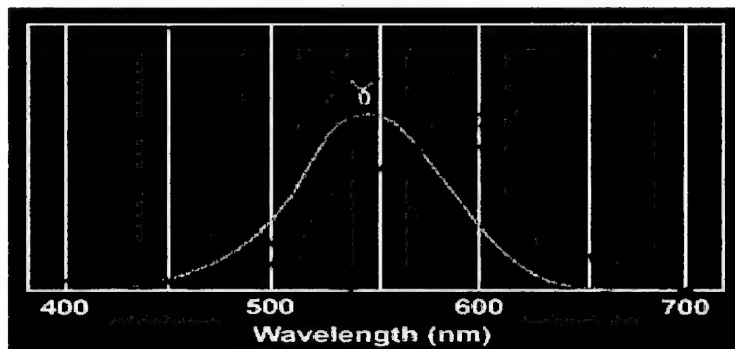
Figure 3.4: Spectral Absorption Curves. (Scott, 1997)

The sensitivity curves of the Rho, Gamma and Beta sensors in our eyes determine the intensity of the colors we perceive for each of wavelengths in the visual spectrum. Figure 3.5 is an approximation of the visual spectrum illustration adjusted for the sensitivity curves of our Rho, Gamma and Beta sensors.

51
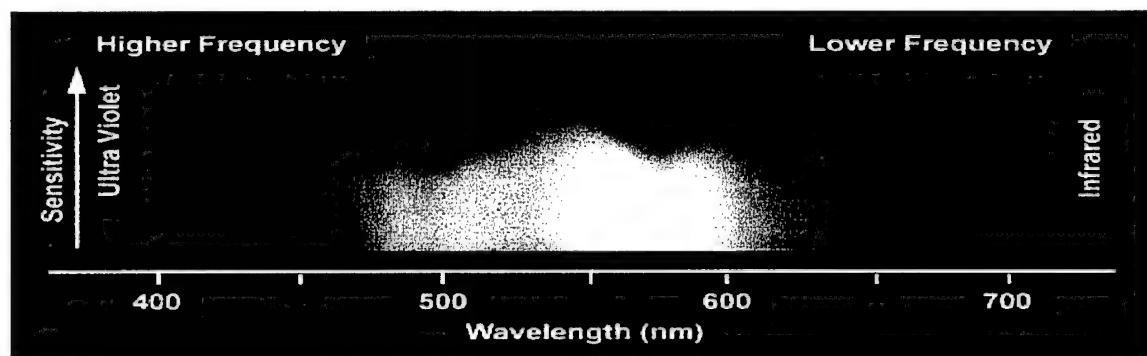
Figure 3.5: Spectral Absorption Curves. (Scott, 1997)

There are three perceptual definitions of light: brightness, hue, and saturation. If we observe two light sources with the same general spectral shape, the source with the greater intensity will generally appear to be perceptually brighter. Hue is the attribute that distinguishes a red color from a green color or a yellow color. Saturation is the attribute that distinguishes a spectral light from a pastel light within the same hue.

B. COMPARISON TO PRINCIPAL COMPONENTS

Processing of color within the human eye is accomplished through an achromatic channel and two opponent-color channels. The opponent-color channels are the red-green opponent and the blue-yellow opponent channel. (Wyszecki and Stiles, 1967; Buchsbaum and Gottschalk, 1983) The A, R-G, and B-Y channels are formed from a principal components analysis, are statistically uncorrelated, and therefore make up orthogonal dimensions in a 3-D color space. Furthermore, it has been shown that there are two fundamental axes within color space comprised of a R-G plane where all colors have an absence of yellowness or blueness and a B-Y plane where all colors have an absence of redness or greenness. The intersection of these two planes is a line with

52

absence of all color, or the gray line, which corresponds to the achromatic channel. (Krauskopf, et al., 1982)

We can use the concept of three orthogonal axes to develop the hue, saturation, and value (H-S-V) color representation system. From the previous section, hue indicates a particular color, e. g. the perceived colors of red, green, blue, etc., saturation indicates the purity of a particular hue, e. g. S=1 denotes a pure hue while S=0 denotes absence of color (gray), and value is related to the brightness or intensity of a particular color. The perceptual color space therefore makes up a cone, with the A axis as the axis of rotation of the cone and the R-G and B-Y axes transverse. Hue is determined by computing an angle in the (red-green) - (blue-yellow) plane, and saturation is determined by the angle between a particular point in color space and the gray axis. Figure 3.6 graphically depicts this conical representation and its associated radial visualization.
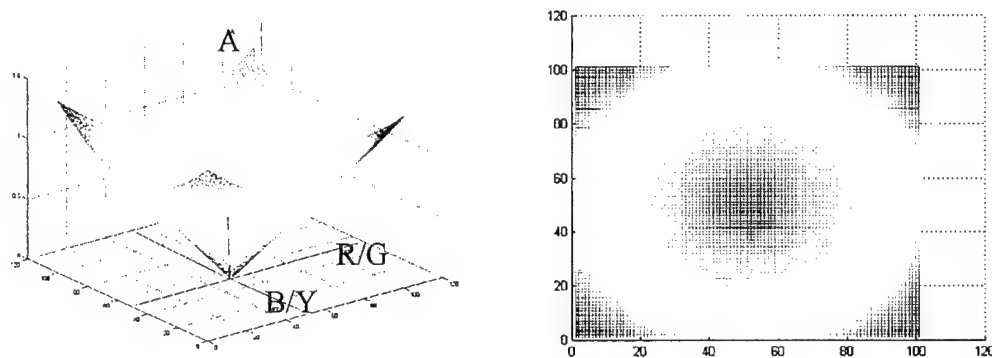

Figure 3.6: Perceptual Color Space.

When mapping color space we encounter three distinct problems. The first is that color space is nonlinear. The non-linearity is related to the spectral response functions of the individual photoreceptors. The second problem is that we typically map red next to

53

violet when they actually appear at opposite ends of the spectrum. This can be seen in Figure 3.1. Thirdly, as intensity is increased, the hue is perceived to shift, and this is the issue of color constancy. (Brainard, et al., 1993, p. 165-170) The fourth problem is associated with the color planes. It has been demonstrated that while red-green and blue-yellow planes exist, other similar color-opponent planes do not seem to exist, hence the term "cardinal directions" used by Krauskopf, et al. This cardinal direction scheme will be utilized for the invariant mapping strategy in later sections.

C.   PSEUDOCOLOR AND OPPONENT COLOR MAPPING STRATEGIES

In the past, pseudocolor displays have utilized a mapping strategy whereby the principal components were directly depicted by mapping the PCs as follows:

$P_1 \rightarrow$ Red $P_1 \rightarrow$ Brightness
$P_2 \rightarrow$ Green   OR $P_2 \rightarrow$ Hue
$P_3 \rightarrow$ Blue $P_3 \rightarrow$ Saturation

Figure 3.7 is a mapping of the first three PCs into (R,G,B) of a scene from Davis-Monthan AFB. Although this method does depict some of the high spatial frequency information, much of it is suppressed and there is an apparent smearing, which is a result of how the observer views the data. These methods are not a good fit to human vision.

It has been shown that for humans, the achromatic spectral channel accounts for approximately 97% of color vision, while the R-G and B-Y channels account for approximately 2% and 1% respectively. (Buchsbaum and Gottschalk, 1983) From the previous discussion of the principal components transformation, it can be readily seen that the first principal component of a spatial image is roughly achromatic in that it

54

samples the mean illumination distribution and can therefore be viewed as the intensity or brightness of a hyperspectral image. Continuing along this reasoning, we note that the second and third PCs contain significantly less scene variance and subsequently higher PCs contain even lower amounts. From this we may be able to conclude that we can map the second and third principal components into the (R/G) – (B/Y) plane.
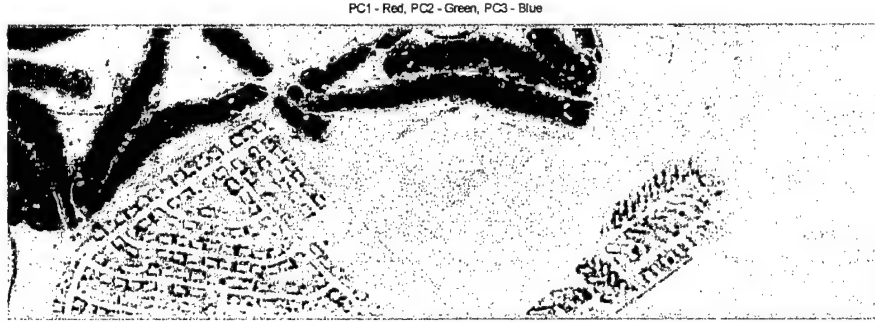
Figure 3.7: Pseudocolor Representation of Davis-Monthan Scene Obtained by Mapping the First Three PCs into (R,G,B).

Mapping the first PC into the achromatic channel, the value of the second PC into the R-G channel and the value of the third PC into the B-Y channel yields

$$\theta = \text{atan}\left(\frac{P_3}{P_2}\right) \rightarrow H \text{ (Hue)}$$

$$\frac{\sqrt{P_2^2 + P_3^2}}{P_1} \rightarrow S \text{ (Saturation)} \tag{3.1}$$

$$P_1 \rightarrow V \text{ (Value)}$$

where P_i is the ith PC. (Tyo, et. al., 2000)

The mapping of the same Davis-Monthan scene with Equation 3.1 yields Figure 3.8 and is a more visually pleasing representation because pixels that don't have a significant projection onto either P_2 or P_3 appear desaturated or gray. This makes the

55

image easier to view because naturally occurring scenes tend to be largely desaturated with low dimensionalities in the visible portion of the spectrum. (Buchsbaum and Gottschalk, 1983)

HSV FROM COVARIANCE, COLOR RESHAPED

Figure 3.8: Pseudocolor Representation of Davis-Monthan Obtained with Equation 3.1.

The mapping strategy in Figure 3.8 was designed with the performance of the human visual system in mind and does not present images that contain large regions of highly saturated hues that vary rapidly. To obtain Figure 3.8 we first needed to adjust the hue representation within MATLAB. MATLABs built-in HSV2RGB function maps the colors starting with red, then runs through yellow, green, blue, and then back to red again in a non-orthogonal manner. The non-orthogonal mapping yields incorrect hue opponency, i.e. red not opposite green. Figure 3.9a depicts MATLABs default non-orthogonal colorwheel and Figure 3.9b is the colorwheel reshaped to correspond to the correct color orthogonality.

Default wheel   Reshaped wheel
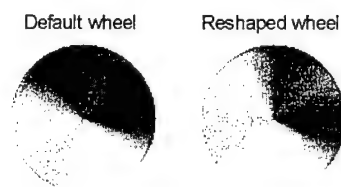
Figure 3.9: Hue Wheels Using MATLAB Default and Reshaped Hue Values.

56

Although the remapping of MATLAB's colorwheel yields the correct orthogonality between the colors, it does not produce an image that maps the materials within the scene to our perception of that material, i.e. vegetation to green, water to blue, etc. Utilizing the HYDICE bands of the original data corresponding approximately to the peak sensitivities of the ρ, γ and β receptors, spectral bands 150, 38 and 10 respectively, we can display a scene that depicts approximately how we would perceive that scene if viewed directly. Figure 3.10 is a Red-Green-Blue image corresponding bands 150, 38 and 10 that accurately portrays the golf course as green and the background sandy soil as tan to slightly red.

True color, R-150, G-38, B-10 (Clipping)

Figure 3.10: RGB Image with Original Data Bands 150, 38 and 10.

Utilizing the RGB mapping strategy of Figure 3.10 and knowledge of linear transformations and eigenvectors from chapter two, we can identify a 3x3 set of RGB eigenvectors for the individual scene. These statistics can then be applied to the RGB transformation of Equation 3.1 to produce an image that preserves the hue of the primary source of variance within the image. (Figure 3.11) This mapping strategy retains the image display advantage achieved with Equation 3.1 and also allows for a

straightforward method of mapping this scene into perceptual colorspace that preserves the expected hues for major scene constituents.
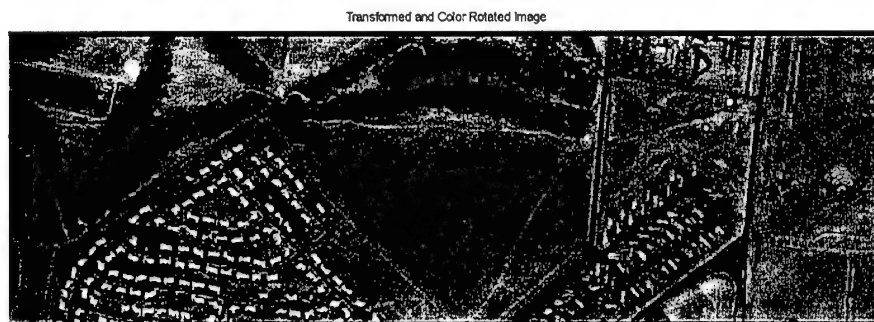
Figure 3.11: HSV Image Transformed with Scene RGB Data.

Keeping human visual perception and the characteristics of PCs in mind, it is clear that if a general set of PCs can be identified, a color mapping strategy can be arranged so that materials are presented in a straightforward manner, i.e. water can always be mapped to blue, etc. As a wider range of wavelengths is considered, it should be expected that more than 3 PCs may be necessary to capture an equivalent amount of the data (99% or more). The next sections will investigate this and develop a coherent method for an invariant display methodology.

IV. DATA ANALYSIS

A.   CASE STUDIES

For this study, the Davis-Monthan HYDICE Collects of June and October 1995 were utilized for analysis. Figure 4.1 is an aerial photograph of the Davis-Monthan collect area. The case studies are subsets of Figure 4.1.

Figure 4.1: Aerial Photograph of Davis-Monthan Collect Area.

B.   CASE STUDY ANALYSIS

Analysis on the data sets were performed utilizing three statistical methods. The first method involved computing the unbiased estimate of the covariance matrix from Equation 2.4. The second method utilized the correlation matrix obtained from the covariance coefficients as identified in Equation 2.5 and the third method used the direct correlation as found from

$$\sum_x = \sum_{j=1}^{N} (\mathbf{x_j})(\mathbf{x_j})^T. \qquad\qquad 4.1$$

As noted earlier, computation of the covariance and direct correlation matrices is computationally expensive. Taking advantage of the symmetric nature of the statistics reduces the number of computations required, but real-time computing of these values is still time consuming and not practical. Table 4.1 highlights this and depicts the number of flops required for the two prevalent data sets from the Davis-Monthan collect.

Data in Mega	Samples, Lines, Bands	
Flops	320x960x210	320x1280x210
Band Mean Computation	64.57	86.0836
Covariance and Direct Correlation	47417.5	63223.984
Correlation Matrix from Coefficients	0.1764	0.1764
Image to PC Transfom Average	27096	36128

Table 4.1: Statistics Computation.

The direct correlation statistics of the data sets were found from Equation 4.1 and were also investigated to identify the effect of removing the mean from each band.

60

Figure 4.2 is a density slice representation of the three statistical matrices for two Davis-Monthan scenes and the average of all sixteen scenes. Notice the similar structure and intensity values for the same matrix type. The first set has a covariance magnitude on the order of 10^6, direct correlation magnitude of 10^{13} and the next set is on the order of 10^6 and 10^{12} respectively.
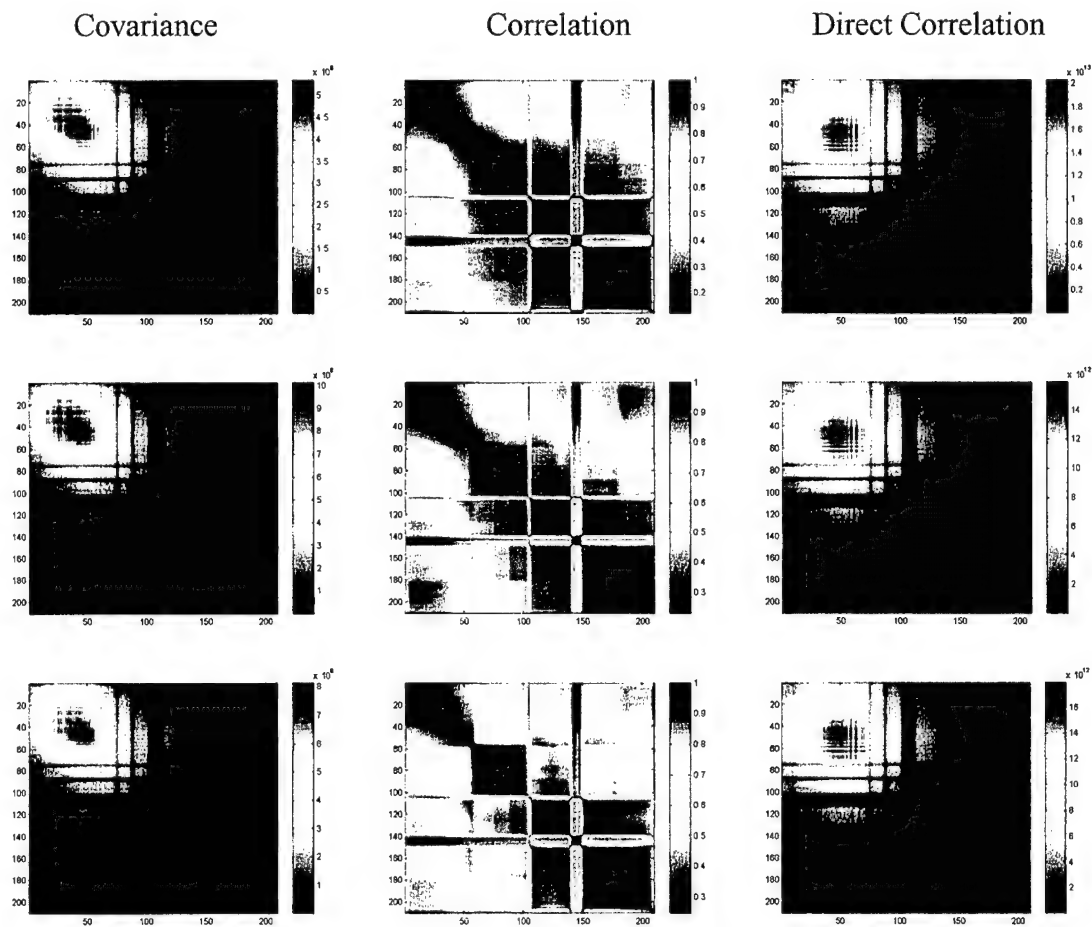

Figure 4.2: Density Slice Representation of Statistics Matrices. First row - Scene One. Second Row - Scene Two. Third Row - Average.

These results are very pleasing in that they graphically depict a structural similarity within the statistics and corresponds very well to results obtained by Brower,

61

et. al., 1996. This structural similarity will be capitalized on to develop an invariant display strategy.

Of the sixteen data sets, all have the same basic characteristics as the two scenes shown in Figure 4.2, and as depicted by the average, the structure remains nearly constant across all sixteen scenes. Further investigation into the physical properties of the data sets revealed that the mean value of all the collects were also structurally similar. Figure 4.3 is an example of a mean obtained from the Davis-Monthan collects. The mean value corresponds to the average radiance for that particular band. This implies that if there is a similar structure within the collection means, then there should be a similar structure for the first eigenvector of all the collections since the first eigenvector is a representation of radiance (Figure 4.4). Furthermore, we would expect that since the covariance and direct correlation matrices are derived directly from the pixel vectors, the eigenvectors and individual pixel vectors will display similar characteristic behaviors, i.e., the pixel vector spectrum will follow the behavior of the eigenvector nulls. (Figure 4.5)

Notice also that the correlation matrices have the same scaling. It is clear from the correlation matrices that there is a certain degree of symmetry between the bands. But, it must be remembered that the correlation matrix as shown here is the statistical correlation between the bands and therefore the eigenvector behavior will not follow that of the scene content, but that of the interband correlation. This is clearly seen in Figure 4.5 where the pixel spectra behavior does not correspond to that of the first eigenvector of the correlation matrix.
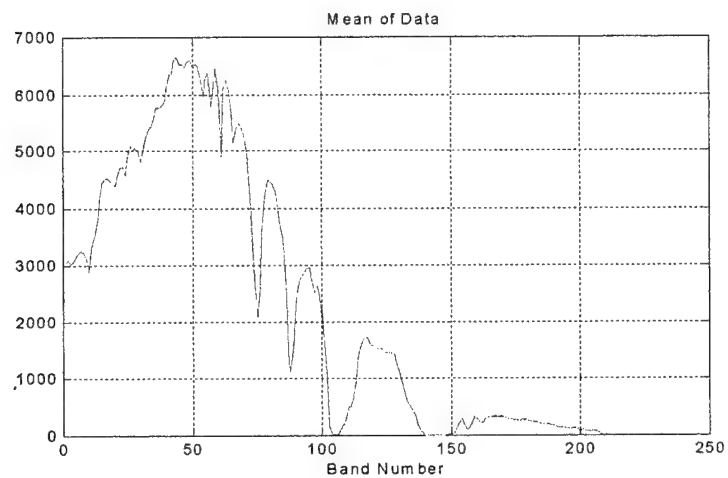
Figure 4.3: Typical Mean Band Plot.
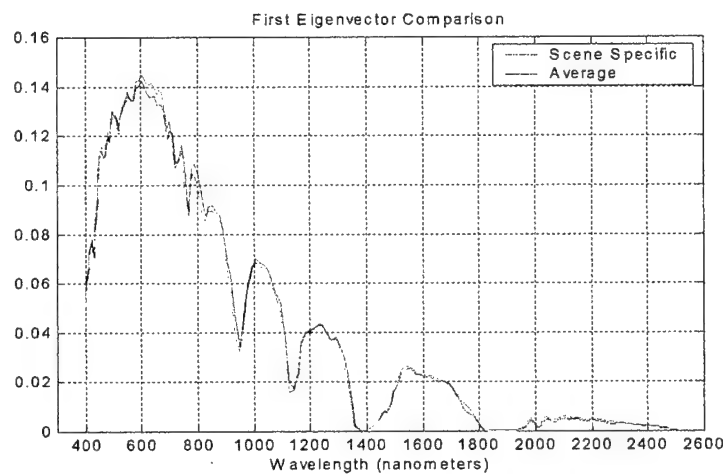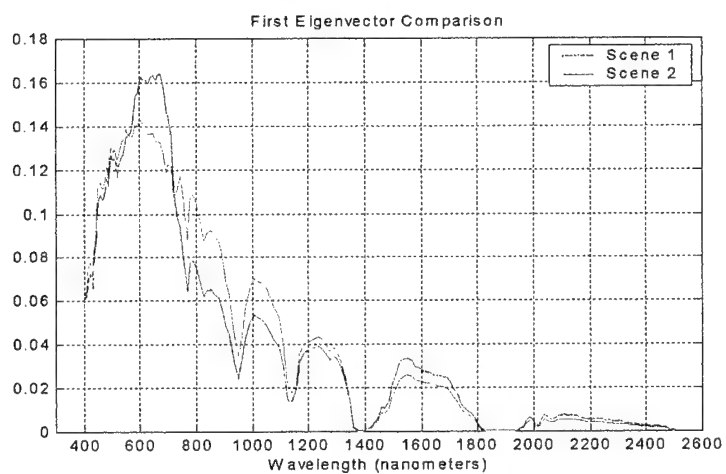
Figure 4.4: First Eigenvector Comparison Between Two Scenes and Comparison of the Average to a Scene.

63
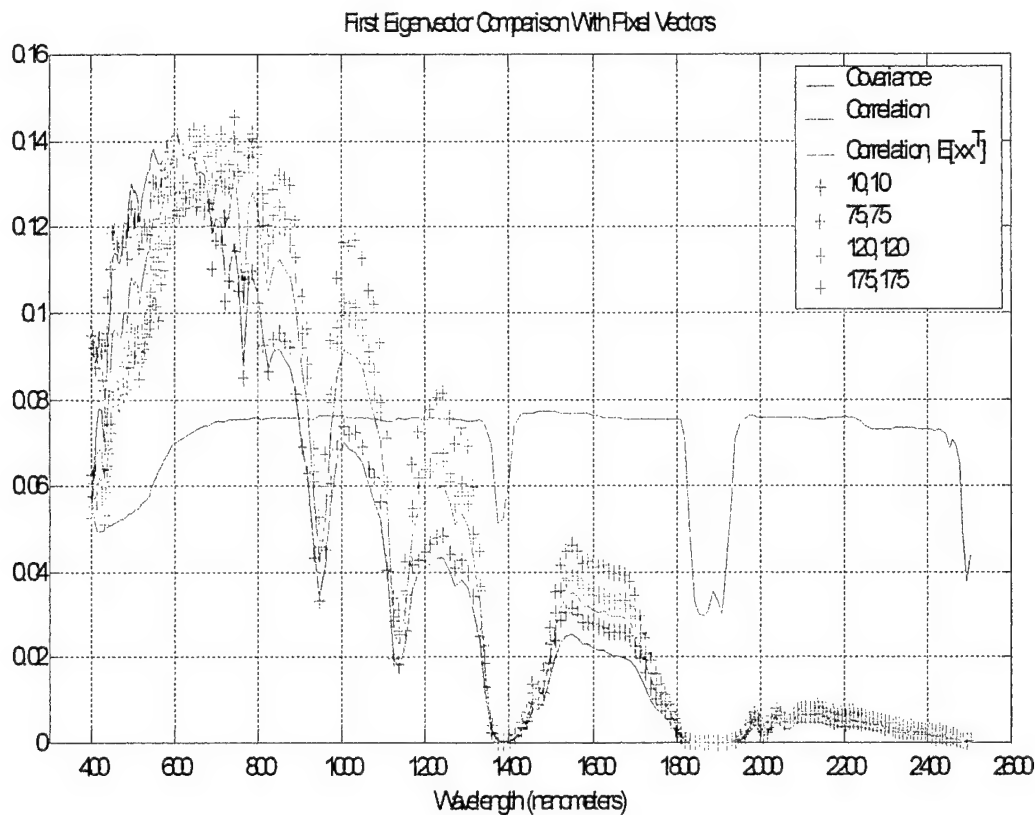
Figure 4.5: Pixel Spectra Comparison to the First Eigenvector.

Taking this further, we also expect that as the eigenvector number increases that the eigenvector behavior will be become more directly correlated to the specifics of the particular scene we are studying, implying that as the eigenvector number increases, the individual scene eigenvectors will become more and more dissimilar (Figure 4.6). But, if we were to utilize an 'average' eigenvector, we would assume that although the lower eigenvectors may no longer be as 'close' as before, that overall, the behavior would be similar across all scenes that the average was taken from. When this comparison is made, we see that the lower numbered eigenvectors remain similar and the higher numbered eigenvectors become more dissimilar as expected. (Figures 4.7-8)

64
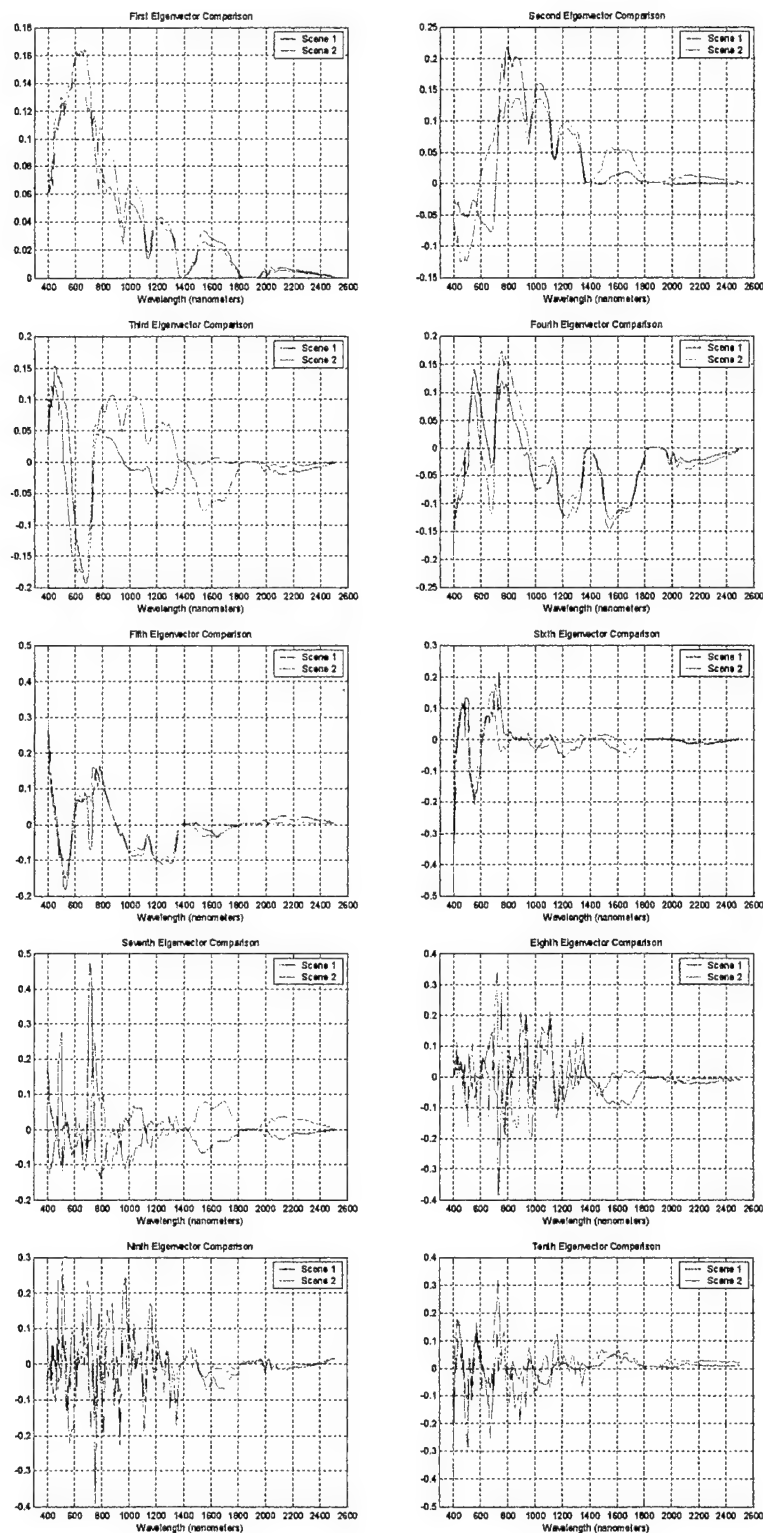
Figure 4.6: Eigenvector Comparison for Two Scenes.

65
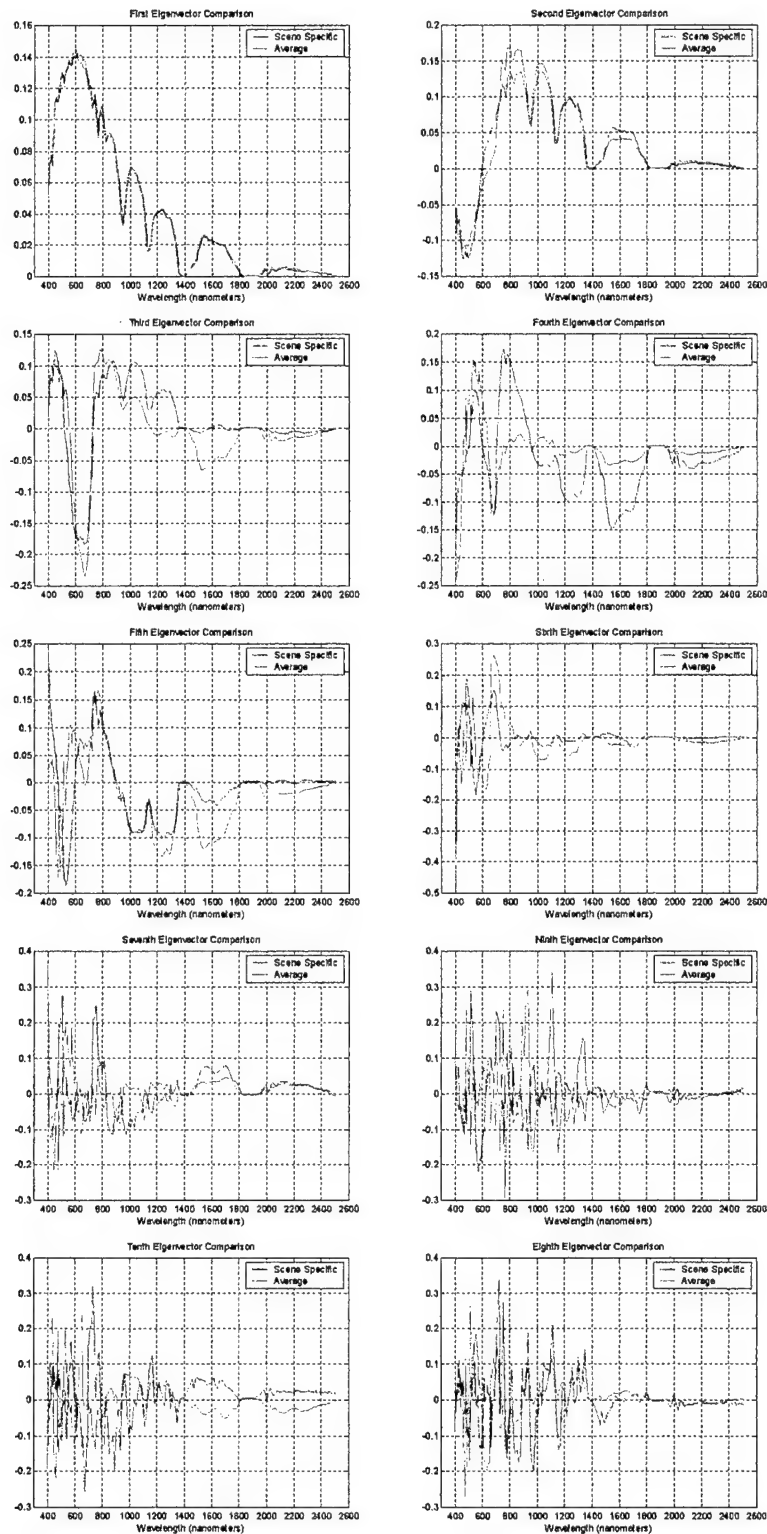
Figure 4.7: Eigenvector Comparison Between the Average and One Scene.

66
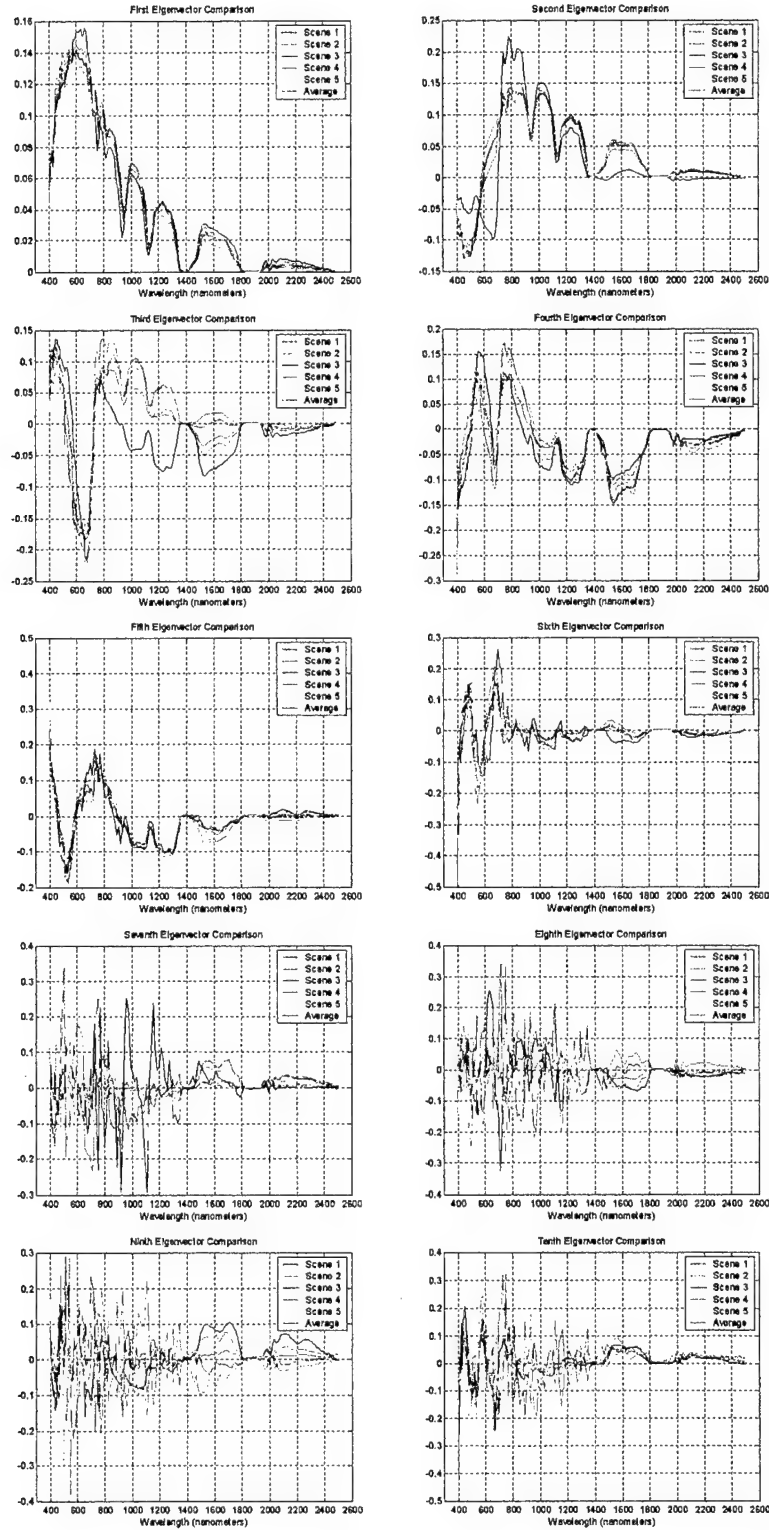
Figure 4.8: Eigenvector Comparison Between the Average and Multiple Scenes.

From the randomly chosen scene comparisons above, it is clear that for the particular data collections from Davis-Monthan, the average eigenvector up to number six is an excellent approximation for all the scenes. It must also be noted that the first three eigenvalues associated with the Davis-Monthan average account for 97.5 percent of the total variance (Figure 4.9) and eigenvalues four and larger only comprise 2.5 percent of the overall variance.
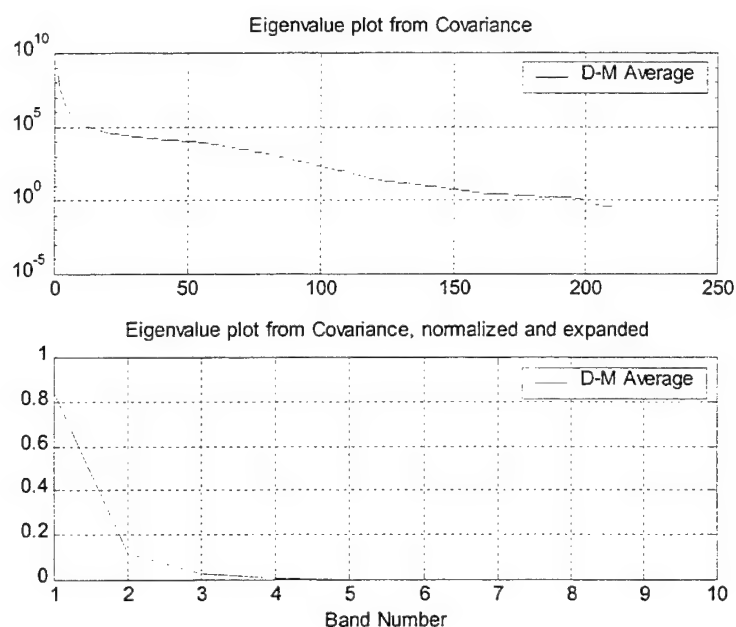
Figure 4.9: Eigenvector Comparison Between the Average and Multiple Scenes.

From analysis of the 16 data sets we can also conclude that the behavior of the RGB eigenvector subset discussed in chapter three should also be similar. Comparison of the average Davis-Monthan RGB eigenvectors with three random scene eigenvectors show that they are indeed similar. (Figure 4.10)
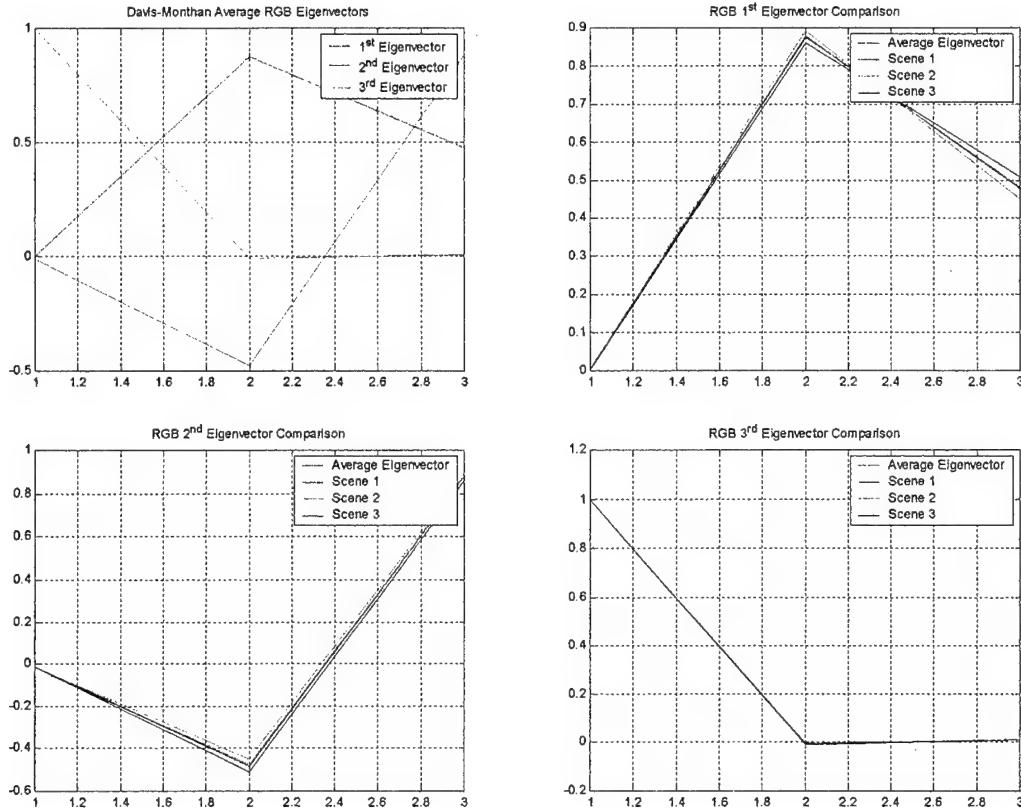
Figure 4.10: RGB Eigenvector Comparison Between the Average and Multiple Scenes.

The next question to be investigated is whether or not these same sets of eigenvectors can be applied to dissimilar scenes and still approximate the overall behavior of the dissimilar scene.

C.   DISSIMILAR SCENE COMPARISONS

For a comparative analysis of the eigenvectors obtained from the Davis-Monthan scenes, a data set from Jasper Ridge and a set from Lake Tahoe will be utilized. Jasper Ridge was chosen because the data was obtained from a different sensor (AVIRIS) of the

same class and the scene is dominated by vegetation. Lake Tahoe was chosen because it is from a HYDICE collect which contains vegetation and a large section of water. Both of these scenes contrast with Davis-Monthan in that they contain much more vegetation and the background is not predominately sand.

The scene statistics of Jasper Ridge (Figure 4.11) and Lake Tahoe (Figure 4.12) also follow the same general structure as Davis-Monthan. The significant differences of note are that while the variance in the Davis-Monthan averages are highest between bands 15-60, the variance is maximum between bands 40 and 60 for Jasper Ridge and 55-70 for Lake Tahoe. Also of important note is the difference in the shape of the mean. (Figure 4.13) The difference in shape around 700nm can be attributed to the chlorophyll absorption spectrum that is characteristic of vegetation.
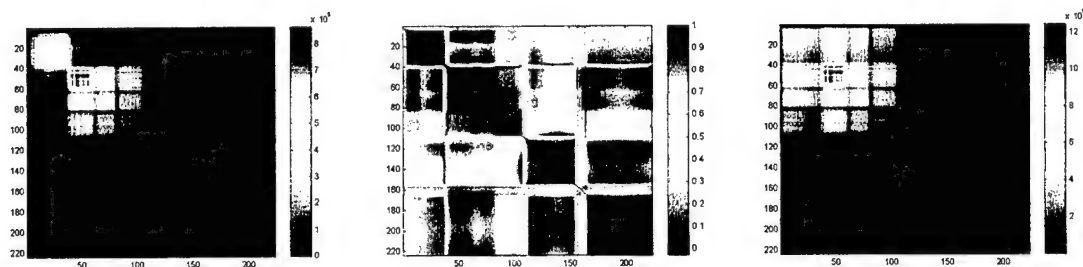
Figure 4.11: Scene Statistics for Jasper Ridge.
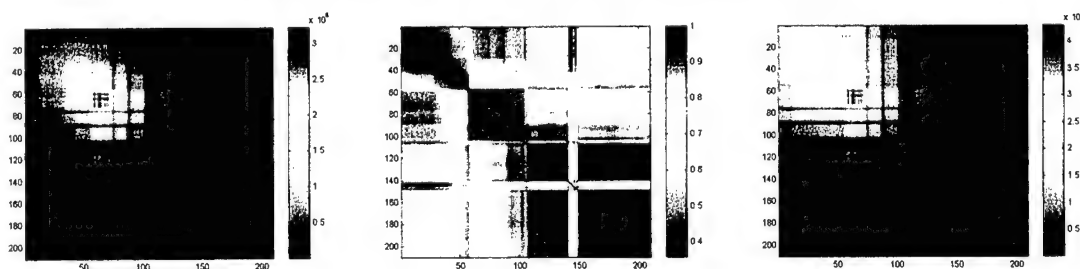
Figure 4.12: Scene Statistics for Lake Tahoe.

70
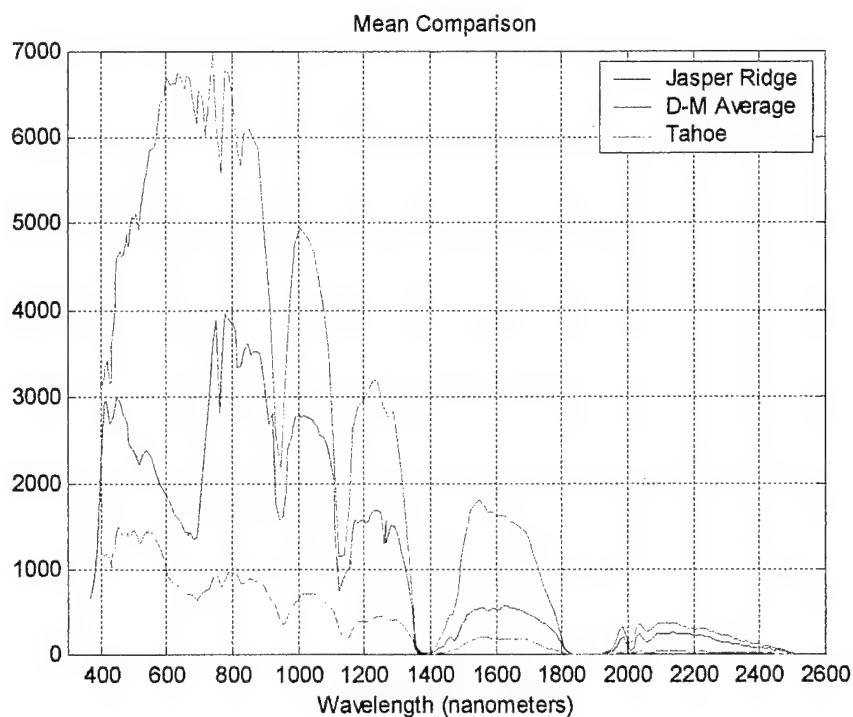
Figure 4.13: Jasper Ridge and Lake Tahoe Mean Compared to Davis-Monthan Average.

With the exception of the wavelengths between 450nms and 750nms, the behavior of the means for Jasper Ridge and Lake Tahoe correspond very closely to that of the Davis-Monthan scene. From this we can conclude that the behavior of the first eigenvector will also be similar in shape, with the exception of the chlorophyll absorption area, as shown in Figure 4.14, even though the scene constituents are different. The comparison of subsequent eigenvectors is not as simple as the first, because as noted earlier, as the eigenvector number increases, the scene specifics will begin to dictate the behavior of the eigenvector. Figure 4.14 depicts this behavior. Eigenvectors number one and two from all three sets are similar in shape, however, starting with eigenvector number three, the shapes begin to diverge significantly from the Davis-Monthan average.

71
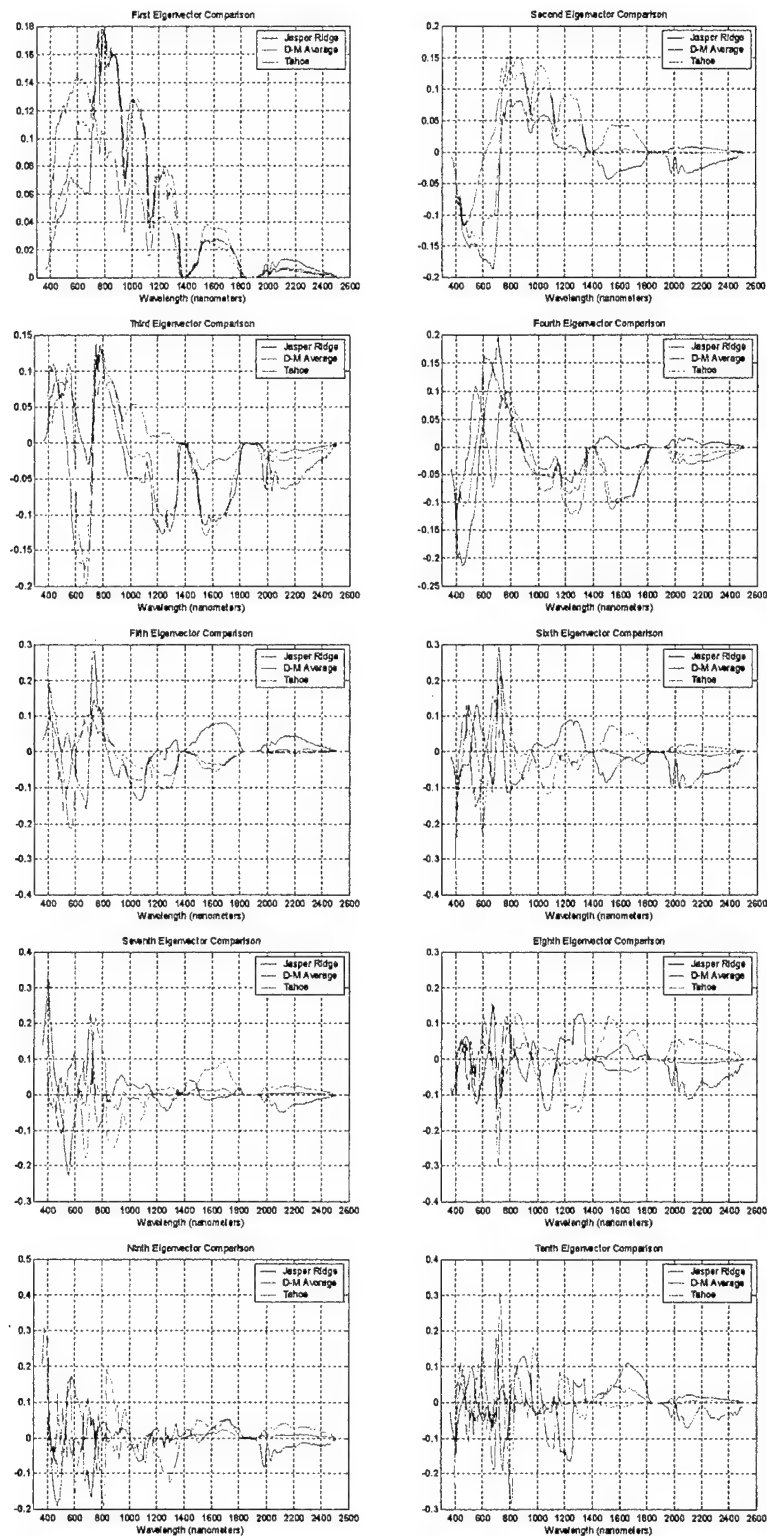
Figure 4.14: Jasper Ridge and Lake Tahoe Eigenvectors Compared to Davis-Monthan Average.

Although the first eigenvector is similar for all scenes, Jasper Ridge and Lake Tahoe's eigenvectors quickly begin to diverge from the Davis-Monthan average by eigenvector number three. Also, both Jasper Ridge and Lake Tahoe's eigenvectors are similarly structured from the first eigenvector up through the fourth eigenvector. (The Davis-Monthan scenes eigenvectors remained similarly structured up through eigenvector number six. (Figure 4.8)) This would seem to indicate that the statistics of Jasper Ridge and Lake Tahoe are more alike to each other than to the Davis-Monthan statistics and that these scenes are from a class that does not include Davis-Monthan.

A comparison of the Davis-Monthan average RGB eigenvectors to Lake Tahoe and Jasper Ridge yields similar results. (Figure 4.15) As expected, the first eigenvectors which correspond to the overall scene color composition are nearly identical while the next two eigenvectors diverge due to variances within the individual scenes.
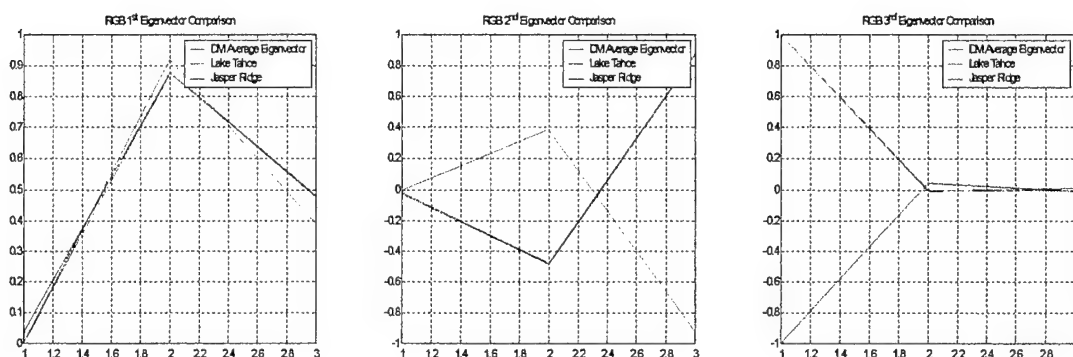
Figure 4.15: Jasper Ridge and Lake Tahoe RGB Eigenvectors Compared to Davis-Monthan Average.

D. APPLICATION OF AVERAGES

To test whether averages of the Davis-Monthan scenes could be applied to other scenes, a subset of 13 data sets from the October 1995 collect were averaged to obtain the PC transformation and RGB eigenvectors. These 'global' eigenvectors were then applied to two different scenes to obtain the PCs, HSV and RGB transformed HSV images. The first scene for comparison was also from Davis-Monthan, but collected during June 1995. The second scene that the Davis-Monthan averages were applied to was the Lake Tahoe data set. The Lake Tahoe data set was chosen for comparison because the data was also collected with the HYDICE sensor, but is of a completely dissimilar scene background.

For comparison of the original PCs and PCs obtained with the 'global' statistics, four scene images are presented. The first is the grayscale image of the first few principal components. (Figures 4.16a/b and 4.17) The second is the direct RGB representation of the principal components, including the variation of setting saturation to one, value to one, and both saturation and value to one. (Figures 4.18a/b and 4.19a) The third image set is the HSV transformation of the principal components, including setting saturation to one, value to one, and both saturation and value to one. (Figures 4.20a/b and 4.21a/b) The fourth set is the RGB transformation of the HSV image. (Figures 4.22a/b and 4.23a/b)

Upon inspection, the grayscale principal component images appear to be very similar in content with only minor variations in scale. However, the direct RGB comparisons clearly show differences, but the differences are similar in their pixel locations, indicating that they contain the same scene information.

74

Figure 4.16a: Davis-Monthan PC and Test Set PC Comparison. Panel A is the Original (Scene Specific) PC1. Panel B is the Test (Average) PC1. Panel C is the Original (Scene Specific) PC2. Panel D is the Test (Average) PC2.
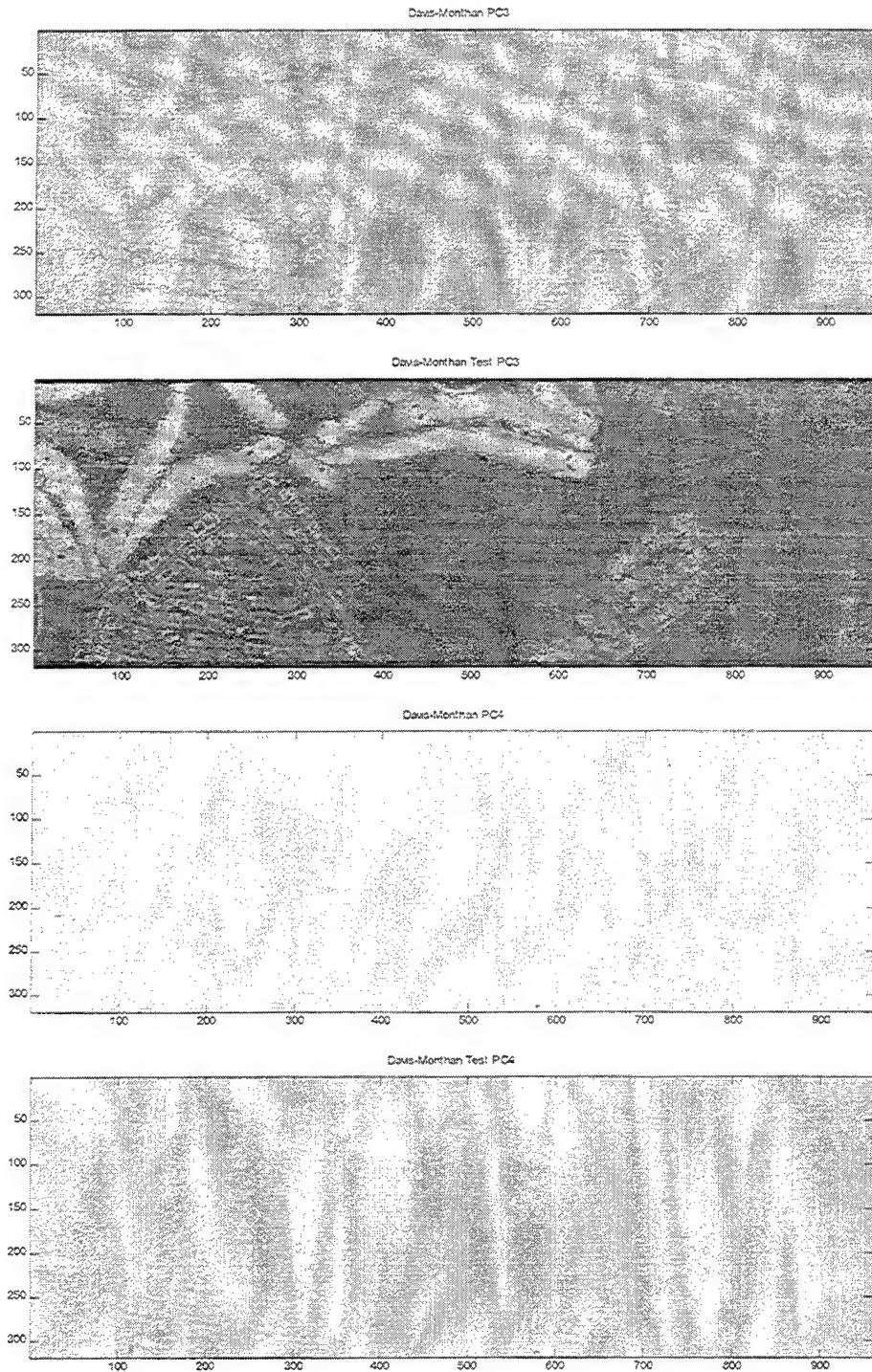
Figure 4.16b: Davis-Monthan and Test Transform PC Comparison. Panel A is the Original PC3. Panel B is the Test PC3. Panel C is the Original PC4. Panel D is the Test PC4. (Note that the test PC4 contains more variance than the original PC4.)

76

Original PCs   Test Set PCs
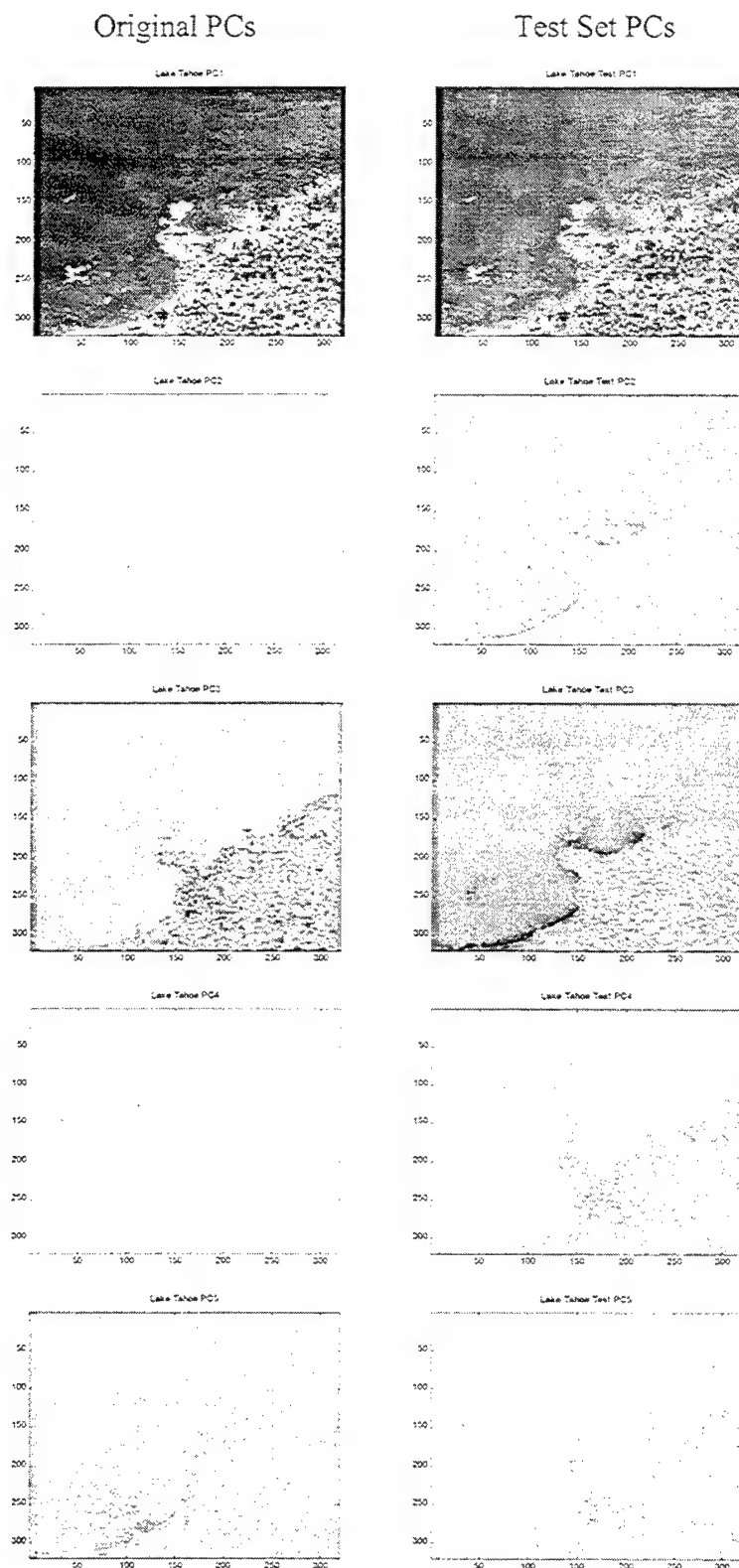
Figure 4.17: Lake Tahoe and Test Transform PC Comparison. (Note that the higher numbered test PCs contain more variance than their counterpart does.)

PC1 - Red, PC2 - Green, PC3 - Blue

PC1 - Red, PC2 - Green, PC3 - Blue

RGB Representation With S=1

RGB Representation With S=1
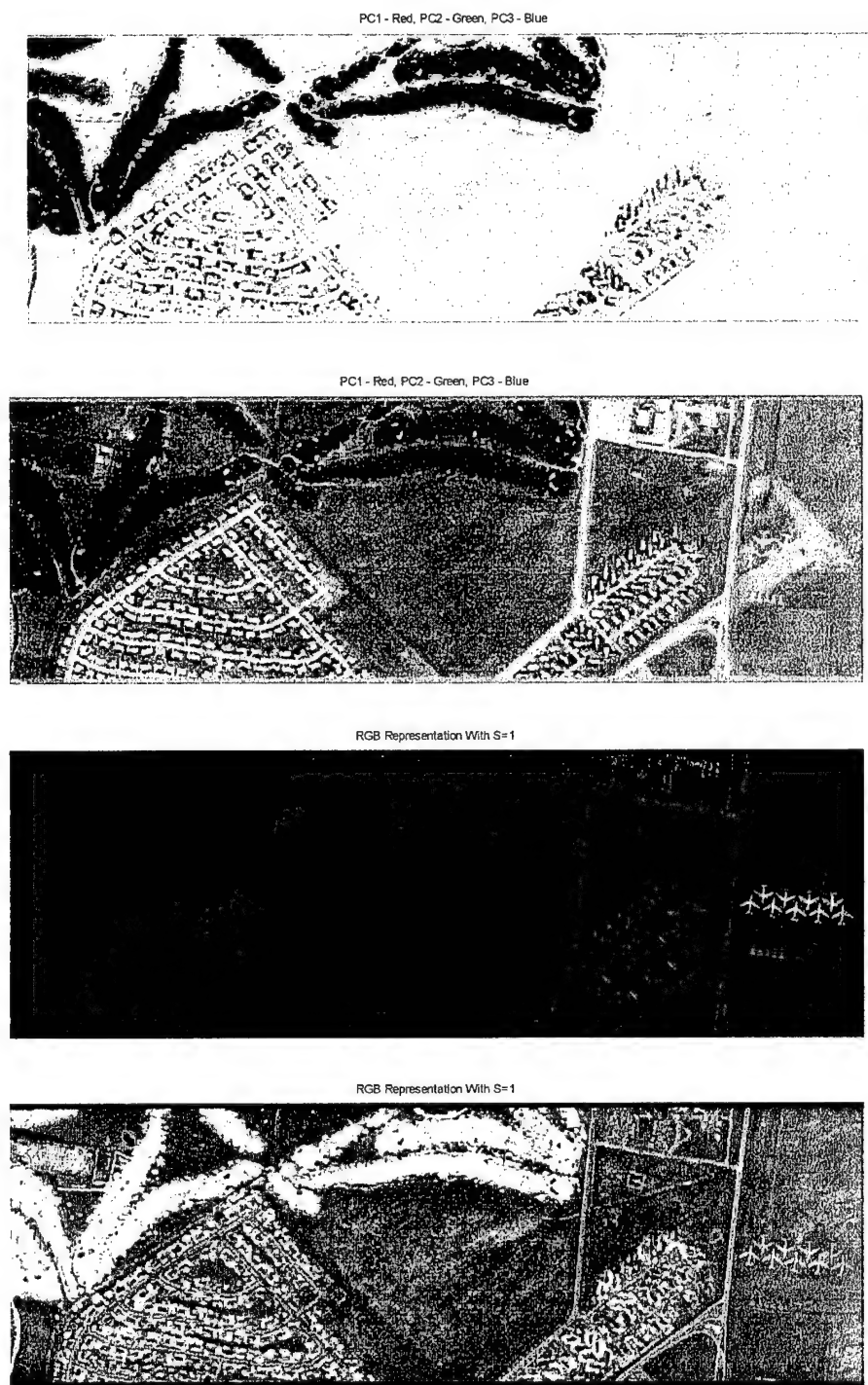
Figure 4.18a: Davis-Monthan Direct RGB Representation of Original PCs and Test PCs. Panels A and C are from the Original Data. Panels B and D are from the Test Set. (Note that with no *a priori* knowledge of the scene, panels A and B may be construed to contain small lakes rather than fairways.)

78
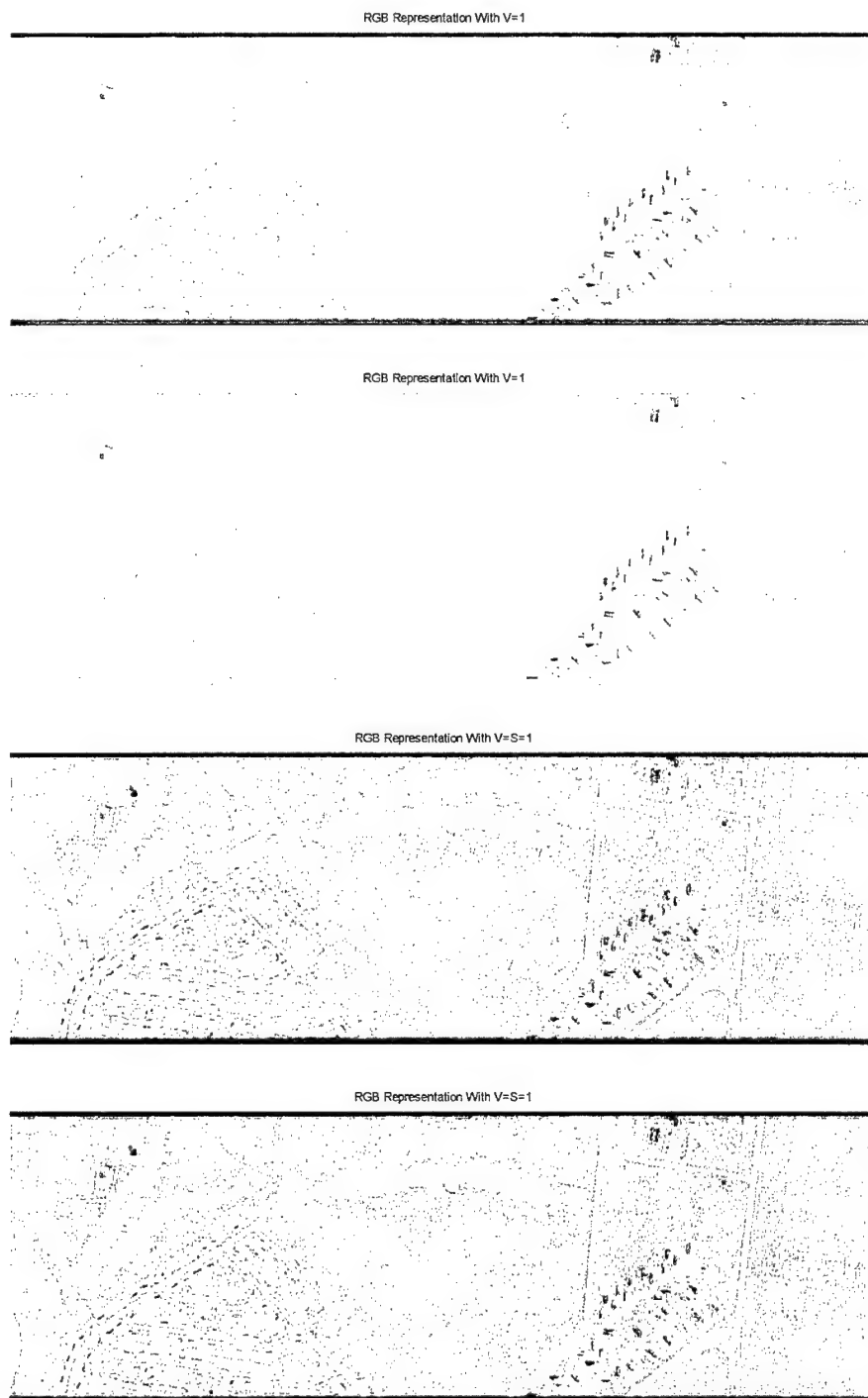
Figure 4.18b: Davis-Monthan Direct RGB Representation of Original PCs and Test PCs. Panels A and C are from the Original Data. Panels B and D are from the Test Set. (Note the similarity between panels A and B, and C and D.)

Original PCs   Test Set PCs

PC1 - Red, PC2 - Green, PC3 - Blue   PC1 - Red, PC2 - Green, PC3 - Blue

RGB Representation With S=1   RGB Representation With S=1

RGB Representation With V=1   RGB Representation With V=1

RGB Representation With V=S=1   RGB Representation With V=S=1
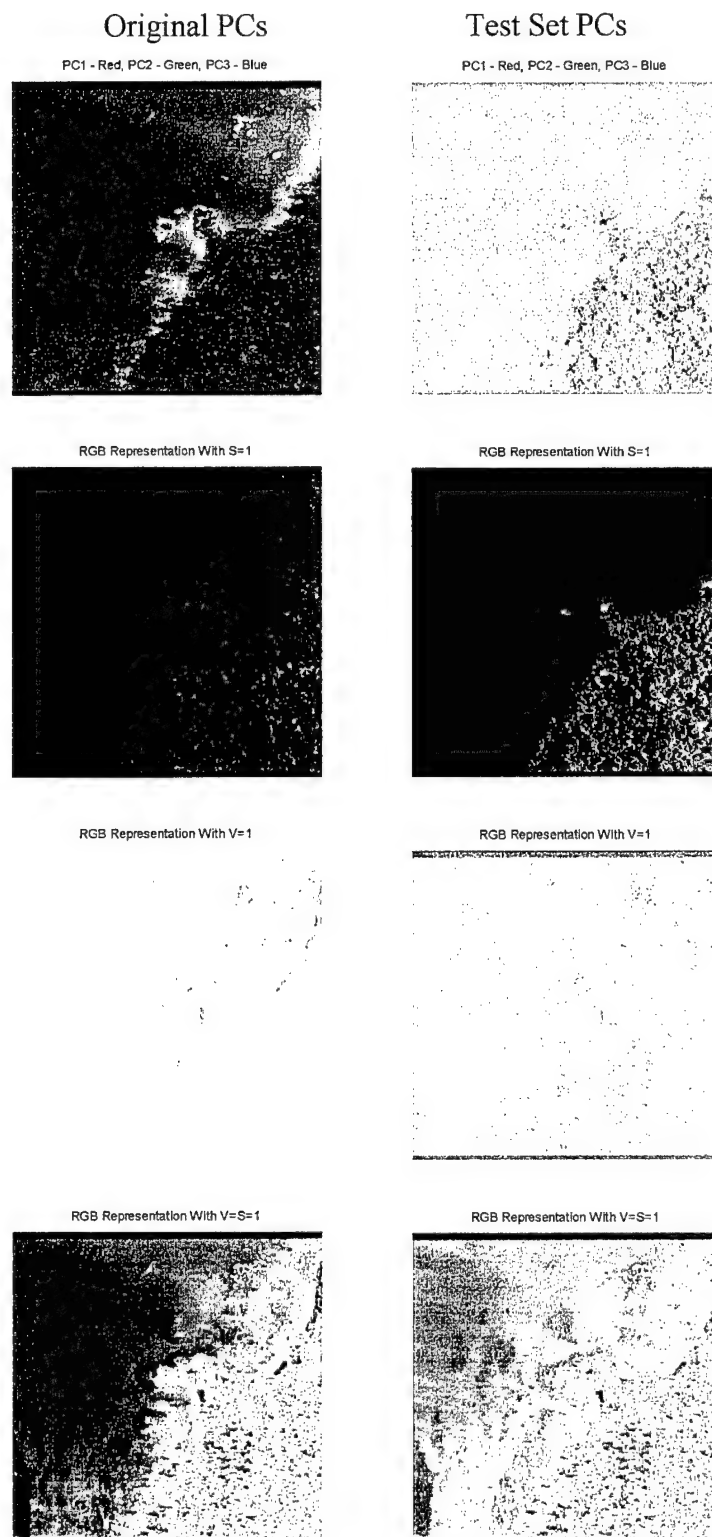
Figure 4.19: Lake Tahoe Direct RGB Representation of Original PCs and Test PCs.
(Note the similarity of scene content.)

80

HSV FROM COVARIANCE, COLOR RESHAPED

HSV FROM COVARIANCE, COLOR RESHAPED (TEST SET)

HSV FROM COVARIANCE, COLOR RESHAPED AND S=1

HSV FROM COVARIANCE, COLOR RESHAPED AND S=1 (TEST SET)
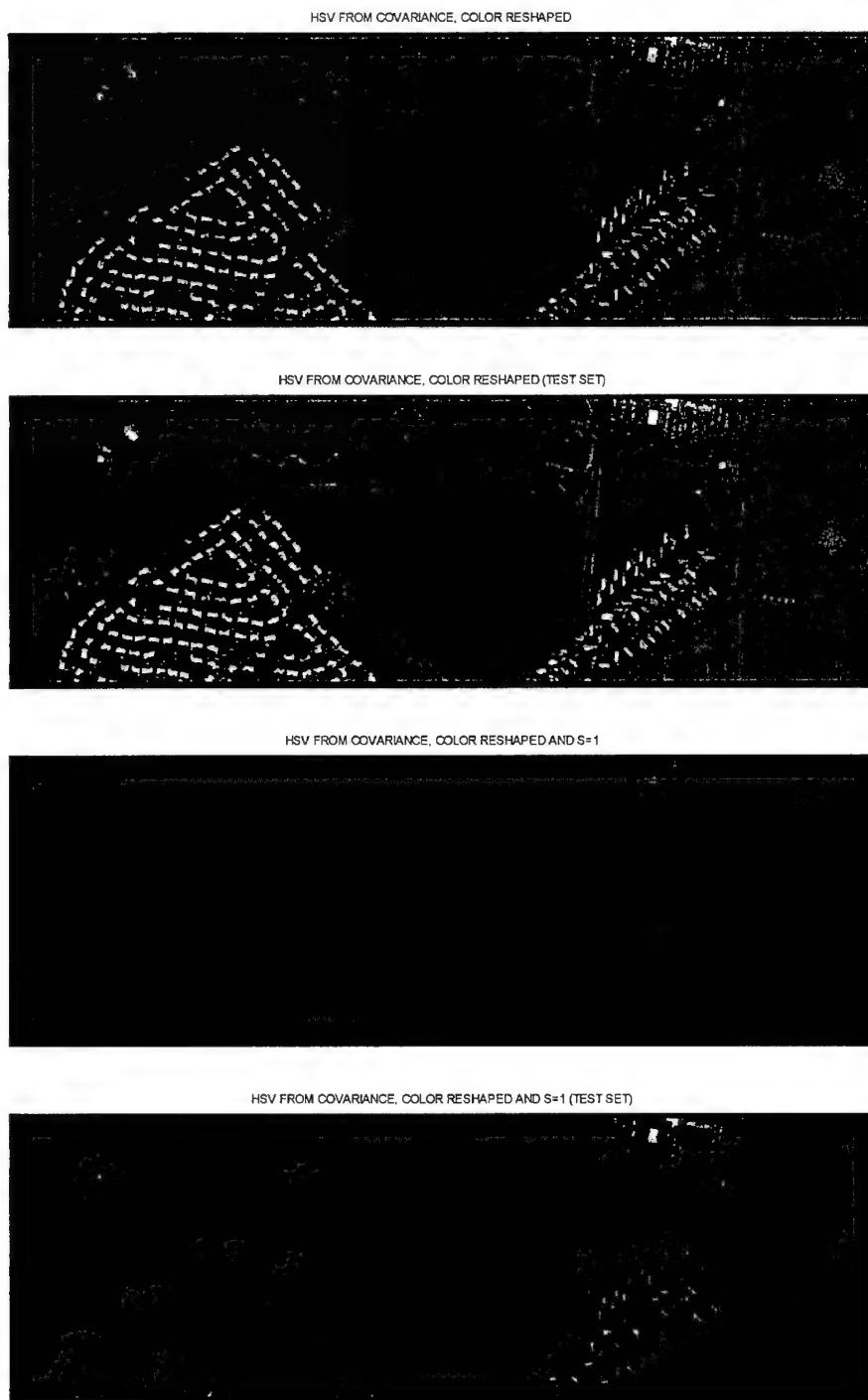
Figure 4.20a: Davis-Monthan HSV and Test HSV Comparison. Panels A and C are
from the Original Data. Panels B and D are from the Test Set.

81

HSV FROM COVARIANCE, COLOR RESHAPED AND V=1

HSV FROM COVARIANCE, COLOR RESHAPED AND V=1 (TEST SET)

HSV FROM COVARIANCE, COLOR RESHAPED AND V=S=1

HSV FROM COVARIANCE, COLOR RESHAPED AND V=S=1 (TEST SET)
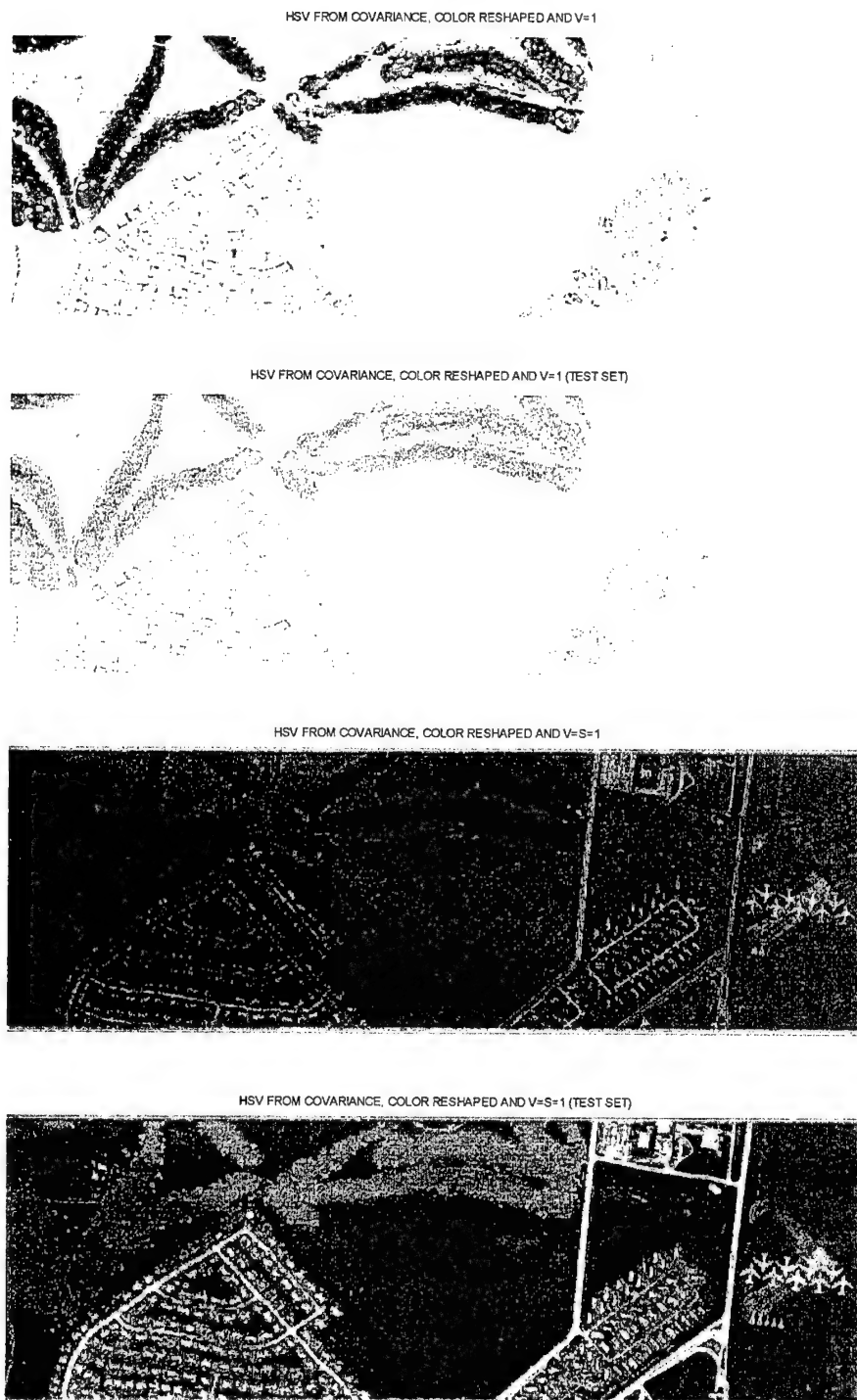
Figure 4.20b: Davis-Monthan HSV and Test HSV Comparison. Panels A and C are from the Original Data. Panels B and D are from the Test Set.

82

HSV FROM COVARIANCE, COLOR RESHAPED

HSV FROM COVARIANCE, COLOR RESHAPED (TEST SET)

HSV FROM COVARIANCE, COLOR RESHAPED AND S=1

HSV FROM COVARIANCE, COLOR RESHAPED AND S=1 (TEST SET)
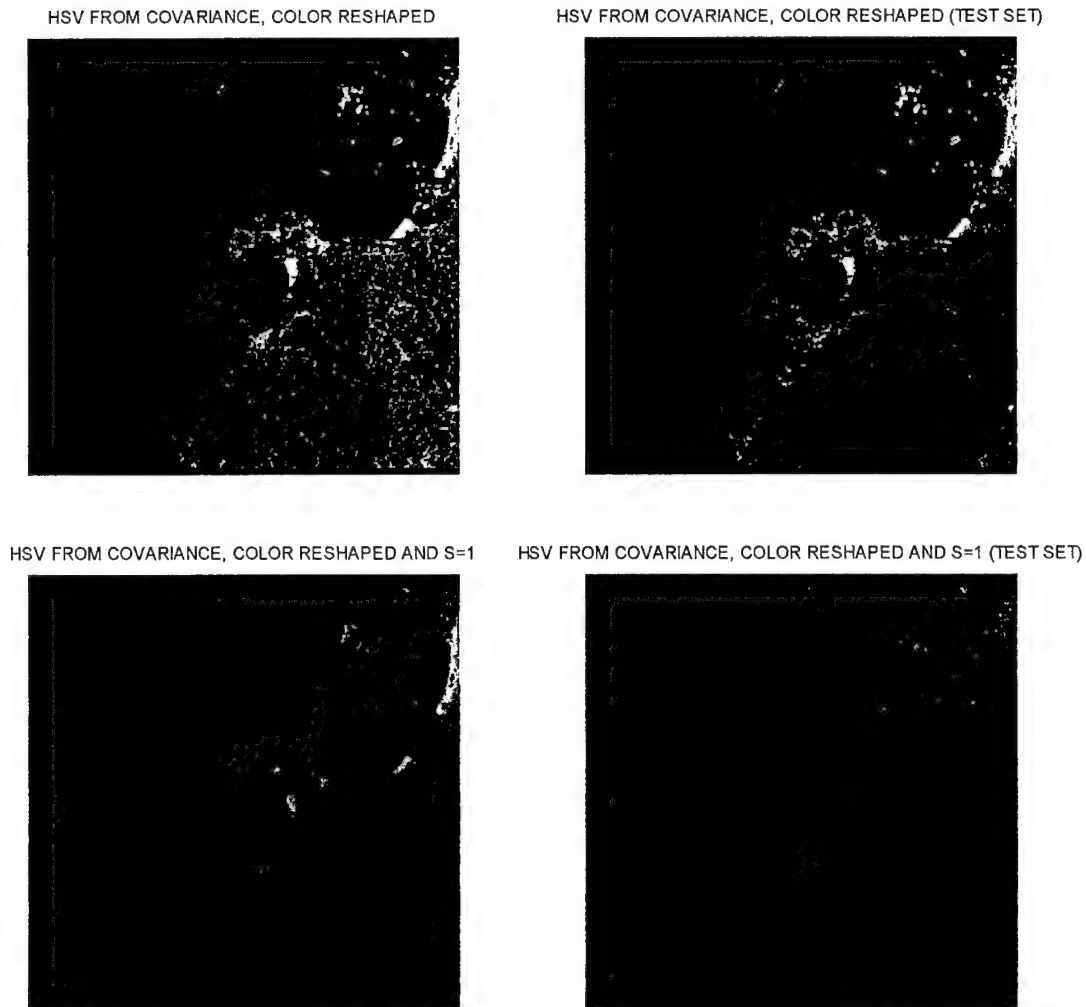
Figure 4.21a: Lake Tahoe HSV and Test HSV Comparison.

The images of Figure 4.20a panel A and 4.21a panel A makes it easier to view, as compared with images like those in Figure 4.18a panel A and Figure 4.19 panel A. Pixels that do not have a significant projection onto either PC2 or PC3 appear largely desaturated. This makes the image easier to view because naturally occurring scenes tend to be largely desaturated with low dimensionalities in the visible portion of the spectrum. (Buchsbaum and Gottschalk,1983) Human observers are not used to examining images with large regions of highly saturated hues that vary rapidly.

83

HSV FROM COVARIANCE, COLOR RESHAPED AND V=S=1   HSV FROM COVARIANCE, COLOR RESHAPED AND V=S=1 (TEST SET)
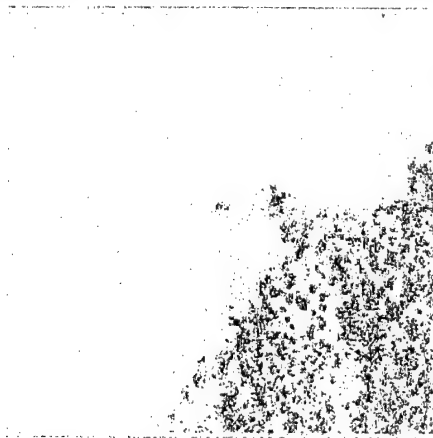
Figure 4.21b: Lake Tahoe HSV and Test HSV Comparison.

The image sets in which the saturation and values are set to one provides a way to go back and forth between highly saturated and less saturated images to make material classification more obvious. From these figures it is clear to see that while the colors of the original PC and test PC sets may be different, the scene content remains the same and visible.
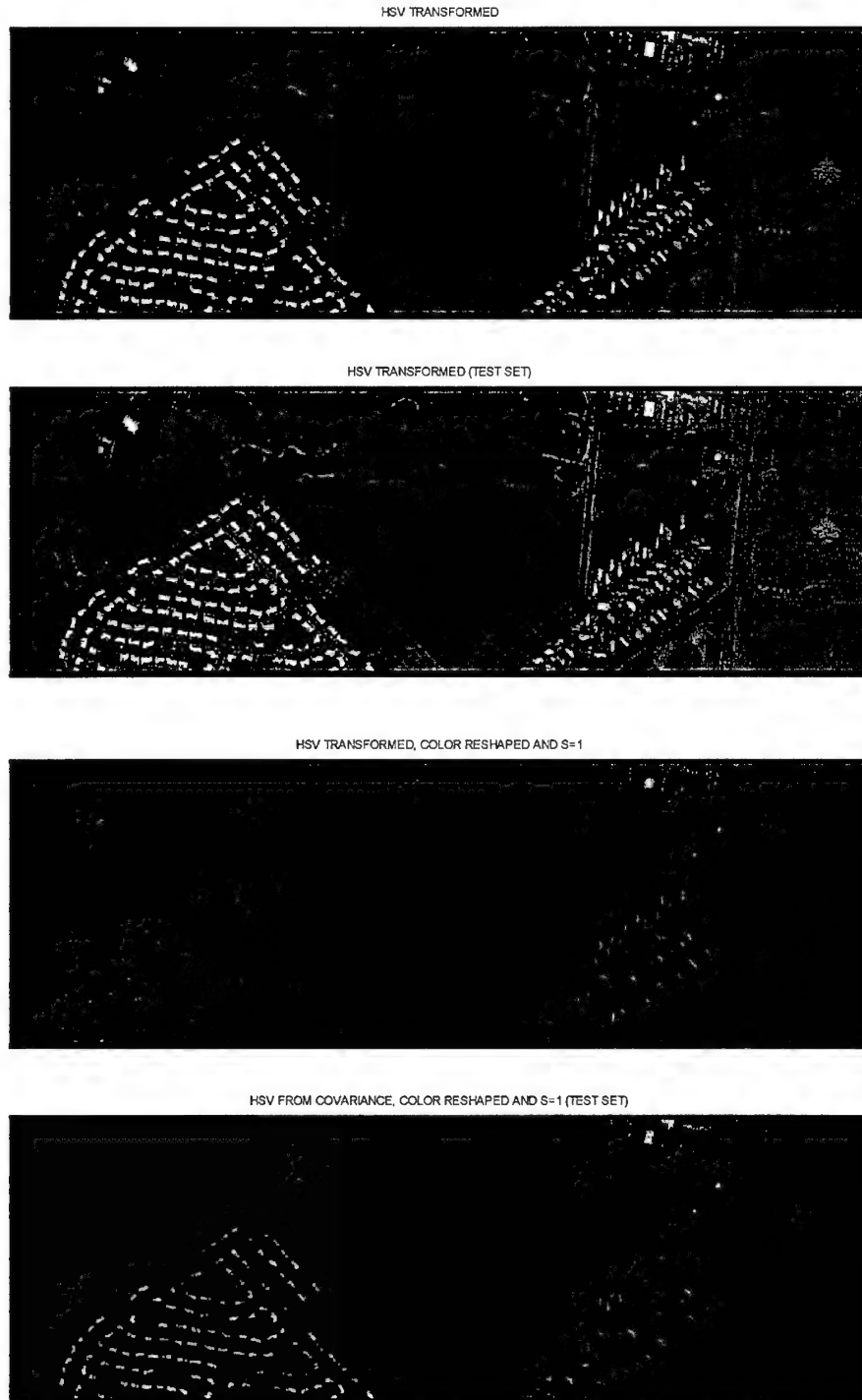
84

Figure 4.22a: Davis-Monthan RGB Transformed HSV and Test RGB Transformed HSV Comparison. Panels A and C are from the Original Data. Panels B and D are from the Test Set.

HSV TRANSFORMED, COLOR RESHAPED AND V=1

HSV FROM COVARIANCE, COLOR RESHAPED AND V=1 (TEST SET)

HSV TRANSFORMED, COLOR RESHAPED AND V=S=1

HSV FROM COVARIANCE, COLOR RESHAPED AND V=S=1 (TEST SET)
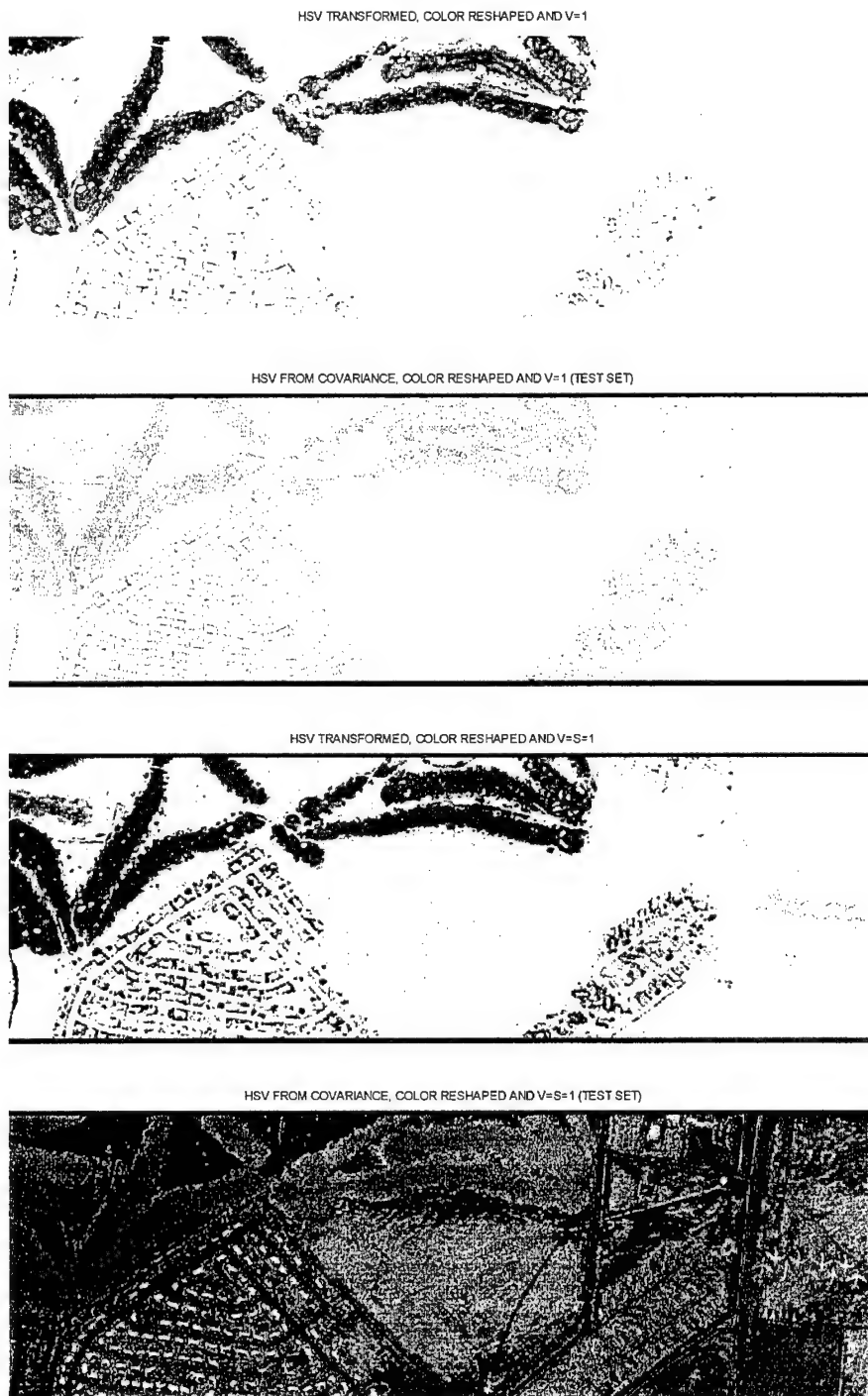
Figure 4.22b: Davis-Monthan RGB Transformed HSV and Test RGB Transformed HSV Comparison. Panels A and C are from the Original Data. Panels B and D are from the Test Set.

RGB Transformed   RGB Transformed Test Set

HSV TRANSFORMED   TRANSFORMED HSV, COLOR ROTATED (TEST SET)

HSV TRANSFORMED, COLOR RESHAPED AND S=1   HSV FROM COVARIANCE, COLOR ROTATED AND S=1 (TEST SET)
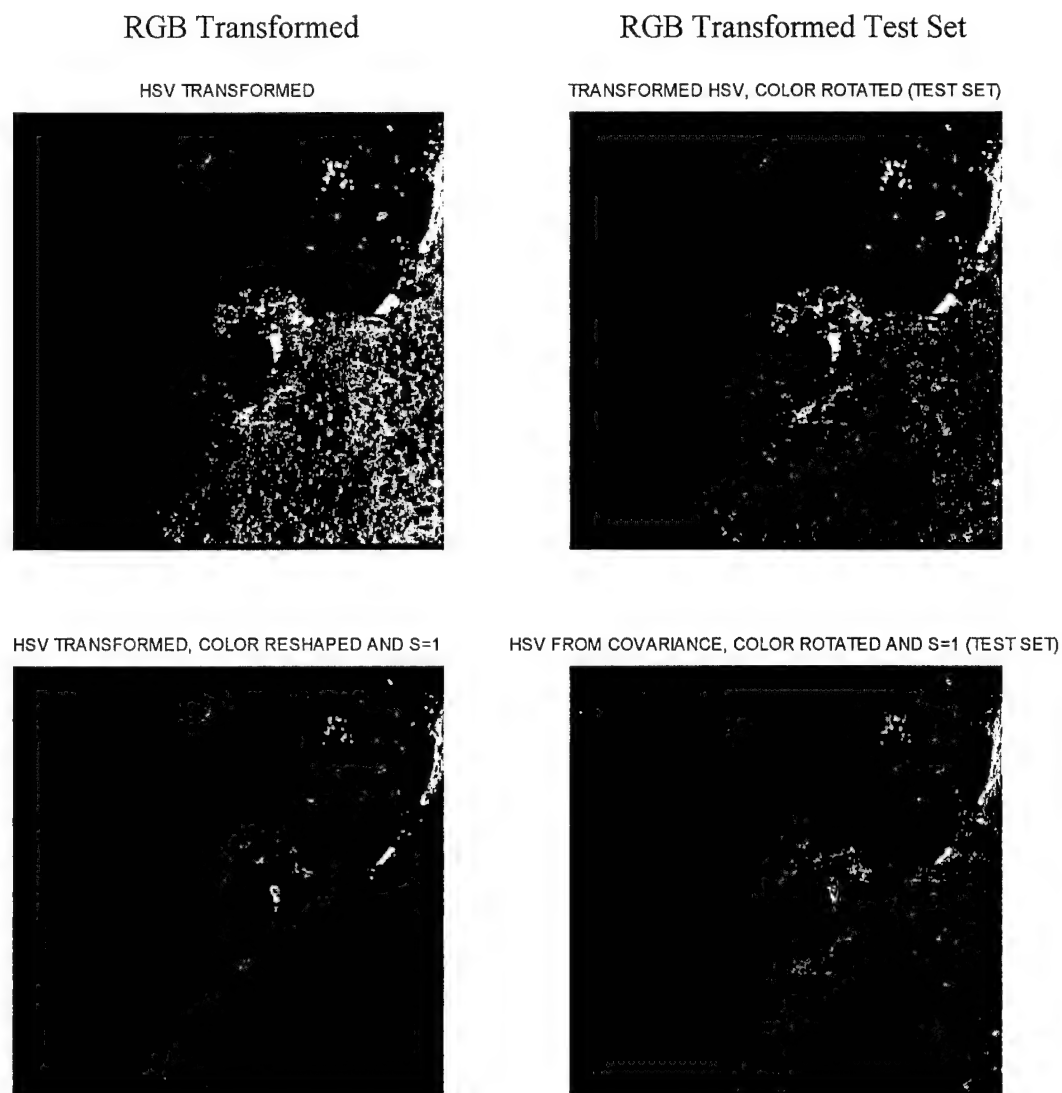
Figure 4.23a: Lake Tahoe RGB Transformed HSV and Test RGB Transformed HSV
Comparison.

Figure 4.23 makes an interesting comparison between the RGB transformed
images. The images on the left which are directly transformed from their own scene
information clearly show the dominance of the 'blue' band corresponding to the high
amount of water represented in the scene while the images on the right which were

transformed with the 'global RGB eigenvectors maintains the appearance of the HSV image.

RGB Transformed

RGB Transformed Test Set

HSV TRANSFORMED, COLOR RESHAPED AND V=1

HSV FROM COVARIANCE, COLOR ROTATED AND V=1 (TEST SET)

HSV TRANSFORMED, COLOR RESHAPED AND V=S=1

HSV FROM COVARIANCE, COLOR ROTATED AND V=S=1 (TEST SET)
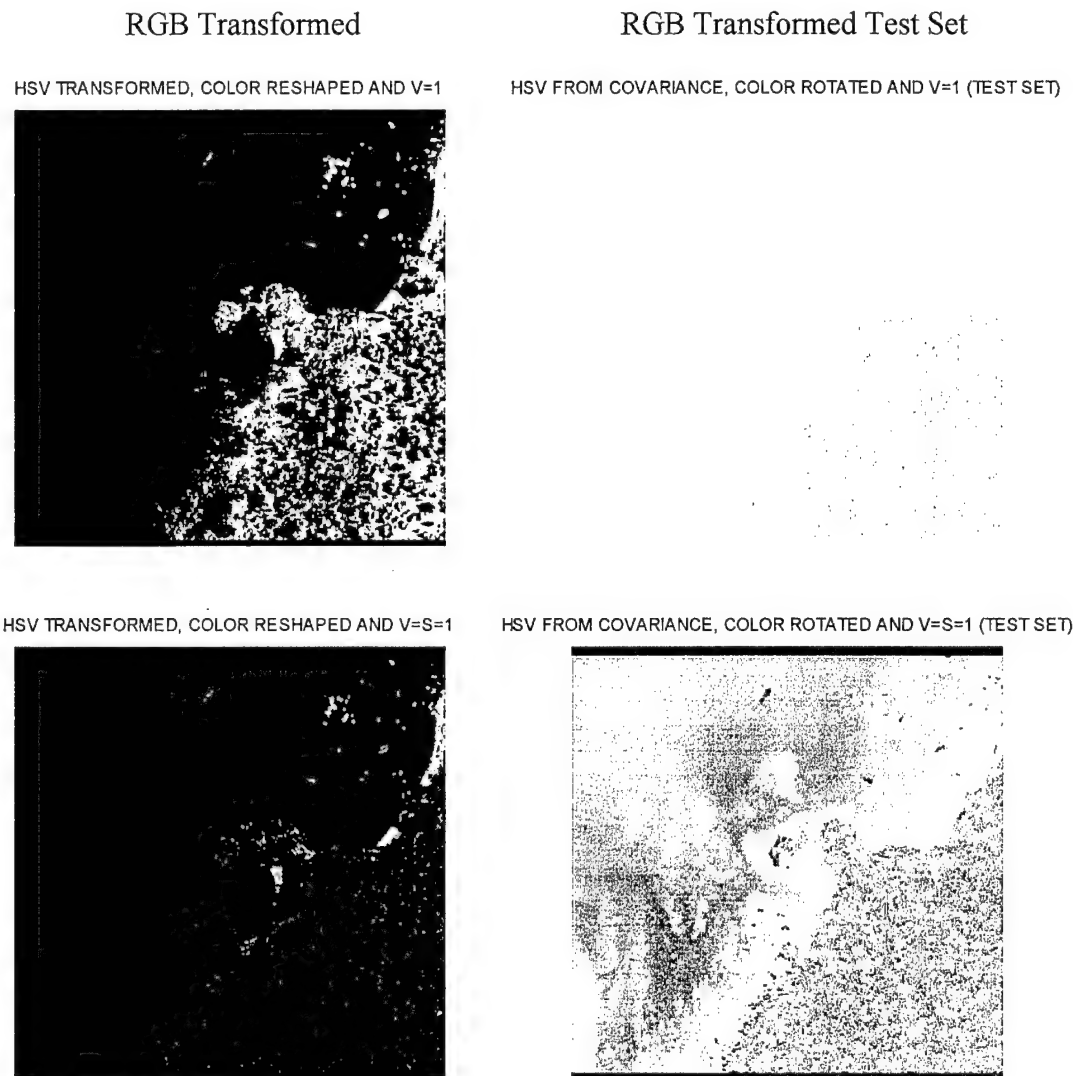
Figure 4.23b: Lake Tahoe RGB Transformed HSV and Test RGB Transformed HSV Comparison.

V. SUMMARY AND CONCLUSIONS

From analysis and comparison of the Davis-Monthan data to dissimilar scenes, it is clear to see that for best analysis, it would be appropriate to maintain scenes such as Davis-Monthan within one group and scenes such as Jasper Ridge and Lake Tahoe within another group. But, for first order unsupervised classification, the first few eigenvalues and associated eigenvectors which contain the largest amount of scene variance can appropriately represent the scene. Figure 5.1 and Table 5.1 reinforce this by showing that over 98 percent of scene variance is contained within the first three eigenvectors. In fact, over 95 percent is located within the first two. Extending this concept further and drawing upon the results in the previous sections, it is clear that a generalized 'global' set of eigenvectors can appropriately depict any scene content. The average eigenvectors investigated in this study provides such a basis and can be further improved upon with an increase in the number of data sets utilized.
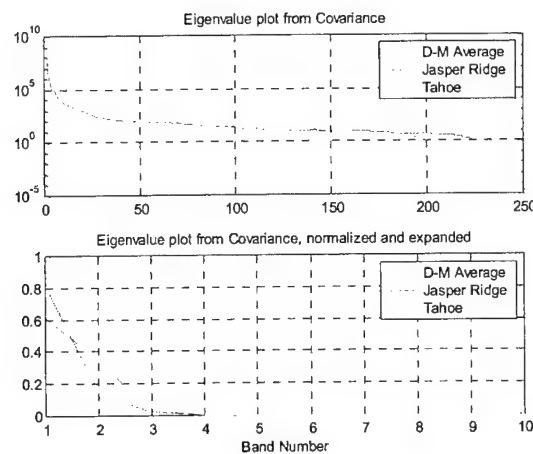
Figure 5.1: Jasper Ridge and Lake Tahoe Eigenvectors Compared to Davis-Monthan Average.

89

Eigenvalue	Davis-Monthan	Jasper Ridge	Lake Tahoe
1	0.8417	0.6164	0.8093
2	0.1159	0.3479	0.1629
3	0.0259	0.0271	0.0147
4	0.0056	0.0026	0.0092
5	0.0028	0.0019	0.0022

Table 5.1: Eigenvalues for Davis-Monthan Average, Jasper Ridge, and Lake Tahoe.

Table 5.1 along with the figures in chapter four graphically depict the fact that the first three eigenvectors are the most important in describing any scene. Referring back to section 3C on color mapping strategies, it is clear that a combination of the first three principal component transforms will appropriately depict any scene.

The principal component-based mapping strategy discussed previously provides an easy way to perform first order unsupervised classification. The inclusion and utilization of 'global' or generalized eigenvectors decreases the overhead required to perform the first order classification and allows for 'real time' classification of hyperspectral imagery. The resultant image is segmented spatially based on a generalized projection of the radiance distribution in the PC2-PC3 plane. By visually inspecting the resulting image, an analyst can then direct attention to appropriate areas of the scene for further processing without the time consuming requirement of calculating the scene specific statistics.

The PC and RGB transformation eigenvectors utilized in this study were derived by averaging the scene statistics from 13 similar scenes. These 'global' or generalized eigenvectors were then applied to a similar and dissimilar scene to observe the effect. It is clear that these eigenvectors appropriately allowed for first order classification and can

be applied to a broad range of spectral imagery classes. These eigenvectors can become even more robust as the number of 'averaged' scenes is increased.

It was shown that the 1st PC will always be related to the mean solar radiance, but the 2nd, 3rd and subsequent PCs depend on the specific contents of the image. However, it was also shown that only the first three PCs are required for a color mapping corresponding to human color vision. The remapping of the MATLAB colorspace in chapter three provides an orthogonal mapping of the colors, but requires further refinement of the colorspace. It remains to be investigated whether or not the RGB transformation of the HSV image presented here can be arranged so that materials are presented in a straightforward manner, i.e. water always mapped to blue, vegetation to green, etc, vice having the dominant scene constituent set the base hue of the image. The author believes that this mapping can be accomplished.

The presentation strategy discussed here is best suited to broad scale geographical classification, not for identifying small, isolated targets. However, objects and variances within the scene which occur only at a few pixels in an image and thus have little effect on the overall covariance matrix and do not contribute significantly to the 2nd and 3rd PCs, appear to stand out and be discernable in this mapping strategy. For this reason, this aspect of the mapping strategy merits further investigation.

The invariant display strategy and generalized eigenvectors presented here is offered as a way to have a first look at a wide variety of spectral scenes. By performing a PC transformation with these eigenvectors and analyzing the three most significant PCs, an initial classification decision can be made 'real time'. Detailed investigation of the

relationship between the PC eigenvectors and dissimilar image content shows that this strategy is robust enough to provide an accurate initial scene classification.

MATLAB CODE

Two MATLAB code files are scripted below. The first was utilized for conversion to Band Interleave format and the second was utilized to generate the statistics and principal components for analysis.

```
%****************************************************************************
%This program will read in a 3-D Hyperspectral Data set from ENVI format
%
%                  by
%            David I. Diersen
%              October 2000
%
clear
%****************************************************************************
%HYPERSPECTRAL DATA FILE READER
%
%     WRITTEN PRIMARILY FOR 'BSQ' BYTE ORDER 0-1 AND 'BIL' BYTE ORDER 0-1
%
%     THIS FIRST SECTION GETS THE NECESSARY INFO ON THE FILE TO PROCESSED
%
filein=input('   What file do you want to process?  ','s');
type=str2num(input('What is the data type? (1,2,3,4,5,or6)  ','s'));
if type == 1
    type=char('int8');
elseif type==2
    type=char('int16');
elseif type==3
    type=char('int32');
elseif type==4            %Not dealing with 4, 5 and right now
    type=char(float);
elseif type==5
    type=char(doubleprecision);
elseif type==6
    type=char(complex);
else string('  You made a mistake, BOOM!    ')
end
byte=str2num(input('What is the byte order? (0=MS-DOS, 1=IEEE)  ','s'));
inter=str2num(input('What is the interleave type? (1=BSQ,2=BIP,3=BIL)
','s'));
l=str2num(input('   What is the number of samples?  ','s'));
%Obtains the size of original data
w=str2num(input('   What is the number of rows?  ','s'));
dim=str2num(input('   How many bands do you have?  ','s'));
hdrsz=str2num(input('   How long is the header?  ','s'));
%****************************************************************************
%   READ IN THE FILE
%
fid1=fopen(filein);                      %Open the binary file
if inter==1                              %Works on BSQ format files
```

```matlab
    if byte==1                              %Byte order is 1
        hdr=fseek(fid1,hdrsz,'bof');    %Sets the pointer to right after
the header
        tmp=fread(fid1,[1,(l*dim*w*2)],'int8');
%Reads the data in 1 byte increments (Splits data in half)
        tmp2=reshape(tmp,2,(length(tmp)/2));
%These next three lines swaps bytes
        tmp3=flipud(tmp2);
        tmp4=reshape(tmp3,1,length(tmp)); %Data is now in LSB-MSB order
        fid2=fopen('tempdata','w');         %Creates a temporary file
        count=fwrite(fid2,tmp4,'int8');
%Writes the Byte swapped data to binary file ro reread as LSB-MSB
        fid2=fopen('tempdata');             %Open the temp file
        data=fread(fid2,[1,(l*w*dim)],'int16'); %Reads the data as an
integer
        dat=reshape(data,l,w,dim);
        [l c d]=size(dat)
        for i=1:d
%Reorders and transposes data because of read in issues
            AA(:,:,i)=dat(:,:,i)';
        end
        fclose(fid2);
        delete tempdata                     %Deletes the temporary read file
    else                                    %Byte order is 0
    two_D_file=fread(fid1,[1,(l*dim*w)],type);
    dat=reshape(two_D_file,l,w,dim);
    [l c d]=size(dat)
    for i=1:d
%Reorders and transposes data because of read in issues, memory size
        AA(:,:,i)=dat(:,:,i)';
    end
end
elseif inter==2
    two_D_file=fread(fid1,[1,(l*w*dim)],type);
elseif inter==3                         %Works on BIL format files
    if byte==1
        fseek(fid1,hdrsz,'bof');        %Sets the pointer to right after
the header
        fid2=fopen('tempdata','w');     %Creates a temporary file
        tmp=(flipud(fread(fid1,[2,(l*w*dim)/4],'int8')));
%Reads the data in 1 byte increments (Splits data up because of size)
        posit=ftell(fid1);
        fwrite(fid2,tmp,'int8');
        clear tmp
        fseek(fid1,posit,'bof');
%This could/should be shortened with a "for" loop
        tmp=(flipud(fread(fid1,[2,(l*w*dim)/4],'int8')));
        clear posit
        posit=ftell(fid2);
        fseek(fid2,posit,'bof');
        fwrite(fid2,tmp,'int8');
        clear tmp
        tmp=(flipud(fread(fid1,[2,(l*w*dim)/4],'int8')));
fwrite(fid2,tmp,'int8');
        clear tmp
```

```
        tmp=(flipud(fread(fid1,[2,(l*w*dim)/4],'int8')));
        fwrite(fid2,tmp,'int8');
        clear tmp
        fid2=fopen('tempdata');        %Open the temp file
        for i=1:w/4            %Reads the file into a concatonated 2-D matrix
            x1(i,:)=fread(fid2,[1,(l*dim)],'int16');
        end
        save X x1
        clear i x1
        for i=1:w/4            %Reads the file into a concatonated 2-D matrix
            x2(i,:)=fread(fid2,[1,(l*dim)],'int16');
        end
        save Y x2
        clear i x2
        for i=1:w/4            %Reads the file into a concatonated 2-D matrix
            x3(i,:)=fread(fid2,[1,(l*dim)],'int16');
        end
        save XX x3
        clear i x3
        for i=1:w/4            %Reads the file into a concatonated 2-D matrix
            x4(i,:)=fread(fid2,[1,(l*dim)],'int16');
        end
        save YY x4
        clear i x2
        fclose(fid2);
        delete tempdata
        load X
        load Y                          %Correctly saved
        load XX
        load YY
        fid3=fopen('tempdata','w'); %Creates a temporary file
        for i=1:(l*dim)
            fwrite(fid3,x1(:,i),'int16');
            fwrite(fid3,x2(:,i),'int16');
            fwrite(fid3,x3(:,i),'int16');
            fwrite(fid3,x4(:,i),'int16');
        end
        clear x1 x2 x3 x4
        fclose(fid3);
        fid4=fopen('tempdata');
        AA=fread(fid4,[w,(l*dim)],'int16');
        AA=reshape(AA,w,l,dim);
        fclose(fid4);
        delete tempdata
        clear fid2 fid3 fid4 hdr tmp tmp2 tmp3 tmp4 count X Y
    else
        two_D_file=fread(fid1,[1,(l*w*dim)],type);
        dat=reshape(two_D_file,l*dim,w);
        tmp=dat';
        AA=reshape(tmp,l,w,dim);    %Resizes the file into correct bands
and size
        AA=reshape(AA,w,l,dim);
    end
end
fclose(fid1);
```

```
clear type l w dim fid1 inter i c d byte count dat data hdrsz posit
%*********************************************************************
% THE OUTPUT OF THE ABOVE BLOCK IS THE HYPERSPECTAL DATA CUBE LABELED AA
%*********************************************************************

%This section takes in the 3-D data set (AA) and processes the stats
%(Mean, Covariance, Correlation, Eigenvalues, Eigenvectors, and
Principal Components)
%
clear
load crf10m012origdata    %DATA IN MATLAB FORMAT
save tmp2 AA
%
%*********************************************************************
[l c d]=size(AA);                 %Obtains the # rows, columns, and bands
N=l*c;                            %Number of pixels in the scene
%  FIND THE MEAN
for i=1:d                         %Applied for each band
   mean_(i)=(1/N)*(sum(sum(AA(:,:,i))));
%Finds the mean for each band, vector form
end
mean_=mean_';                     %Mean into column form
save stats2 mean_
%  SUBTRACT THE MEAN FROM EACH BAND
for i=1:d
   AA(:,:,i)=(AA(:,:,i)-mean_(i));
%Subtracts the mean from each band and replaces AA
end
clear i x
%The above works well and fast.  Now working by pixels, slows down
%  FIND THE CORRELATION AND COVARIANCE MATRIX
k=1;                              %Initialize the pixel count
Cov=zeros(d,d);                   %Initialize covariance matrix
Auto_Corr=zeros(d,d);            %Initialize Auto Correlation matrix
for i=1:N
%Run for each pixel              THIS TAKES A LONG, LONG, LONG TIME.....
   z=k:(l*c):(l*c*d);
   cov=((1/(N-1)).*(AA(z)'*AA(z))); %Normalized pixel covariance
   corr=((AA(z)')+mean_)*(AA(z)+(mean_')); %Adds mean back in
%Get the Auto correlation at the same time E[(x)(x)']
   Cov=Cov+cov;                   %Summing over entirety
   Auto_Corr=Auto_Corr+corr;     %Summing over entirety
   clear cov corr
   k=k+1;                         %Advances pixel
end
save stats2 Cov Auto_Corr -append
clear AA i j k tmp z mean_
[S_C Eval Evect]=svd(Cov);        %SVD decomp to get evals and evectors
save stats2 S_C Eval Evect -append  %Save stats to save memory
clear S_C Eval Evect
%
%  NOW GET THE CORRELATION MATRIX WITH COEFFICIENTS
%
D=(diag(Cov))*(diag(Cov))';
%Use the diagonal of the cov matrix to get the denominator of corr
matrix
```

96

```matlab
for i=1:length(Cov)^2
Corr(i)=(Cov(i))/sqrt(D(i));        %Builds Correlation vector
end                                 %Next reshapes correlation matrix
Corr=reshape(Corr,sqrt(length(Corr)),sqrt(length(Corr)));
[S_Corr Eval_Corr Evect_Corr]=svd(Corr);
%SVD decomp to get evals and evectors of the Correlation matrix
clear x i D l c d
save stats2 Corr S_Corr Eval_Corr Evect_Corr -append
clear Corr S_Corr Eval_Corr Evect_Corr Cov
%
%   NOW THE DECOMPOSITION OF E[x*x']
%
[S_AC Eval_AC Evect_AC]=svd(Auto_Corr);
%SVD decomp to get evals and evectors
save stats2 S_AC Eval_AC Evect_AC -append
clear Auto_Corr S_AC Eval_AC Evect_AC
%*********************************************************************
%   This section will find the principal components, pixel by pixel
%
clear
load stats2                %Loads the statistics file
load tmp2                  %Loads the MATLAB format original data
[l,c,d]=size(AA);          %Rows, columns and dim of orig data
k=1;
N=(l*c);
      for i=1:N   %Run for each pixel, THIS TAKES A LONG, LONG TIME......
   z=k:(l*c):(l*c*d);
   AA(z)=(Evect')*(AA(z)'); %Transform from covariance
   k=k+1;
end
PC=AA;                %Creates principal component transform variable
clear AA
i=1:25;
PCs(:,:,i)=PC(:,:,i);%Only want the first 25 Principal components
clear PC
PC=PCs;
save xforms2 PC        %Saves to a MATLAB file
clear PC i k z AA
clear                  %Clears to keep memory from becoming full
load stats2            %As above
load tmp2
[l,c,d]=size(AA);      %Rows, columns and dim of orig data
k=1;
N=(l*c);
for i=1:N              %Run for each pixel, THIS TAKES A LONG TIME.....
   z=k:(l*c):(l*c*d);
   AA(z)=(Evect_Corr')*(AA(z)');%Transform from coefficients
   k=k+1;
end
PC_R=AA;
clear AA
i=1:25;
PCs(:,:,i)=PC_R(:,:,i);%Only want the first 25 transforms
clear PC_R
PC_R=PCs;
```

97

```
save xforms2 PC_R -append    %Saves the transfom from coefficients
clear PC_R i k z AA
clear                        %Make more memory room
load stats2
load tmp2
[l,c,d]=size(AA);            %Rows, columns and dim of orig data
k=1;
N=(l*c);
for i=1:N                    %Run for each pixel, THIS TAKES A LONG TIME.
   z=k:(l*c):(l*c*d);
   AA(z)=(Evect_AC')*(AA(z)');   %Transform from E[xx']
   k=k+1;
end
PC_AC=AA;
clear AA
i=1:25;
PCs(:,:,i)=PC_AC(:,:,i);     %Only want the first 25 transforms
clear PC_AC
PC_AC=PCs;
save xforms2 PC_AC -append
clear PC_AC i k z AA c d N
%***************************************************************
% Outputs three files, tmp2 which is the original data file, stats2 %
%    which is the statistics from the three methods, and xforms2 which is
%    the first 25 bands of the principal component transforms.
%***************************************************************
```

LIST OF REFERENCES

Anderson, T. W., *An Introduction to Multivariate Statistical Analysis,* Second Edition, John Wiley & Sons, New York, NY, 1984.

Brainard, D. H., Wandell, B. A., and Chichilnisky, "Color Constancy: From Physics to Appearance," *Current Directions in Psychological Science*, pp. 165-170, October 1992.

Brower, B. V., Haddock, D. H., Reitz, J. P., and Schott, J., "Spectrally and Spatially Adaptive Hyperspectral Data Compression," *SPIE Proceedings,* vol. 2821, August, 1996.

Buchsbaum, G. and Gottschalk, A., "Trichromacy, Opponent Colours Coding and Optimum Colour Information Transmission In The Retina" *Proc. R. Soc. Lond. B 220* pp. 89-113, 1983.

Farrand, W. H. and Harsanyi, J. C., "Discrimination of Poorly Exposed Lithologies in Imaging Spectrometer Data," *Journal of Geophysical Research,* vol. 100, no. El, pp. 1565-1578, January 25, 1995.

Fukunaga, K., *Introduction to Statistical Pattern Recognition,* Academic Press, New York, NY, 1972.

Goetz, A. F. H., "Imaging Spectrometry for remote sensing: Vision to reality in 15 years." *Proceedings of SPIE, vol. 2480: Imaging Spectrometry*, pp. 2-13, 1995.

Golub, G. H., and Van Loan, C. F., *Matrix Computations,* Johns Hopkins University Press, Baltimore, MD, 1983.

Gorman, J. D., Subotic, N. S., and Thelen, B. J., "Robust Material Identification in Hyperspectral Data via Multiresolution Wavelet Analysis," *1995 International Conference on Acoustics, Speech, and Signal Processing Proceedings,* vol. 5, pp. 2805-2808, May 9-12, 1995.

Haykin, S., *Adaptive Filter Theory,* Third Edition, Prentice Hall, Upper Saddle River, NJ, 1996.

Hotelling, H., "Analysis of Complex Statistical Variables into Principle Components," *The Journal of Educational Psychology,* vol. 24, pp. 417-441 and 498-520, September and October 1933.

Jenson, S. K. and Waltz, F. A., "Principal Components Analysis and Canonical Analysis in Remote Sensing," *Proceedings of the American Society of Photo Grammetry, 45th Annual Meeting,* pp. 337-348, 1979.

Johnson, P. E., Smith, M. 0., and Adams, J. B., "Quantitative Analysis of Reflectance Spectra with Principal Components Analysis," *Proceedings of the J₅Jh Lunar and Planetary Science Conference, Part 2, Journal of Geophysical Research,* vol. 90 supplem ant, pp. C805-C8 10, February 1985.

Jolliffee, I. T., *Principal Component Analysis,* Springer-Verlag, New York, NY, 1986.

Kapur, J. N., *Maximum-Entropy Models in Science and Engineering,* John Wiley & Sons, New York, NY, 1989.

Kerekes, J., Siracusa, C., Orloff, S., Manolakis, D., Shaw, G., Biehl, L., "Hyperspectral Data Characterization for Object Detection Applications," *IEEE International Geoscience and Remote Sensing Symposium*, Honolulu, HI, 2000.

Krauskopf, J., Williams,D. R., and Heeley, D. W. "Cardinal Directions of Color Space," *Vision Res. 22*, pp. 1123-1131, 1982,

Leon-Garcia, A., *Probability and Random Processes for Electrical Engineering,* Second Edition, Addison-Wesley, Reading, MA, 1994.

Pratt, W. K., *Digital Image Processing, Second Edition*, John Wiley & Sons, New York, NY, 1991.

Rao, A. K. and Bhargava, S., "Multispectral Data Compression Using Bidirectional Interband Prediction," *IEEE Transactions on Geoscience and Remote Sensing,* vol.34, no. 2, pp. 385-397, March 1996.

Ready, P. J. and Wintz, P. A., "Information Extraction, SNR Improvement, and Data Compression in Multispectral Imagery," *IEEE Transactions on Communications,* vol. COM-21, no. 10, pp. 1123-1130, October 1973.

Research Systems, Inc., Boulder, CO. *Interactive Data Language User's Guide,* Version Four, March, 1995.

Richards, J. A., *Remote Sensing Digital Image Analysis,* Springer-Verlag, New York, NY, 1993.

Rinker, J. M., "Hyperspectral Imagery . What Is It? . What Can It Do?" *USA CE Seventh Remote Sensing Symposium,* May 7-9, 1990.

Roger, R. E., and Cavenor, M. C., "Lossless Compression of AVIRIS Images," *IEEE Transactions on Geoscience and Remote Sensing,* vol.5, no.5, pp. 713-719, May 1996.

100

Scharf, L. L., *Statistical Signal Processing: Detection, Estimation, and Time-Series Analysis,* Addison-Wesley, Reading, MA, 1991.

Scott, Ed, and Bewley, Hollis, Spectral Selectivity, [http://www.photo.net/photo/edscott/spectsel.htm], 1997.

Searle, S. R., *Matrix Algebra Useful for Statistics,* John Wiley & Sons, New York, NY, 1982.

Singh, A. and Harrison, A., "Standardized Principal Components," *International Journal of Remote Sensing,* vol. 6, no. 6, pp. 883-896, 1985.

Smith, M. O., Johnson, P. B., and Adams, J. B., "Quantitative Determination of Mineral Types and Abundances from Reflectance Spectra Using Principal Components Analysis," *Proceedings of the J₅Ih Lunar and Planetary Science Conference, Part 2, Journal of Geophysical Research, vol. 90 supplement*, pp. C797-C804, February 1985.

Stefanou, M S, *A Signal Processing Perspective of Hyperspectral Imagery Analysis Techniques*, Master's Thesis, Naval Postgraduate School, Monterey, CA, June 1997.

Therrien, C. W., *Discrete Random Signals and Statistical Signal Processing,* Prentice Hall, New York, NY, 1992.

Tyo, J. S., Pugh, E. N., Engheta, N., "Colorimetric Representation for use with Polarization-Difference Imaging in Scattering Media," *J. Opt. Soc. Am. A*, vol. 15 pp.367-374, 1998.

Tyo, J. S., Diersen, D. I., Olsen, R. C., "Development of an Invariant Display Strategy for Spectral Imagery," *Proceedings of SPIE, vol. 4132: Imaging Spectrometry VI*, 2000, In Press.

Tyo, J. S., Robertson, J. C., Wallenbecker, J., Olsen, R. C., "Statistics of Target Spectra in HSI Scenes", *Proceedings of SPIE, vol. 4132: Imaging Spectrometry VI*, 2000, In Press.

Vane, G. and Goetz, A. F. H., "Terrestrial Imaging Spectroscopy," *Remote Sensing of the Environment,* vol. 24, pp. 1-29, 1988.

Wald, G., "Human Vision and the Spectrum," Science, vol. 145, 3636, pp.1007-1017, September 1964.

Watkins, D. S., *Fundamentals of Matrix Computations,* John Wiley & Sons, New York, NY, 1991.

Wyszecki, G., and Stiles, W. S., *Color Science*, Wiley, New York, NY, 1967.

INITIAL DISTRIBUTION LIST

1. Defense Technical Information Center..2
    8725 John J. Kingman Road, Suite 0944
    Ft. Belvoir, VA 22060-6218

2. Dudley Knox Library...2
    Naval Postgraduate School
    411 Dyer Road
    Monterey, CA 93943-5101

3. Director, Training and Education 1
    MCCDC, Code C46
    1019 Elliot Road
    Quantico, VA 22134-5027

4. Director, Marine Corps Research Center..2
    MCCDC, Code C40RC
    2040 Broadway Street
    Quantico, VA 22134-5107

5. Marine Corps Representative...1
    Naval Postgraduate School
    Code 037, Bldg. 330, Ingersoll Hall, Room 116
    555 Dyer Road
    Monterey, CA 93943

6. Marine Corps Tactical Systems Support Activity 1
    Technical Advisory Branch
    Attn: Librarian
    Box 555171
    Camp Pendleton, CA 92055-5080

7. Chairman, Code EC 1
    Department of Electrical and Computer Engineering
    833 Dyer Road, Room 437
    Naval Postgraduate School
    Monterey, CA 93943-5121